

University of Montana

## ScholarWorks at University of Montana

---

Graduate Student Theses, Dissertations, &  
Professional Papers

Graduate School

---

2003

### Imaging the shallow subsurface using ground penetrating radar at the Nyack floodplain Montana

Christopher R. Hawkins  
*The University of Montana*

Follow this and additional works at: <https://scholarworks.umt.edu/etd>

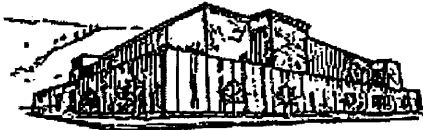
**Let us know how access to this document benefits you.**

---

#### Recommended Citation

Hawkins, Christopher R., "Imaging the shallow subsurface using ground penetrating radar at the Nyack floodplain Montana" (2003). *Graduate Student Theses, Dissertations, & Professional Papers*. 8158.  
<https://scholarworks.umt.edu/etd/8158>

This Thesis is brought to you for free and open access by the Graduate School at ScholarWorks at University of Montana. It has been accepted for inclusion in Graduate Student Theses, Dissertations, & Professional Papers by an authorized administrator of ScholarWorks at University of Montana. For more information, please contact [scholarworks@mso.umt.edu](mailto:scholarworks@mso.umt.edu).



**Maureen and Mike  
MANSFIELD LIBRARY**

The University of

**Montana**

---

Permission is granted by the author to reproduce this material in its entirety, provided that this material is used for scholarly purposes and is properly cited in published works and reports.

**\*\*Please check "Yes" or "No" and provide signature\*\***

Yes, I grant permission

    X    

No, I do not grant permission

Author's Signature: Christopher R. Hawkins

Date: June 6, 2003

Any copying for commercial purposes or financial gain may be undertaken only with the author's explicit consent.

---



IMAGING THE SHALLOW SUBSURFACE USING GROUND PENETRATING  
RADAR AT THE NYACK FLOODPLAIN, MONTANA

by

Christopher R. Hawkins

B.S., University of Tennessee 1999

presented in partial fulfillment of the requirements

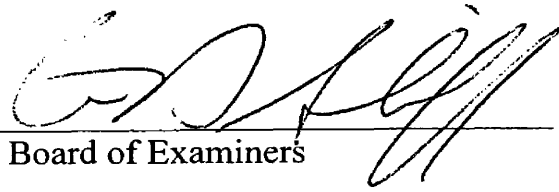
for the degree of


Master of Science

The University of Montana

2003

Approved by:

  
Chair, Board of Examiners

  
Dean, Graduate School

6-9-03  
Date

UMI Number: EP38959

All rights reserved

INFORMATION TO ALL USERS

The quality of this reproduction is dependent upon the quality of the copy submitted.

In the unlikely event that the author did not send a complete manuscript and there are missing pages, these will be noted. Also, if material had to be removed, a note will indicate the deletion.



UMI EP38959

Published by ProQuest LLC (2013). Copyright in the Dissertation held by the Author.

Microform Edition © ProQuest LLC.

All rights reserved. This work is protected against unauthorized copying under Title 17, United States Code



ProQuest LLC.  
789 East Eisenhower Parkway  
P.O. Box 1346  
Ann Arbor, MI 48106 - 1346

## Imaging the Shallow Subsurface using Ground Penetrating Radar at the Nyack Floodplain, Montana

Director: Dr. Steven Sheriff



The Nyack floodplain of the Middle Fork of the Flathead River is an intermontane floodplain in northwest Montana. It is the location of interdisciplinary research that focuses on the dynamic relationships between physical and biological processes that link flux and retention of materials to evolution of the fluvial landscape. Paleochannels are hypothesized zones of preferential flow that serve as injection and drain points for the aquifer. Furthermore, these paleochannels are localities of diverse above and below ground food webs that facilitate biogeochemical cycling.

To determine the presence of paleochannels, image shallow subsurface stratigraphy, and detect the water table of the Nyack floodplain, I collected twenty kilometers of data using high-frequency ground-penetrating radar (GPR). I applied standard post-processing procedures to the raw GPR data to improve visualization of the shallow subsurface.

Post-processed radargrams consisted of chaotic, discontinuous reflection patterns mixed with zones of absorption. I identified four locations within the Nyack floodplain where trough-shaped reflectors, indicative of paleochannels, are present. These trough-shaped reflectors are evident in one percent of the data collected. In addition, multiple diffraction hyperbolae are located throughout the floodplain at depths between three and twelve meters.

Imaged paleochannels are present underneath three swales at Nyack. However, the longitudinal extent of a swale does not correlate with the longitudinal extent of the associated paleochannel. Furthermore, there is no connectivity between the imaged paleochannels or with the Middle Fork of the Flathead River.

Diffraction hyperbolae are due to boulders deposited before the imaged paleochannels. These boulders are most likely the result of glacial deposition or fluvial lag deposits. The depths of the boulders show increase in depth as one traverses from the northeast to the southwest across the floodplain. This indicates that faulting in the area has downdropped the southwest side deeper than the northeast side of the floodplain.

## **Acknowledgements**

Thank you to Steve Sheriff for your wisdom, insight, guidance, patience, and enthusiasm. Also, thank you to my committee members Bill Woessner and Mark Lorang for their guidance, time, and effort.

This research supported through a National Science Foundation grant entitled Biocomplexity: Controls on Emergent Properties of River Floodplains.

Thank you to the Dalimata family for granting access to their property.

Thank you to everyone who helped me collect GPR transects, at Nyack and points elsewhere, including Adam Johnson, Brian Boer, Tony Berthelote, Nate Harrison, Michael Hoffman, and Noel Phillips.

Thank you to Brian Collins for your time, expertise and effort in creating works of wonder with GIS.

Thank you to Marc Hendrix for your time and effort in analyzing radargrams.

Thank you to Erik Katvala and Rebecca Kunz for your friendship and willingness to be distracted at any given time.

Thank you to Loreene Skeel and Christine Foster for helping me navigate through the land of forms.

Thanks to my family for their support and encouraging words. This is for you.

Thank you to Becky Vorhes, the future Mrs. Becky Hawkins (August 17, 2003). Your presence in my life is the greatest blessing I could ever receive. Thank you for being you, princess.

## **Table of Contents**

<b>Section</b>	<b>Page</b>
Abstract	ii
Acknowledgements	iii
Table of Contents	iv
List of Figures	vi
1. Introduction	1
2. Experimental Design	6
3. Data Acquisition	11
4. Post-Processing	13
5. Results	19
6. Interpretation	25
6.1. Site 1	27
6.2. Site 2	32
6.3. Site 3	35
6.4. Site 4	38
6.5 Channel Form	39
6.6 Diffraction Hyperbolae	41
7. Conclusion	43
References	46
Appendix A: GPS Coordinates of Transect Start and End Points	49
Appendix B: Representative Radargrams of the Nyack Floodplain	53
Appendix C: Polson, MT Gravel Pit	90



**Section**

**Page**

Appendix D: RAMAC GPR Protocol Guide

92

## List of Figures

<b>Figure</b>	<b>Page</b>
1. Nyack floodplain, northwestern Montana	3
2. GPR wave transmission and reflection	6
3. Radargram generated by transect in Figure 2	6
4. GPR survey sections	10
5. GPR transects acquired	12
6. Progression of radargram from raw data to post-processed	15
7. Comparison of Groundvision and REFLEX post-processed data	16
8. Pre- and post-statics correction for transect hf30	18
9. Determination of value for velocity squared	20
10. Two representative transects that imaged the water table	21
11. Representative transect showing diffraction hyperbolae	23
12. Representative transect of the Nyack floodplain	24
13. Example of trough-shaped reflector	25
14. Sites of Interest	26
15. Site 1 detail	28
16. Site 1 radargrams	29
17. Fence diagram for Site 1	30
18. 3-D channel surface for Site 1	31
19. Site 2 detail	33
20. Site 2 radargrams	34
21. Site 3 detail	35

<b>Figure</b>	<b>Page</b>
22. Site 3 radargrams	37
23. Site 4 detail	38
24. Site 4 radargram	39
25. Distribution of diffraction hyperbolae	42
26. Boulder frequency with depth	43

## **1. Introduction**

In recent years, multidisciplinary research has begun to focus on the interaction between groundwater and surface water in intermontane floodplains as well as the associated biodiversity of such systems. Stanford et al. (1994) note that complex groundwater food webs and riparian plant assemblages are due to interactions between river inflow and aquifer discharge. Stanford & Ward (1993) hypothesize that the convergence of surface and groundwater in alluvial intermontane aquifers is a primary determinant of biodiversity and bioproduction in the floodplain. One aspect of this research has been to determine the role, if any, that preferential flow zones may have in the dynamics of intermontane floodplains. Huggenberger et al. (1998), hypothesize that zones of preferential flow through highly permeable gravels allow for rapid exchange between surface and groundwater. Stanford and Ward (1993) and Poole et al. (2002) theorize that these zones of preferential flow are in the form of paleochannels.

Paleochannels are preserved cobble-boulder beds of previous river channels that fill with an upwardly fining sequence after avulsion (Stanford et al. 1994). Furthermore, these paleochannels serve as injection and drain points for the exchange of surface and groundwater. With respect to floodplain biodiversity, previous research (Stanford and Ward, 1988; Stanford et al. 1994, Ward et al. 1994) indicates that invertebrates in the food webs of the floodplain are more abundant in paleochannels than in other parts of the sedimentary matrix that comprise the floodplain aquifer.

Current research at the Nyack floodplain, an intermontane floodplain in northwestern Montana, focuses on dynamic interactions between physical and biological processes that link flux and retention of water, heat, and materials (particularly biota, sediment, and nutrients) to changes in the fluvial landscape. The Nyack floodplain is a gravel dominated floodplain of the Middle Fork of the Flathead River located near West Glacier, Montana (Figure 1), approximately three km wide by eight km long. The floodplain consists of a matrix of unconsolidated fine-grained media, such as silts and clays, intermixed with coarse-grained deposits, such as sands, gravels, and cobbles (Poole et al 1997; Johnson, 2003). These materials placed by fluvial and glacial processes, sit in a glacially modified, fault-bounded valley. Preferential flow zones or paleochannels within the floodplain play an important role in guiding current research because they probably facilitate the existence of diverse above and below ground food webs. These food webs, in turn, likely drive the biogeochemical cycling of carbon, nitrogen, and phosphorus within the floodplain. Previous work at this locality by Stanford and Ward (1993), Stanford et al. (1994), Pool et al. (1997,2002) hypothesize that paleochannels are usually associated with surface depressions, also referred to as swales, and definable using aerial photographs. However, none of these studies focused on the extent to which paleochannels occur within the Nyack floodplain.

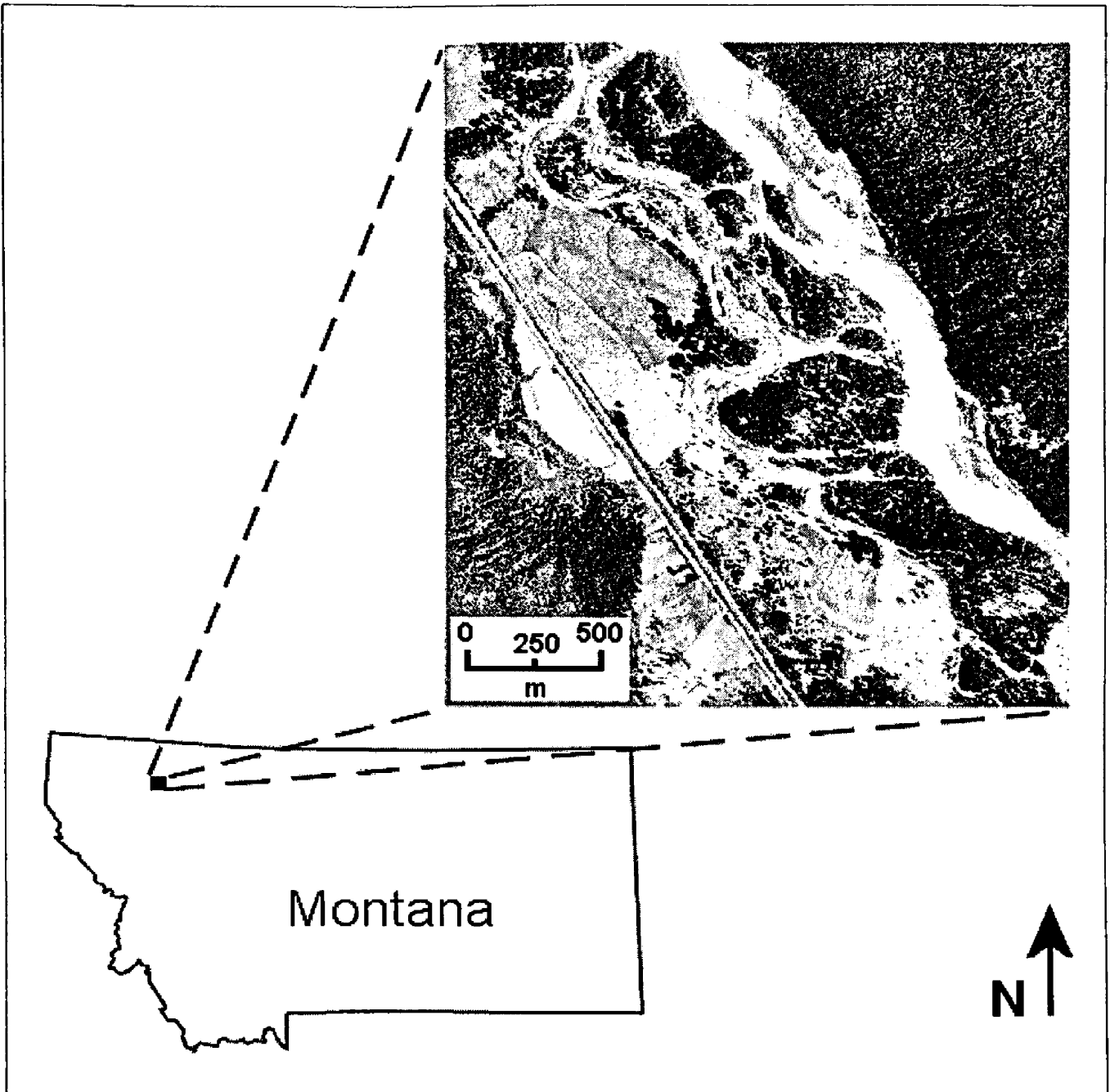


**Figure 1. Nyack floodplain, northwest Montana  
(Modified from USGS Nyack, MT Aerial Photograph)**

Various studies show that ground penetrating radar is an effective geophysical technique in many different geological environments. Dominic et al. (1991) successfully used ground penetrating radar to delineate shallow stratigraphy and detect the sediment-bedrock boundary at depths ranging from one and a half to four meters at three localities in Southwestern Ohio (a glaciated upland, a sand and gravel quarry, and a dam comprised of hydraulic-fill materials) and one site in the Bahamas (a beach/strand plain system). Jol et al. (1996) imaged coastal barrier stratigraphy, at sites on the Atlantic, Gulf, and Pacific coasts, up to depths of twelve meters. Bridge et al. (1998) used ground penetrating radar to examine large-scale structure of channel deposits of a braided, low-sinuosity river in Nebraska. Thus, ground penetrating radar is effective in a wide variety of subsurface media. Previous work shows that some of the best results occur in unconsolidated gravels and sands that have minimal clay and water content in their pore spaces (Beres and Haeni, 1991; van Overmeeren, 1998). These results suggest GPR would be useful in interpreting the subsurface character of a river floodplain.

Intermontane river floodplains, such as those that one would find associated with the Rocky Mountains of northwestern Montana, and other similar localities, are comprised of reworked deposits by bed load dominated streams. Characteristics of these streams include a shifting network of channels, deposition of a variety of gravel bedforms, and the abandonment of channels (Miall, 1996). van Overmeeren (1998) used a 200 MHz GPR system to accurately image two paleochannels, from a braided river system, exposed in a gravel pit. Both paleochannels exhibited trough-shaped reflection patterns in the radargram. The reflection patterns lined up with the position of the respective

paleochannels exposed in outcrop. A joint study of gravel-sand braided systems by Vandenberghe and van Overmehren (1999) tested the ability of GPR to image well-defined channels in the Rhine Valley of the Netherlands. At one locality, a gravel pit, GPR produced a trough-shaped reflection indicating the presence of a paleochannel. The position of the trough-shaped reflection correlated with the position of an observed paleochannel in the pit face. As another example, Poole et al. (1997) effectively used ground penetrating radar to detect features with the geometry of paleochannels on two reaches of gravel dominated braided floodplains of the Flathead River, one on the mainstem and one the Middle Fork.

A ground penetrating radar system, generally speaking, transmits electromagnetic waves of a given frequency into the subsurface. The waves propagate through the subsurface and reflect back electromagnetic waves when the transmitted wave encounters subsurface materials that have differing electromagnetic properties (Figure 2). Variations in these properties are usually associated with changes in the volumetric water content of a given material (Davis and Annan, 1989). The receiver antenna collects reflected electromagnetic waves and transmits the information to a computer via the GPR control unit. The transmitted information, or trace, combined with other traces creates a radargram, which displays an image of the subsurface geometry, in time-distance space (Figure 3).



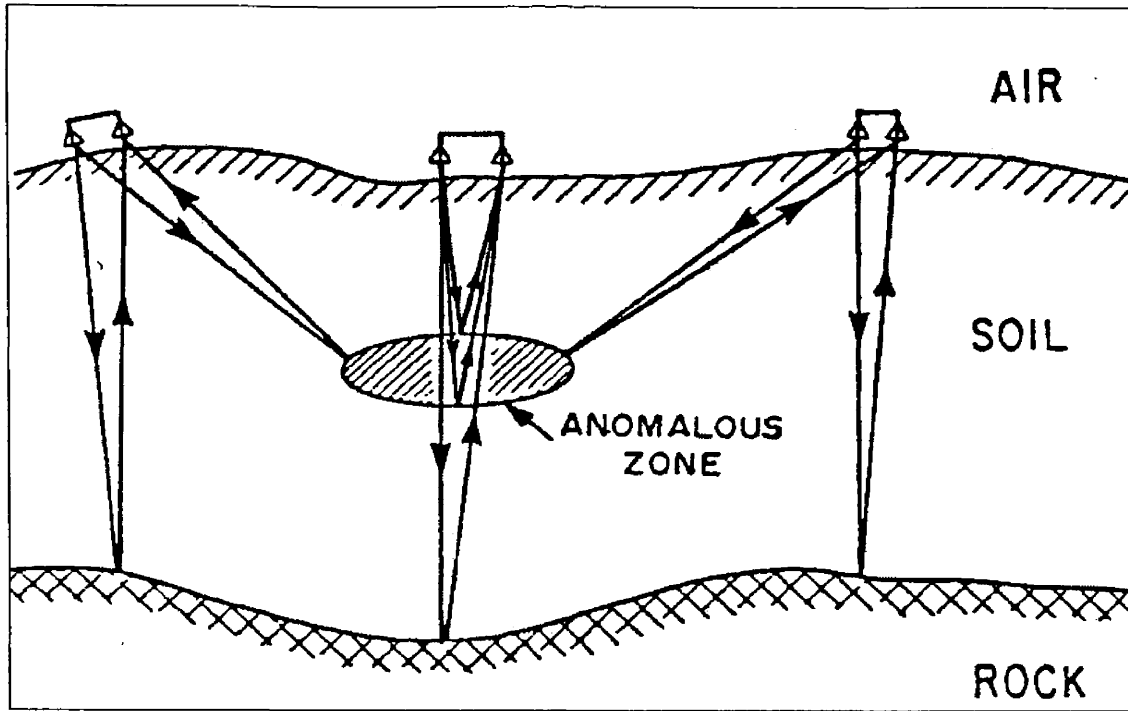


Figure 2. Wave transmission and reflection (Modified from Davis and Annan, 1989)

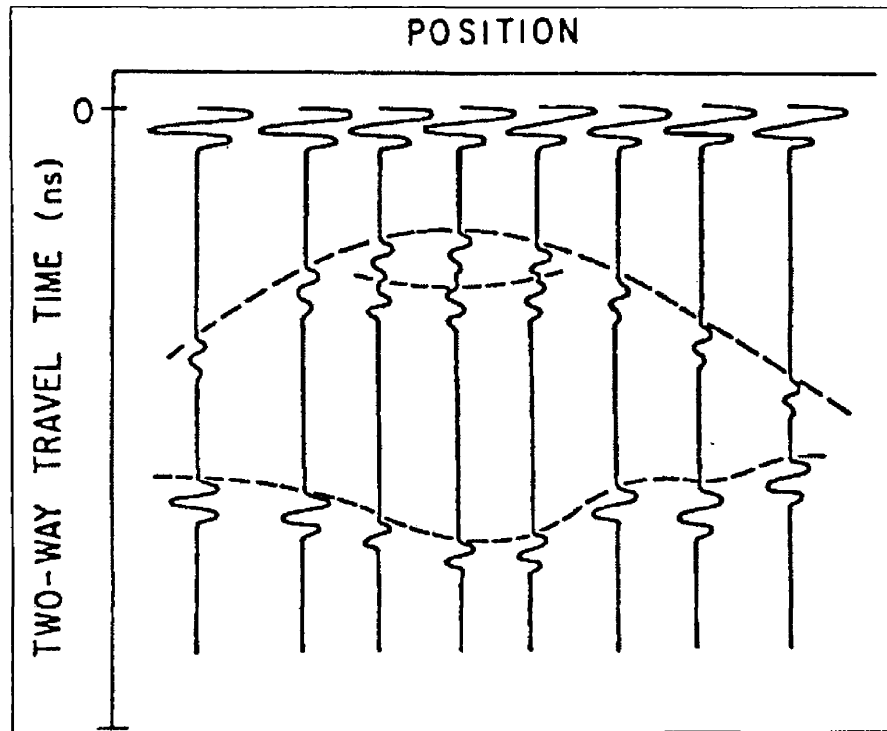


Figure 3. Radargram generated by transect in Figure 1 (Modified from Davis and Annan, 1989)

This work assesses if ground penetrating radar can be applied to identify the presence, frequency, and extent of paleochannels within a gravel dominated floodplain, and if successful to infer the role that they play in influencing groundwater and surface water exchange within the floodplain. Theoretically, ground penetrating radar is an ideal tool to image such a subsurface. Unlike other methods, it provides assessment of sediment architecture up to depths of 20m with little to no disturbance of floodplain deposits (Huggenberger et al. 1998). The objectives of this study are 1) to use ground penetrating radar to locate paleochannels within the floodplain, 2) determine their longitudinal and lateral extent and depth, 3) determine their relationship to surface swales, 4) locate the position of the water table, 5) image shallow subsurface stratigraphy, and 6) infer if direct linkage between the river and paleochannels are likely.

## **2. Experimental Design**

To accomplish the objectives of this study, I used a coarse survey of the floodplain with transect to transect spacing equal to, approximately, thirty meters to trace out large-scale features. For the survey, the floodplain was broken into three sections, with one containing a small subset (Figure 4). The division of the floodplain into multiple sections is due to a) man-made parameters such as fence lines that interfere with data collection, b) natural parameters such as creeks, and c) an ongoing hydrogeological study. The Upstream Pasture area (Figure 4, green shade) is constrained by fence on all sides, which separates it from the Hayfield (Figure 4, yellow shade). The third survey section, predominantly located in forest cover (Figure 4, blue shade), takes its name from

Beaver Creek, a side-channel of the Middle Fork that separates it from the two aforementioned sections. The last survey section, Wally Creek (Figure 4, purple shade) is the location of a hydrogeological investigation of a hypothesized preferential flow zone (Johnson, 2003).

The next step in the design of the experiment is the selection of the antenna frequency. There are two key facts that control this selection, the desired resolution and the depth of penetration. Unfortunately, there is an inverse relationship between these two factors; therefore, one must decide if it is more important to have better resolution of the subsurface or to have deeper penetration.

Antenna resolution is ideally equal to one-quarter the wavelength (Beres and Haeni, 1991). For low frequency antennae (25-50 MHz), the resolution is approximately five meters whereas for high frequency antennae (500-1000 MHz) the resolution is about one-tenth of a meter. Conversely, penetration depth for low frequency antennae (25-50 MHz) is between 50 and 60 meters while high frequency antennae (500-1000 MHz) can image only the first few meters of the subsurface (Smith and Jol, 1995). However, signal absorption can negatively impact resolution and depth of penetration. Signal absorption is due to waves encountering geologic materials that are highly conductive, such as clays and clay-rich soils (Beres and Haeni, 1991). In a gravel-dominated floodplain, such as Nyack, there is probably a minimal amount of clay present.

For this survey, I selected 200 and 100 MHz antennae to maintain a balance between resolution and penetration depth. Resolutions of these antennae, theoretically, are on the order of four tenths to three-quarters meters, respectively. Depth of penetration in ideal settings for these antennae is between 18 meters for 200 MHz and 23 meters for 100 MHz (Smith and Jol, 1995). Furthermore, given the present location of the channel bottom, approximately six meters below the surface of much of the floodplain indicates that subsurface geomorphic features are likely located within the first six meters of the subsurface. Therefore, 200 and 100 MHz antennae, theoretically, are ideal for studies in such a locality.

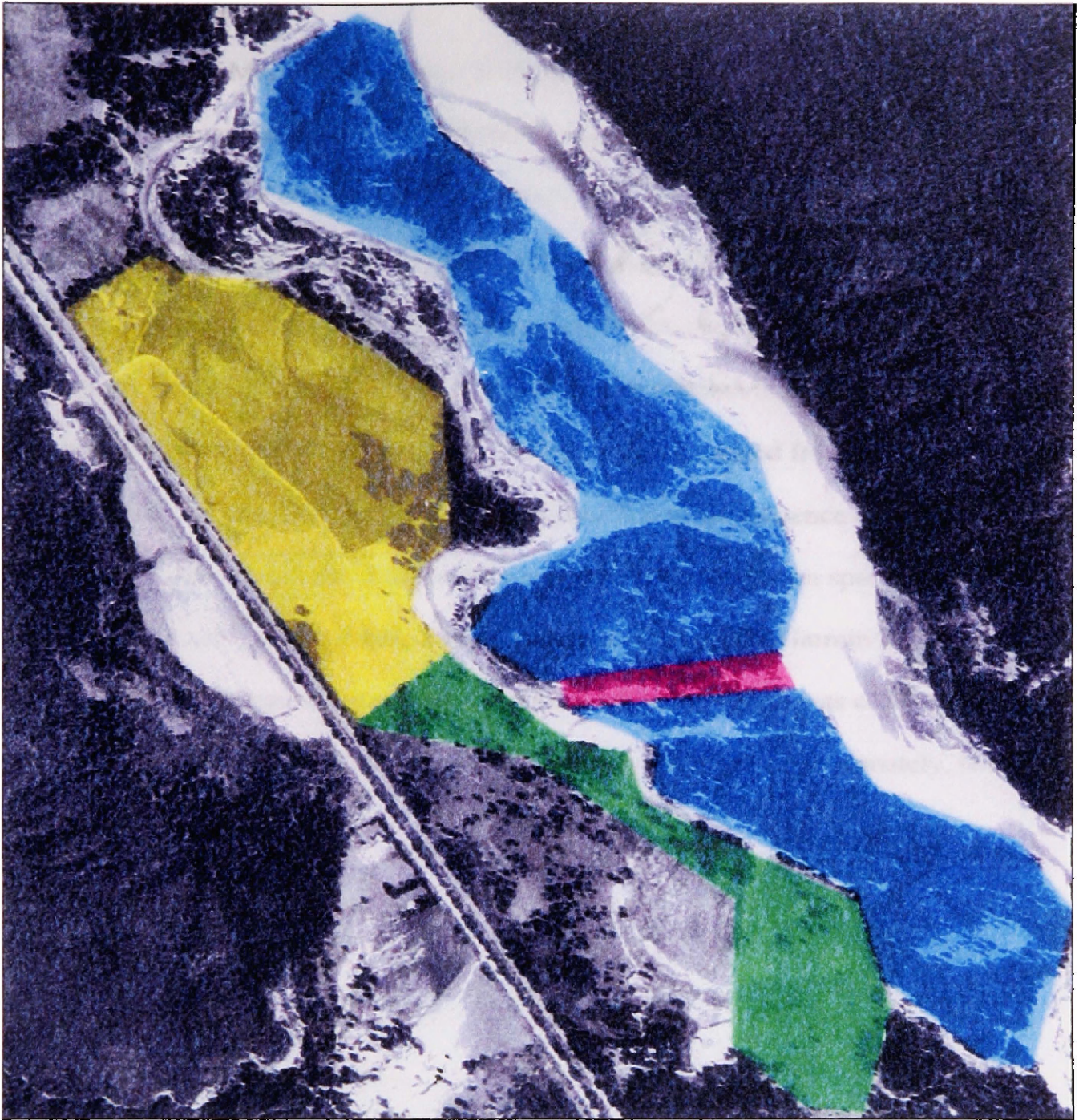


**Figure 4. GPR survey sections. Green: Upstream Pasture, Yellow: Hayfield, Blue: Beaver Creek, and Purple: Wally Creek subset of Beaver Creek.**

### **3. Data Acquisition**

This survey used a MALA Geoscience RAMAC GPR system with a CUII control unit and antenna frequencies of 100 and 200 MHz, set up in the common-offset mode with separation distances of one meter and one-half meter, for collection of data (Appendix A contains a protocol guide for the RAMAC GPR system). For any given transect, sampling took place every one-quarter to one-half meter, dependent on pace which was constant per single transect, but slightly variable from transect to transect. Pace values, determined by dividing transect length by collection time, ranged from eight-tenths to two meters per second. I collected data using pace due to the presence of brush, fences, and other obstacles that made it difficult to maintain an exact station spacing from transect to transect. Before acquisition of each transect, I used a Garmin handheld GPS system to obtain the transect start and end points, while the length was collected using a measuring tape and wheel (Appendix A). The survey acquired, approximately, twenty kilometers of transects (Figure 5).

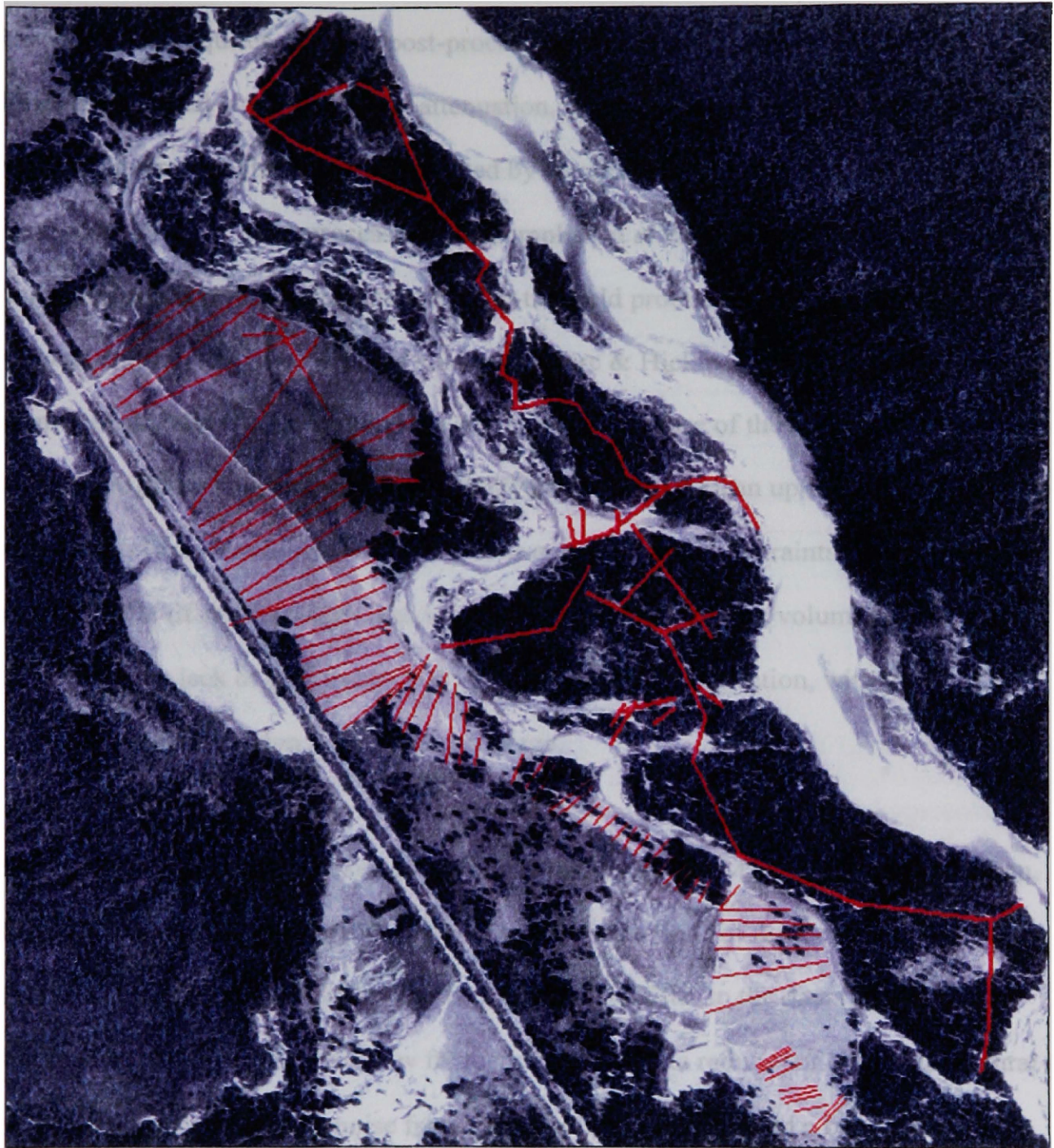


**Figure 5. GPR transects acquired.**

#### **4. Post-Processing**

Raw GPR data requires standard post-processing to overcome signal loss due to such things as spherical wave spreading, attenuation, scattering, heat loss, and absorption as well as to overcome signal noise generated by electronics and ground coupling effects (Reynolds, 1997). Post-processing is accomplished at varying scales of detail. In consulting applications, quick and simple in-the-field processing is quite common (Isbell, personal comm.). In more detailed studies (Leclerc & Hickin, 1997; Olhoeft, 2000; Lesmes et al. 2002) processing is long and involved because of the aim to refine a particular GPR technique for a given locality and to further clean up the data from a site where collection was hampered by natural or anthropogenic constraints. For this study I used a middle-of-the-road approach to post-processing, due to the volume of data collected and a lack of constraints that interfered with data collection, with the MALA Geoscience Groundvision 3.0 software package.

Figure 6A shows an example of raw data collected by the RAMAC GPR system. Often, there is a constant offset in the raw data due to imperfections of the electronics.

Therefore, my first step in processing is to apply a DC filter to the data (Figure 6B).

Removal of unwanted high and low frequencies in the data reduces or eliminates natural background noise as well as noise from electronics. Thus, I applied a band pass filter to the previously DC filtered data (Figure 6C). Electromagnetic waves spread out from their source and proportionally lose energy with increasing distance from the input location (Reynolds, 1997). Fine-grained sediments, such as clay and silt-sized particulate that is likely to fill some of the pore spaces between the coarser deposits can attenuate the



signal (Reynolds, 1997). To compensate for these effects, I passed the data through a time-varying gain filter to boost the strength of the signal (Figure 6D). Often in electronics, there is ringing in the data. This ringing is known as “wow” and is due to distortion in the data caused by speed variation between the antenna frequency and the performance of the laptop that transmits instructions and records the data. The final filter applied to the data, subtract mean trace, removes this ringing effect (Figure 6E).

Upon completion of post-processing with Groundvision, I tested the validity of this approach using the post-processing software REFLEX on a representative transect, hf30. For this particular transect, I removed DC shift from the data, applied an automatic gain control (AGC), and removed the average trace from the data. A comparison of the Groundvision and REFLEX processed data (Figure 7), shows a minor amount of increased detail from the REFLEX processed data. Most notably, REFLEX removed more of the ringing from the data and improved recognition of diffraction hyperbolae than did the Groundvision software. In general, when I used both packages on a number of profiles, Groundvision was more than adequate.

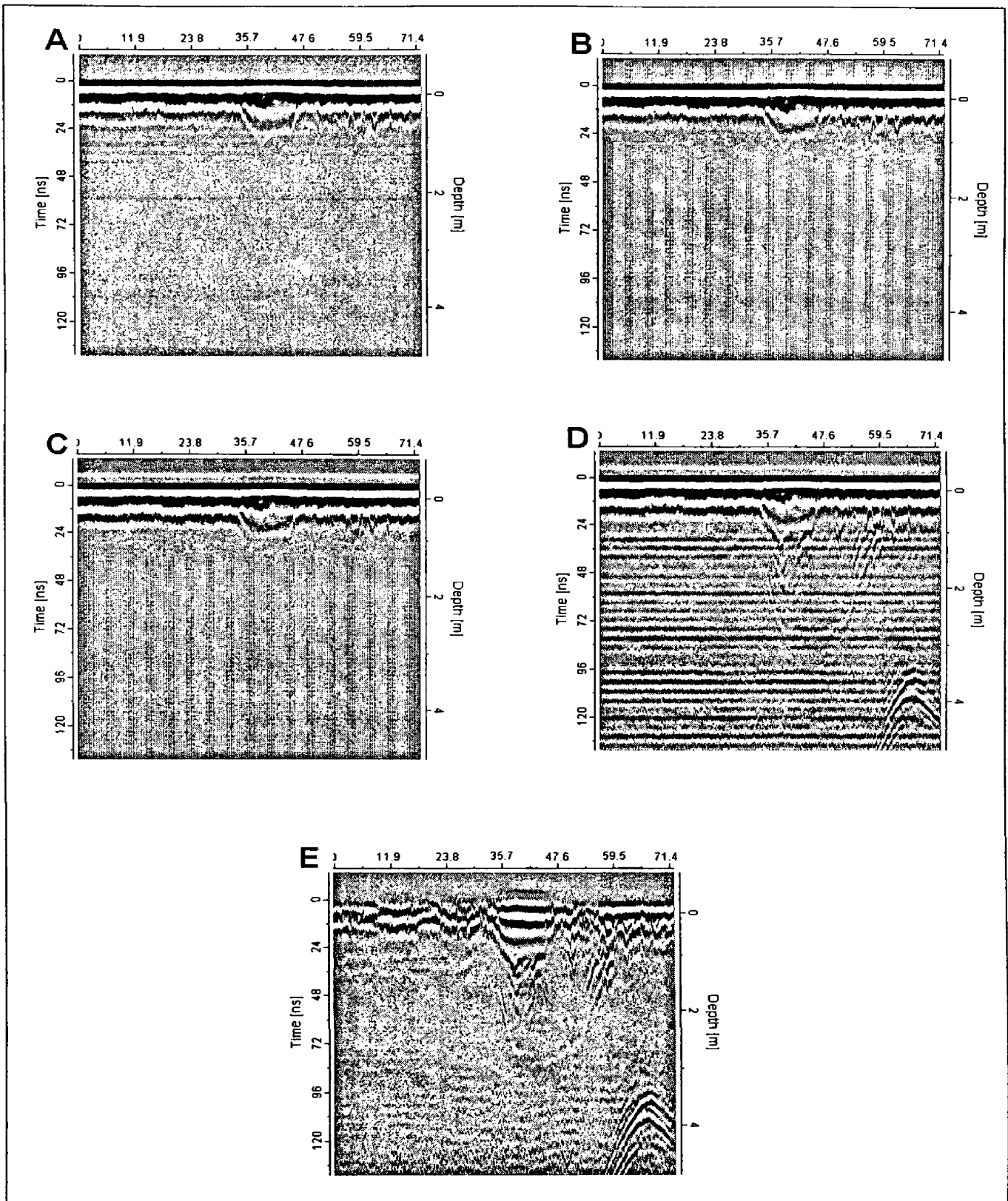


**Figure 6. Progression of radargram (15x vertical exaggeration) from raw data (A) to DC filtered (B) to band pass filtered (C) to time-gain filtered (D) to post-processed (E).**

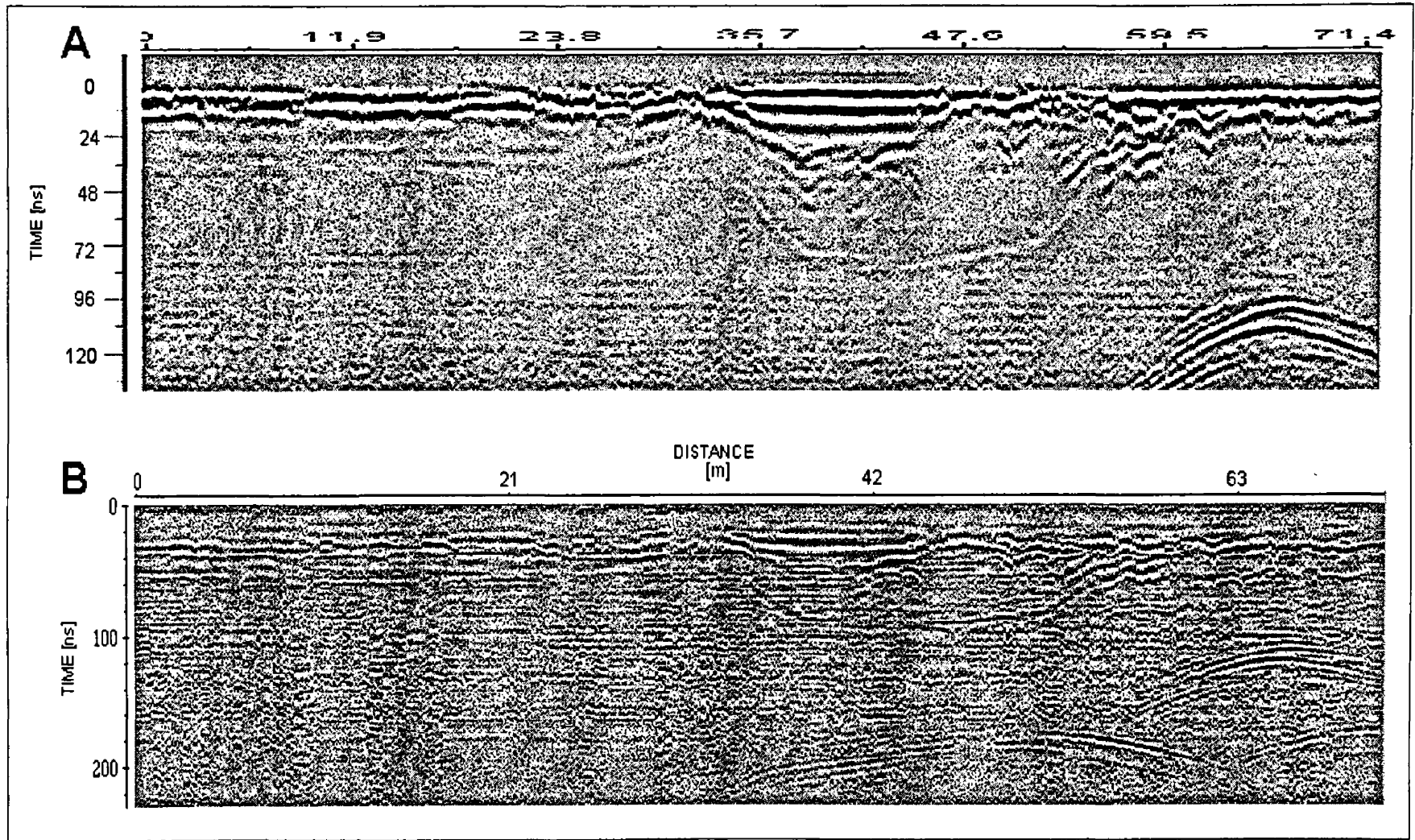
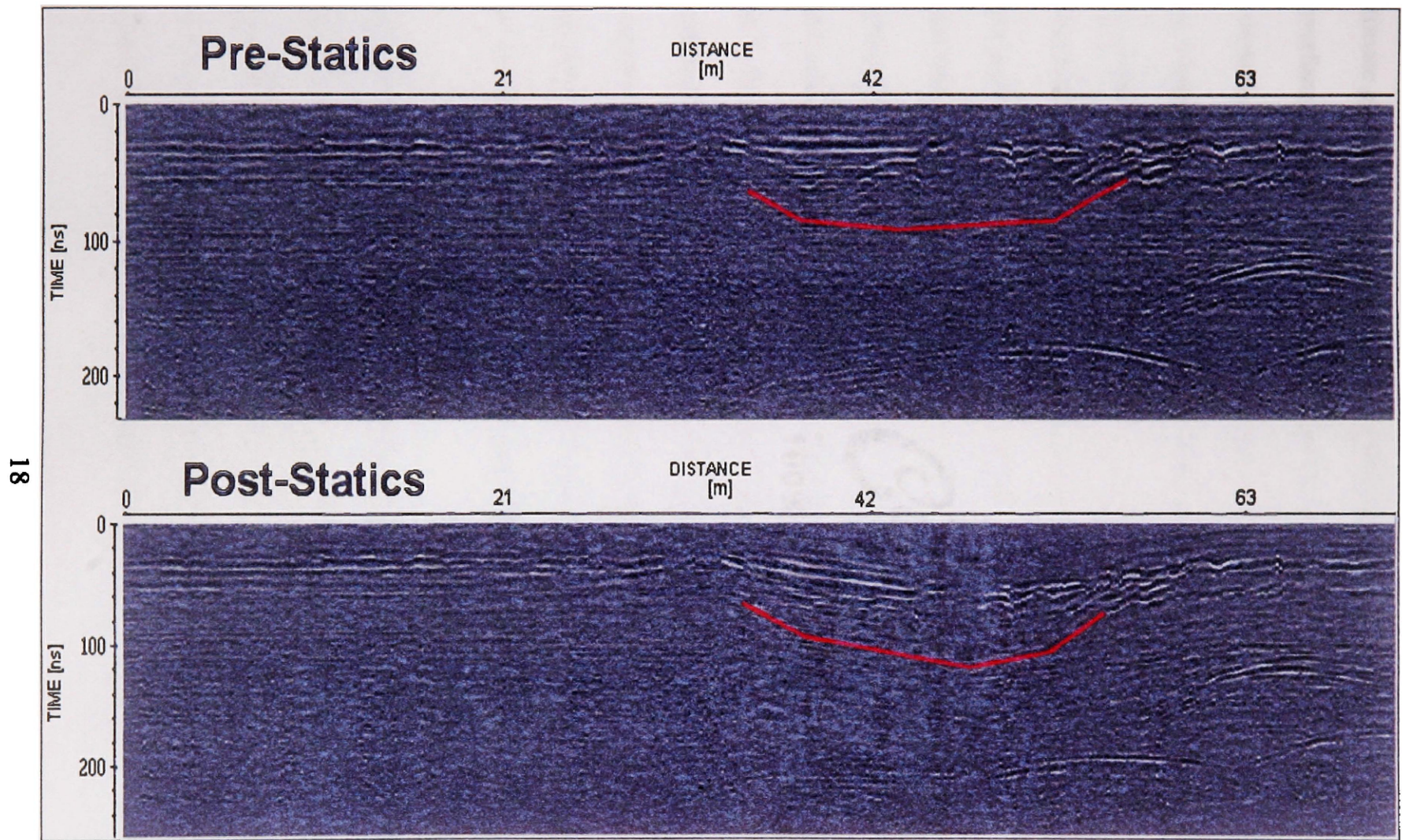


Figure 7. Comparison of Groundvision (A) and REFLEX post-processed data (B).

There are some additional processing steps that are often applied to raw GPR data. Where topography is variable, investigators apply a statics correction to the data to normalize the gathered data to a constant datum. This is because if one travels into a depression or swale, the two-way travel time between a horizontal reflector and the GPR system is less than if when the system is recording the two-way travel time when not within the depression. The variation in two-way travel times from topography results in a reflector that is no longer horizontal, but rather mirrors the surface topography. Therefore, a radargram of a trough-shaped reflector located within a swale will exhibit minimal curvature. For this survey, a statics correction was applied to a representative transect that traversed the largest topographic change, a two-meter deep swale, of the study area. A before and after view of the statics correction applied to transect hf30 is shown in Figure 8. The most notable aspect of this correction is the increased curvature of the trough-shaped paleochannel reflector (highlighted in red) after the application of the statics correction. The pre-statics depth of the bottom of the trough-shaped reflector was 85ns. Post-statics the depth is 120ns, yielding a forty-one percent change in depth. The depth of the left end of the trough-shaped reflector pre- and post-statics is 60ns and 55ns, respectively. This yields an eight percent change in the position of the left end of the reflector. For the right end, the depths are 40ns and 75ns, pre- and post-statics, yielding a percent change in position of eighty-seven percent. No other locality in this survey has a large topographic expression comparable to the representative line and the large expression does not prevent this survey from imaging a paleochannel that lies beneath.



**Figure 8. Pre- and post-statics correction of transect hf30. Trough-shaped reflector of interest denoted by red line. Application of statics restores curvature of trough-shaped reflector.**

## 5. Results

The ultimate goal of a ground penetrating radar survey is to provide a 2D radar image of the subsurface in depth versus distance. However, raw GPR data is in the form of time versus distance. To convert the radar reflection times to depth, one needs the subsurface velocity. I used the common midpoint method (CMP) to determine the subsurface velocity of the Nyack floodplain. The CMP method involves moving the transmitter and receiver antennae away from each other in incremental steps. By doing this, a predetermined midpoint stays between the two antennae at a fixed location. A radargram produced from such an experiment will consist of a linear air reflection, due to the electromagnetic wave traveling through the air from the transmitter to the receiver, a linear ground reflection, due to the wave traveling across the ground surface from one antenna to the other, and a parabolic shaped reflector that represents the subsurface. From this parabolic reflector, select time values and their associated separation distance values. Then, square the time-distance pairs to create a linear plot of distance squared as a function of time squared. The slope of the trend line for this plot will be equal to the value of the square of the velocity (Beres and Haeni, 1991).

After obtaining  $v^2$  from the slope (Figure 9), the square root of that value yields the subsurface velocity. The calculated velocity for the area, from CMP data, is seventy meters per microsecond with a standard error of +/- 0.84 meters per microsecond. This value is comparable to published values for saturated sand, sixty meters per microsecond (Davis and Annan, 1989), and gravel, eighty meters per microsecond (Smith and Jol,

1997). In all subsequent analysis and images, the depth scale is based on this calculated velocity.

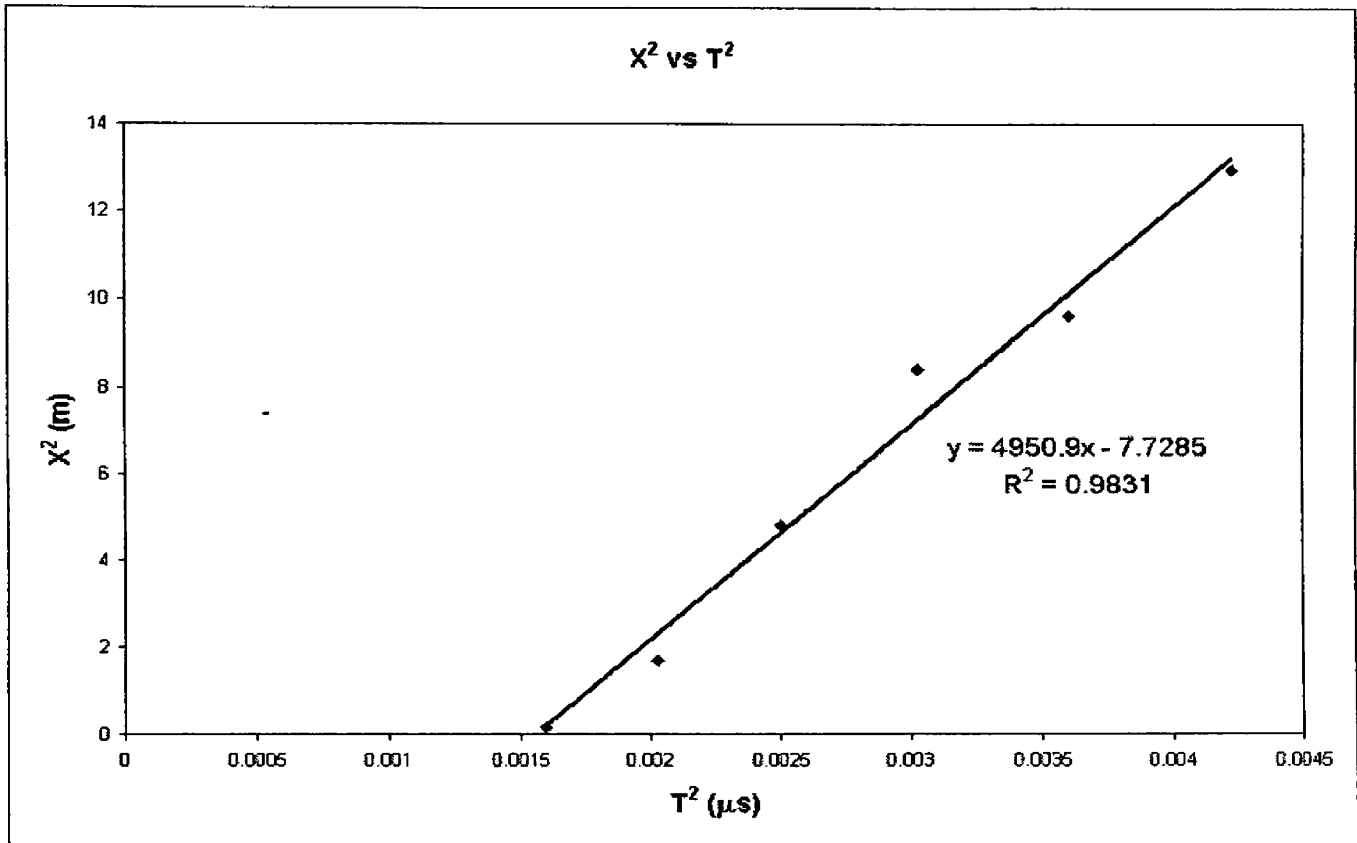
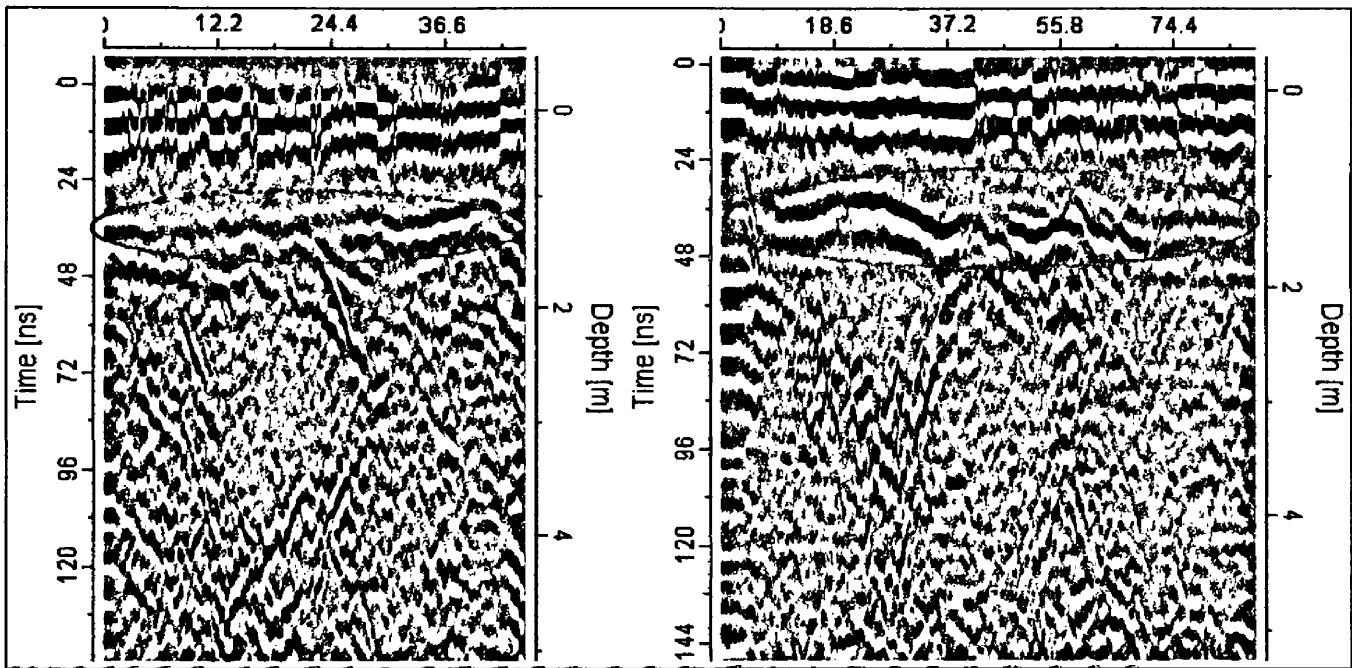


Figure 9. Plot to distance squared versus velocity squared to obtain a value for velocity squared. The resolved velocity obtained from this value is 70 meters per microsecond.

Detection of the water table, one of the goals of this survey, was not possible, with the exception of a few transects in the Beaver Creek area of the floodplain (Figure 10). The lack of detection of the water table is due to 1) the shallowness of the water table, less than one and a half meters, for much of the field season (Johnson, in prep.) and 2) the input pulse of the wave transmitted by the GPR system. Due to the electronic configuration of a GPR system, the input pulse is not a pure spike, but rather a damped

pulse that consists of, in general, a couple of small spikes surrounding the main input spike of the pulse. Due to this damped nature of the input pulse, it obscures the uppermost parts of the subsurface under most conditions. In the case of 200 and 100 MHz antennae, the input pulse, generally, obscures the upper one-half to one and a half meters of the subsurface, respectively. Therefore, the shallowness of the water table makes it nearly impossible to detect unless using an antenna frequency of 500 MHz or greater.



**Figure 10. Two transects from the Beaver Creek section of the floodplain, bc06 and bc39, that imaged the water table (circled in red).**

Common complications in GPR images are reflectors off boulders, tree roots and canopies, buried pipes, steel drums, etc. that produce hyperbolic features in radargrams. Previous work indicated that diffraction hyperbolae, at times, are associated with highly conductive above ground objects such as power lines (Bano et al. 2000) or subsurface



anthropogenic artifacts (Olhoeft, 2000). Due to the pristine nature of the Nyack floodplain, diffraction hyperbolae are not due to subsurface anthropogenic artifacts. In addition, diffraction hyperbolae recorded at Nyack were not adjacent to above ground features, natural or anthropogenic, that would cause such patterns. Furthermore, several transects near forest cover do not show diffraction hyperbolae. In the Missoula, MT area, a survey taken near a row of trees did not yield any diffraction hyperbolae with the unshielded antennae I deployed in my survey. Therefore, diffraction hyperbolae present in radargrams from transects near trees is most likely not due to the canopies or root balls of those trees. It is most likely that diffraction patterns detected at Nyack are due to large boulders (Figure 11).

Beres and Haeni (1991) as well as van Overmeeren (1998) show that for various sediment packages there are characteristic reflection patterns. For example, parallel reflection patterns are indicative of massively bedded silts or sands. A chaotic reflection configuration is discontinuous and non-layered (Beres and Haeni, 1991). Reflection patterns at Nyack are, generally, chaotic in nature (Figure 12; further representative transects are in Appendix B). In addition, Beres and Haeni (1991) compared reflection patterns to drill cores where subsurface stratigraphy was not evident in outcrop. They found that chaotic reflection patterns are indicative of interbedded sand and gravel. For comparison to the Nyack reflection patterns, I completed a survey at a sand and gravel pit, composed of exposed glaciated sediments, near Polson, MT. The survey yielded reflection patterns that are not indicative of layered stratigraphy, but rather interbedded sand and gravel (Appendix C). Another feature evident in Figure 12 that can be found in

radargrams from various transects are zones of absorption. Such zones are due to signal attenuation from very fine-grained sediments such as silts and clays (Beres and Haeni, 1991). These types of sediments have high values of conductivity, which causes the electromagnetic wave to attenuate as it propagates through these areas.

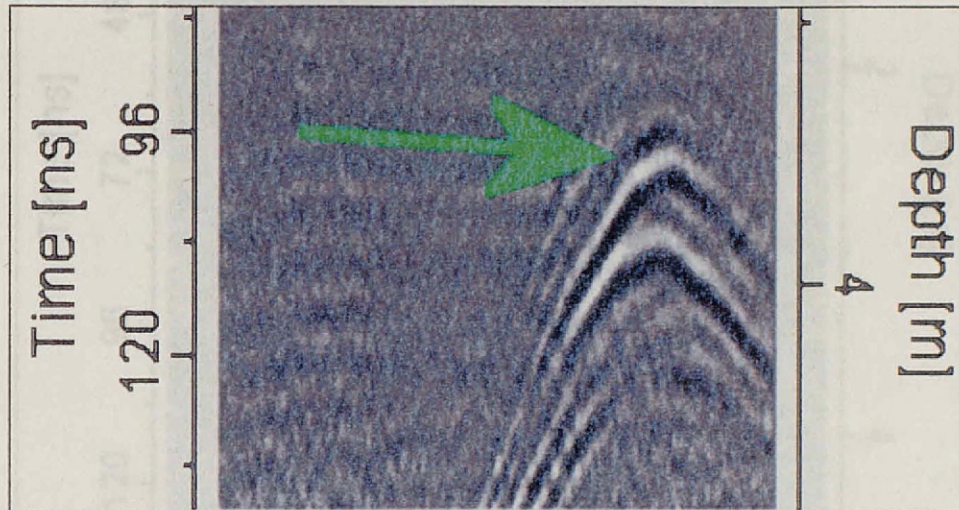
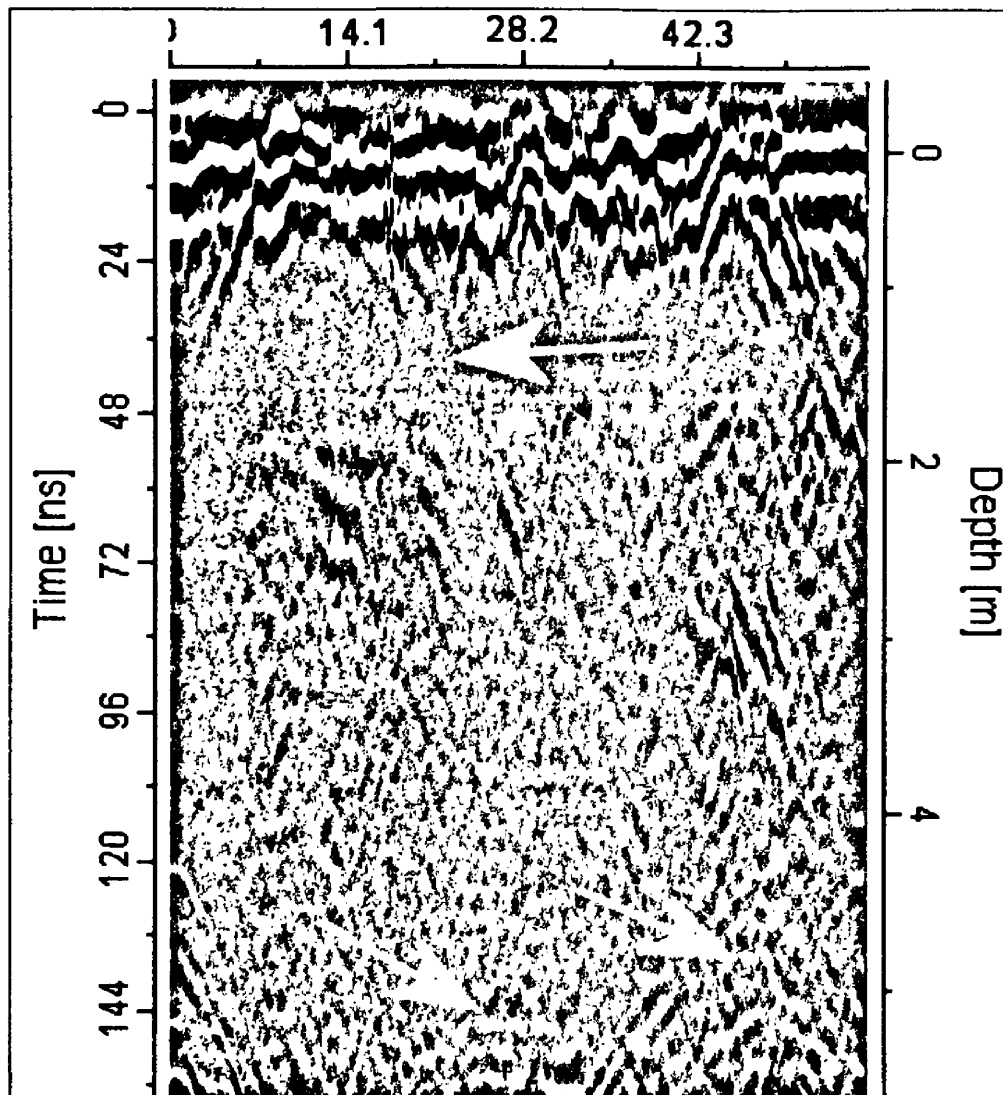


Figure 11. Representative example of diffraction hyperbolae (green arrow).

Figure 12. Representative transect, both with and without absorption, displaying discontinuous, non-layered (i.e. chaotic) reflections, a zone of absorption (white arrow), and diffraction hyperbolae (green arrows).

Trough shaped reflector patterns (Figure 13) are present in ten of the one hundred twenty transects collected. In some localities there is continuity of these patterns from transect to transect. However, there is no interconnection from one locality to another and there is no linkage between them and the Middle Park. Furthermore, transects collected parallel to the channel flow direction do not show evidence of trough shaped reflector patterns.



**Figure 12. Representative transect, bc05, (15x vertical exaggeration) displaying discontinuous, non-layered (i.e. chaotic) reflections, a zone of absorption (yellow arrow), and diffraction hyperbolae (green arrows).**

Trough shaped reflector patterns (Figure 13) are present in ten of the one hundred twenty transects collected. In some localities there is continuity of these patterns from transect to transect. However, there is no interconnection from one locality to another and there is no linkage between them and the Middle Fork. Furthermore, transects collected parallel to the channel flow direction do not show evidence of trough shaped reflector patterns.

The lack of interconnectedness of trough-shaped reflector patterns and discontinuity of chaotic patterns and zones of absorptions suggests a subsurface stratigraphy that is lacking in continuous identifiable layers at the scale of this survey.

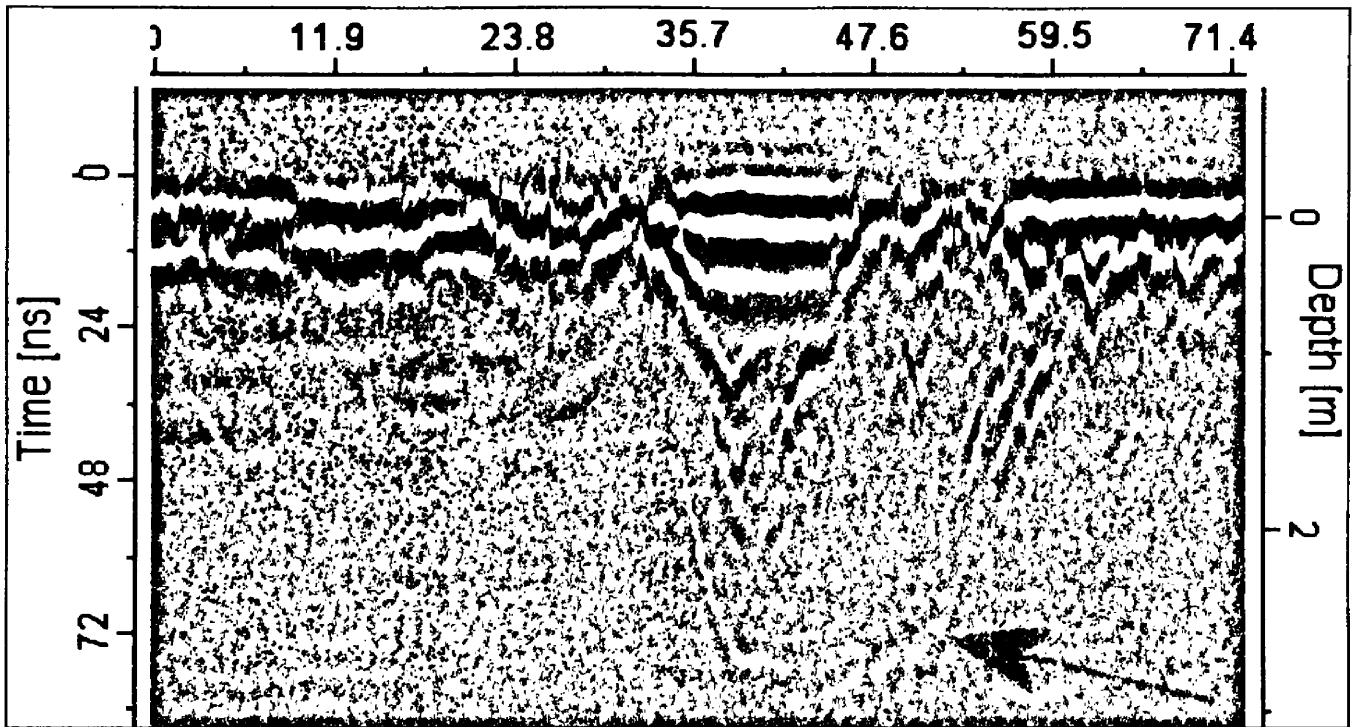


**Figure 13.** Example of a trough shaped reflector (denoted by red arrow) from transect hf30.

## **6. Interpretation**

There are four sites of interest (Figure 14) with respect to reflector patterns that indicate the existence of subsurface geomorphic features. Three of the sites are localities where several hundred meter long swales, possible indicators of paleochannels, are present on the floodplain. The fourth site is the location of a study by Johnson (2003) evaluating the hydrogeological evidence to support a hypothesized preferential flow zone.

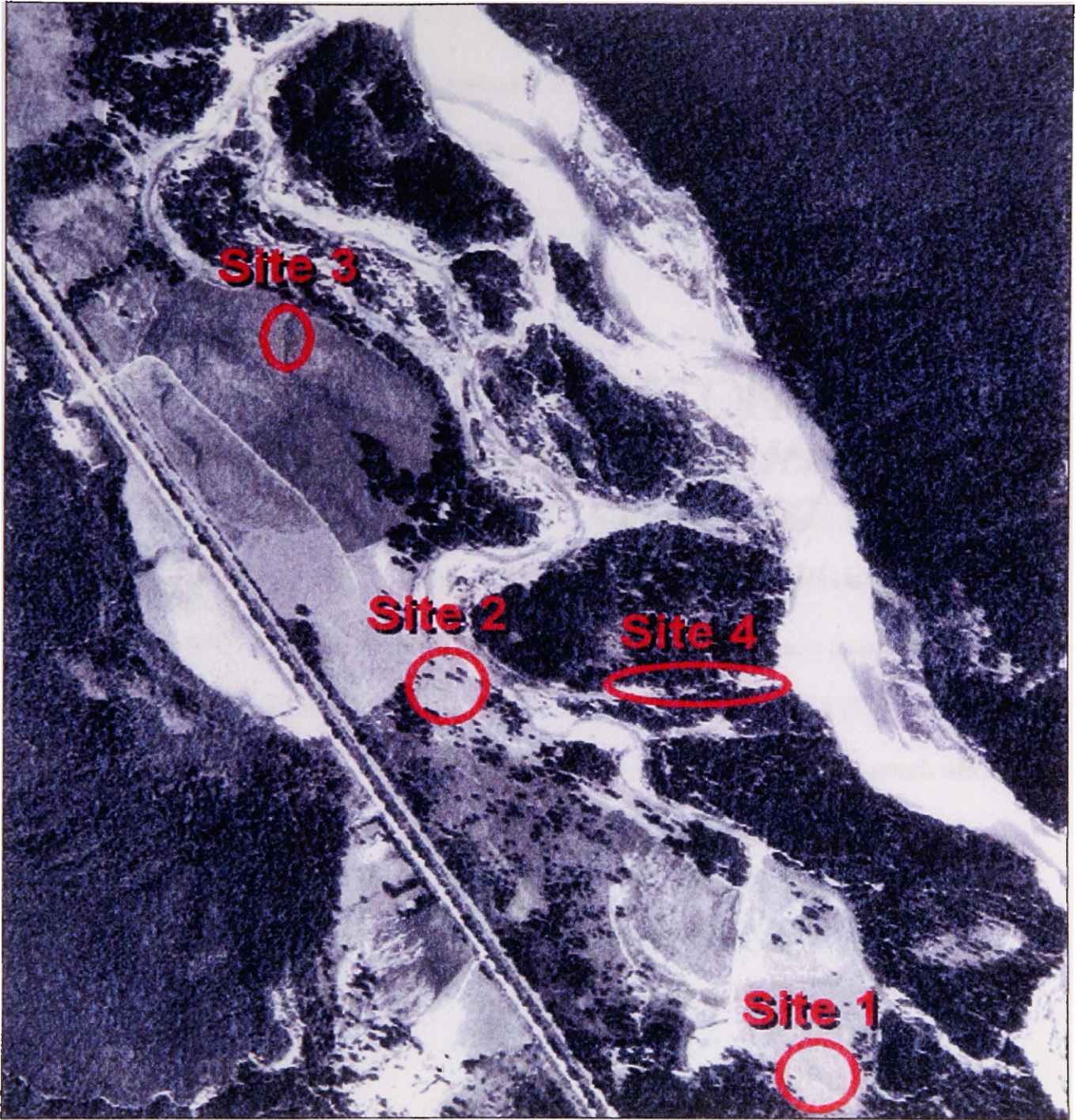


**Figure 14. Sites of interest with respect to paleochannels. Site 1: Upstream Pasture A, Site 2: Upstream Pasture B, Site 3: Hayfield, and Site 4: Wally Creek.**

## 6.1. Site 1

The first site (Figure 15), known as Upstream Pasture A, is a two hundred fifty meter long surface swale located in the southeastern end of the study area. A series of seven transects cross the swale with a rough line-to-line spacing of twenty meters. As evidenced in Figure 16, a trough shaped reflector, denoted by red arrows, develops at the south end and subsequently fades away to the north. Such a reflector clearly has the shape of a paleochannel. The imaged paleochannel has a width of approximately 27.5 meters and a depth of 1.95 meters. A fence diagram (Figure 17) of transects up03 to up07 and a 3-D representation of the channel surface (Figure 18) both show, at two different scales of vertical exaggeration, the evolution of the channel surface from transect to transect. Concurrent with the development of the trough-shaped paleochannel reflector is the development of an absorption zone above and below it (Figure 16, yellow arrows). These zones of absorption are likely due to the filling of the channel, after avulsion, with a fining upward sequence.

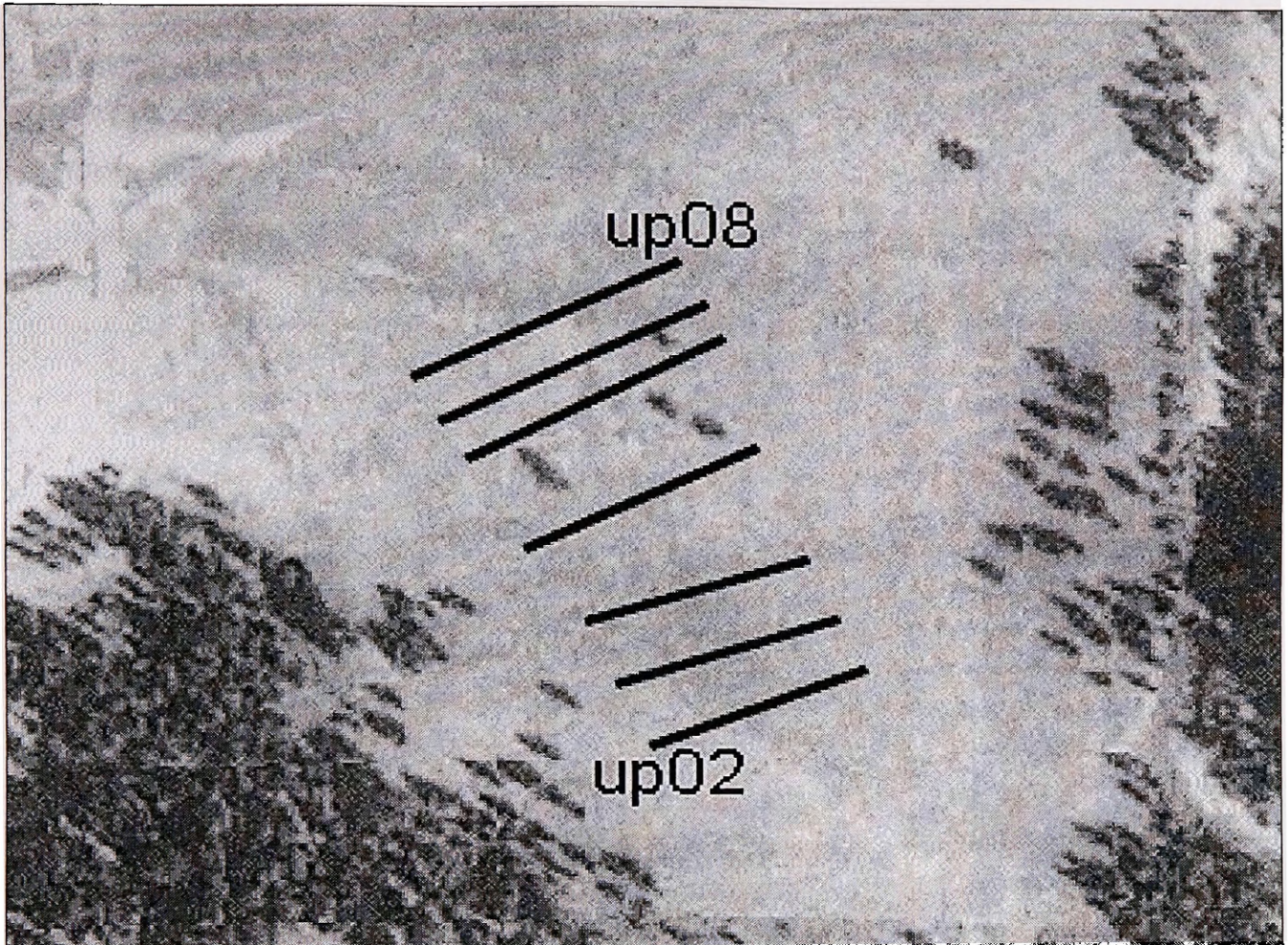


**Figure 15. Upstream Pasture A transects up02 through up08 (black lines). Total distance from up02 to up08 is approximately 140 meters.**

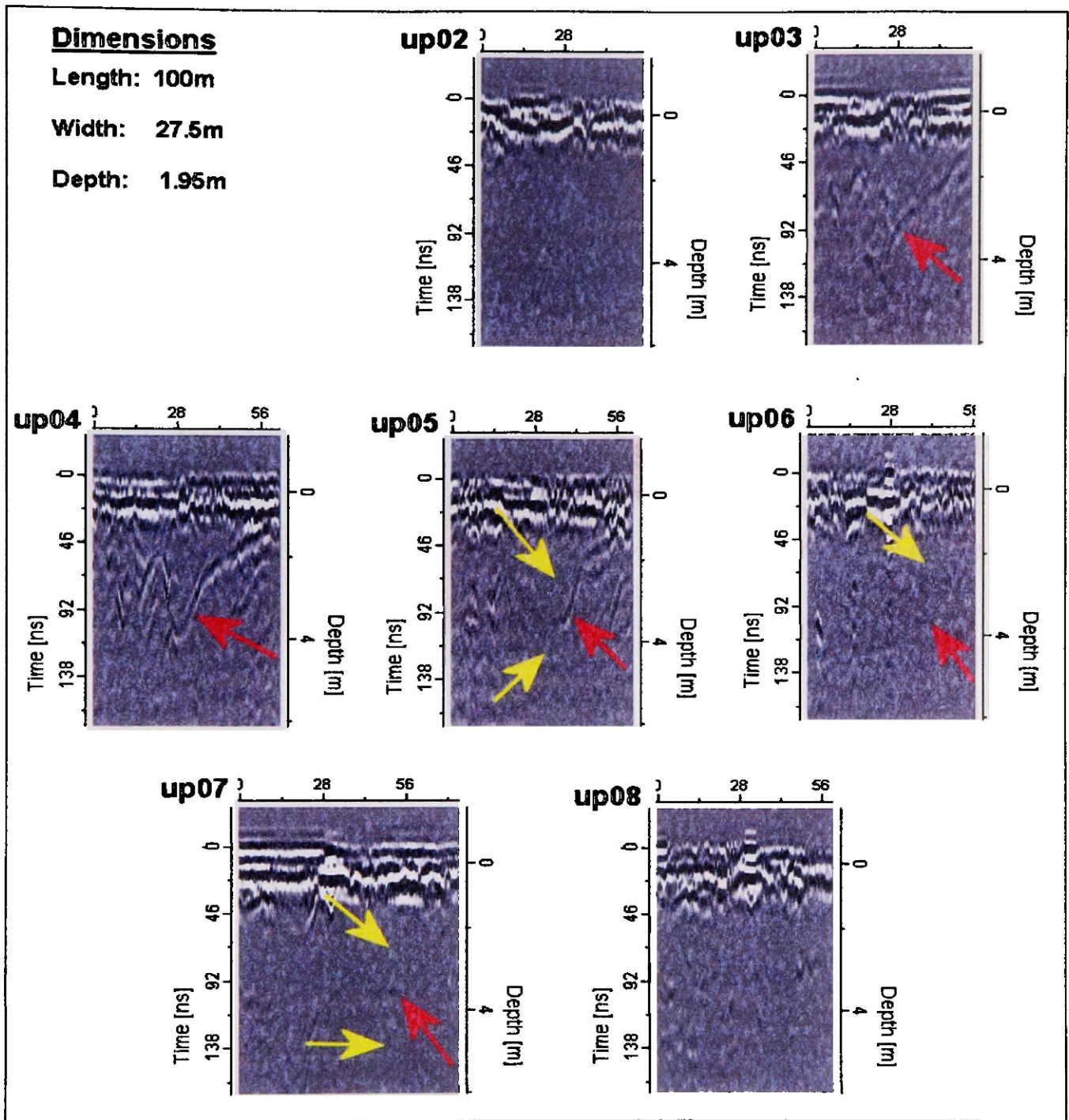


**Figure 16. Upstream Pasture A transects up02 to up08 (15x vertical exaggeration). Trough-shaped paleochannel reflector denoted by red arrow. Zone of absorption, due to silts and clays, denoted by yellow arrows. Width and depth dimensions of the imaged paleochannel are average values.**



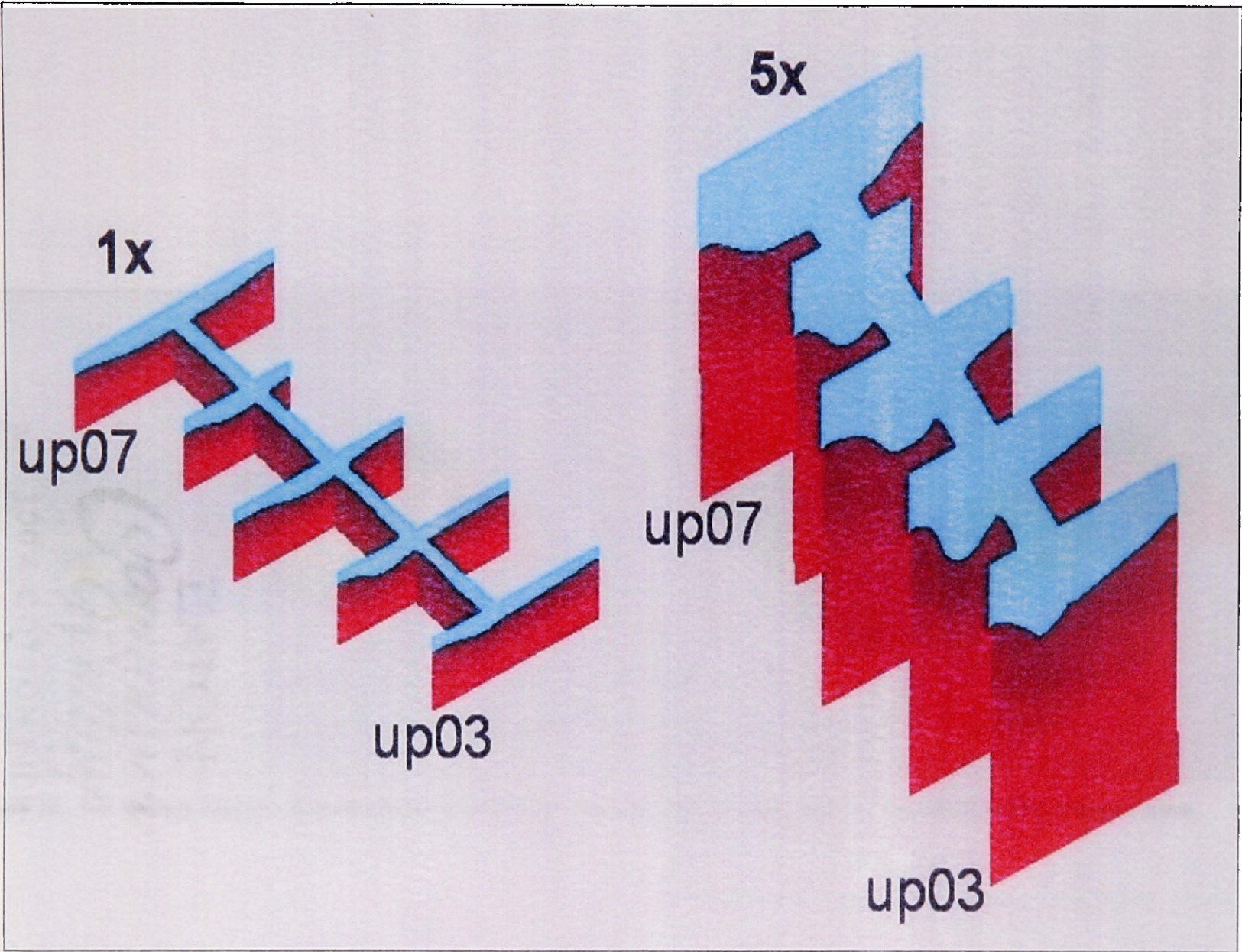
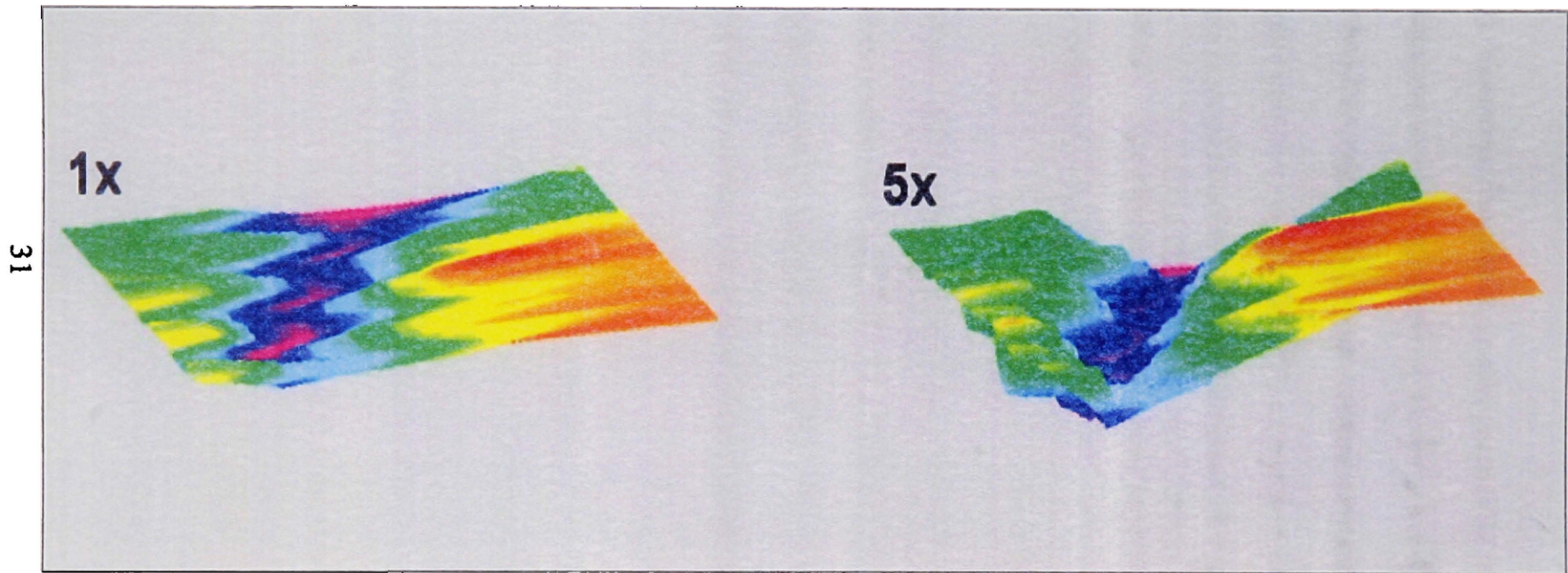


Figure 17. Fence diagram of transects up03 through up07 at 1x and 5x vertical exaggeration.



**Figure 18. 3-D surface diagram of paleochannel imaged in transects up03 through up07 at 1x and 5x vertical exaggeration.**

## 6.2. Site 2

The second site (Figure 19), Upstream Pasture B, is also located in the Upstream Pasture section of the floodplain, adjacent to a side channel of the river locally known as Beaver Creek, and is part of a two hundred meter long swale. Three transects, up38 to up40, cross this particular swale and each line is roughly 20 meters from the next. A trough-shaped, concave up reflector is evident in Figure 20 (red arrows). This type of reflector has the shape of a paleochannel. The dimensions of this interpreted paleochannel are 19.4 meters wide by nine-tenths meter deep.

Diffraction hyperbolae (transect up39, green arrows) and zones of absorption (transect up40, yellow arrows) are also evident in Figure 20. The diffraction hyperbolae, due to boulders, are located at depths of approximately six meters. The zones of absorption are similar to those seen in the first site as they exist both above and below the paleochannel reflector.

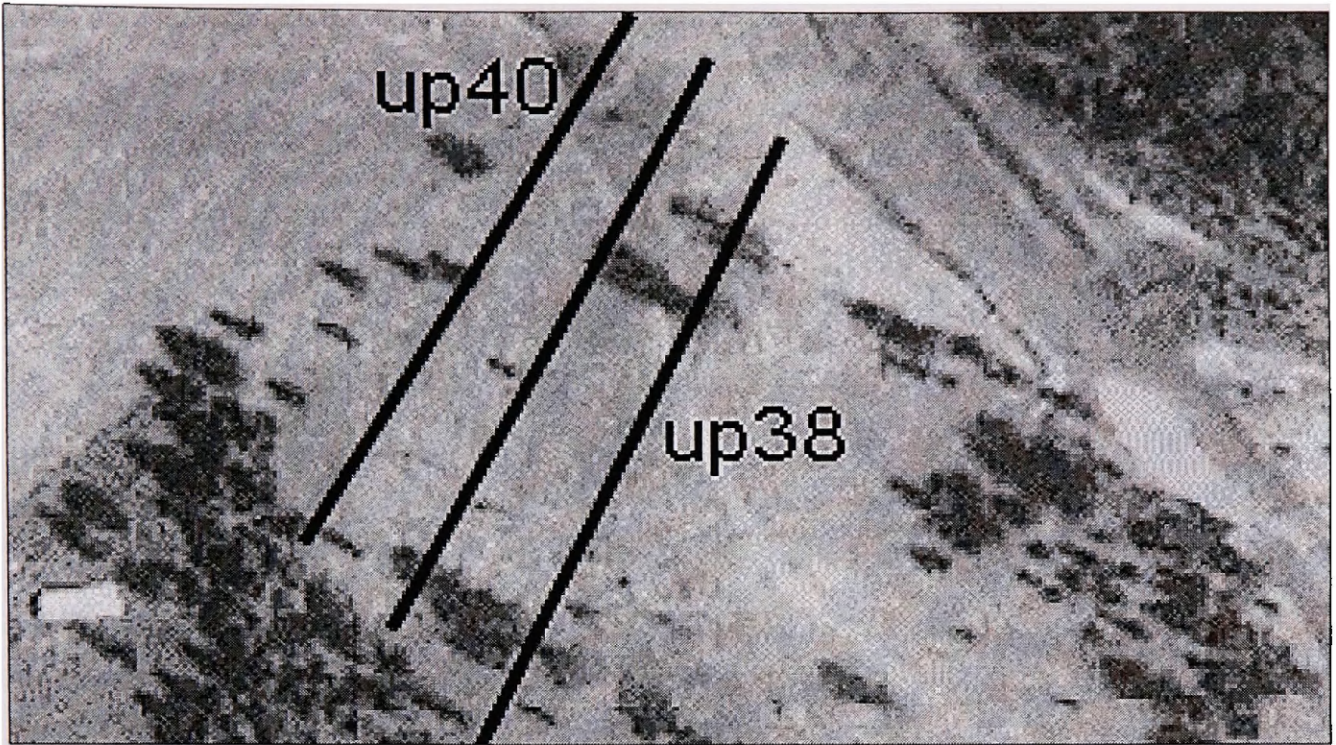


**Figure 19. Upstream Pasture B transects up38 to up40 (black lines). Total distance between transects is approximately 60 meters.**

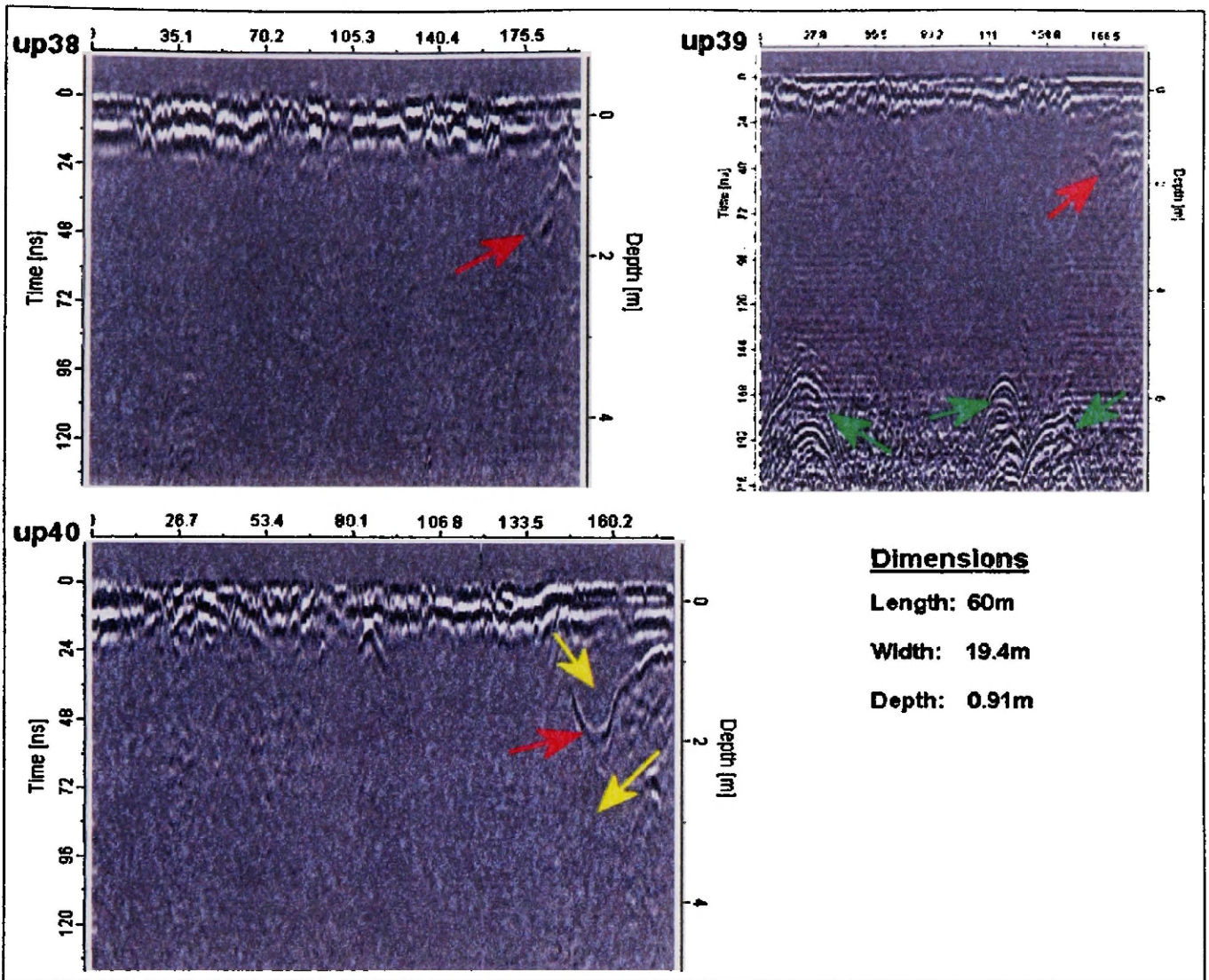
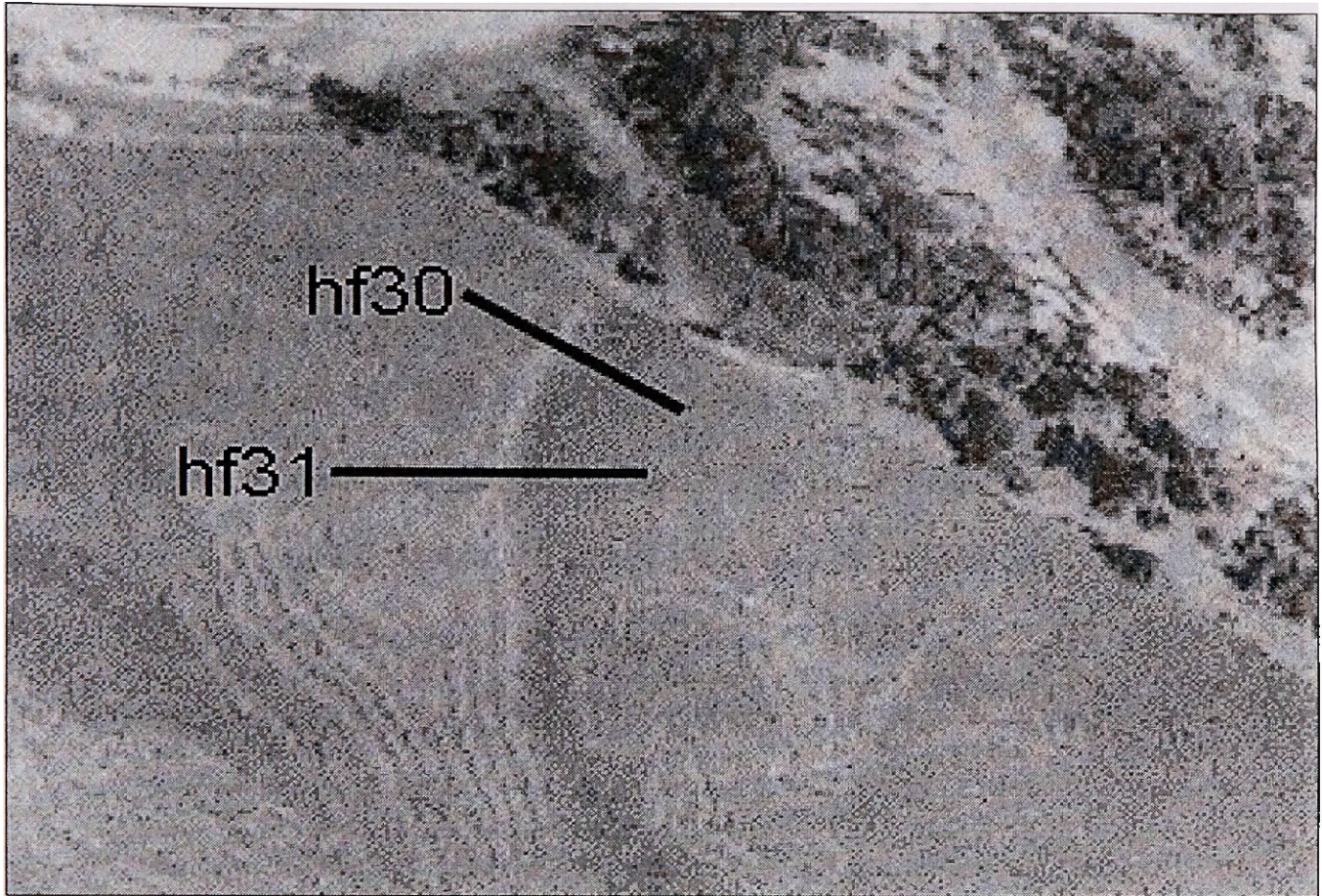


Figure 20. Upstream Pasture B transects up38 to up40 (15x vertical exaggeration). Trough-shaped reflector denoted by red arrow, zone of absorption denoted by yellow arrow, boulders denoted by green arrows. Width and depth dimensions of the imaged paleochannel are average values.

### 6.3. Site 3



**Figure 21. Hayfield transects hf30 and hf31 (black lines). Distance between transects is approximately 40m.**

The Hayfield section of the floodplain is to the northwest of the Upstream Pasture section and a fence separates the two sections. There are two transects, approximately 40 meters apart, that are of interest (Figure 21). I collected them across an, approximately, 30 meter wide swale that is two hundred meters long. In transect hf30 (Figure 22) there is a trough-shaped reflector that is indicative of a paleochannel. This imaged paleochannel has an approximate width of twenty-five meters and an approximate depth of two meters.

Other features evident in transect hf30 are diffraction hyperbolae (green arrows) at a depth of approximately 4m and a zone of absorption (yellow arrow) above the paleochannel reflector.

In transect hf31, the trough-shaped paleochannel reflector is no longer present (Figure 22). Instead, there is a right-dipping reflector, denoted by red arrow, which is present from a horizontal position of thirty-three meters at a depth of near one meter to a horizontal position of fifty-two meters at a depth of three meters, a slope of approximately six degrees. The dipping reflector represents a change between two different facies of electromagnetic properties. Given that this particular transect is located near a transect with a paleochannel reflector and that it is across a feature that in other localities on the floodplain produced paleochannel reflectors, the dipping reflector probably represents one side of a paleochannel bank. The lack of a reflector for the other bank of the paleochannel could be the result of the paleochannel not being on strike with the surface swale making it difficult to detect with geophysical techniques or an event in the history of the paleochannel that has reworked the other bank in such a manner that the electromagnetic properties of the materials comprising it are too similar to resolve.

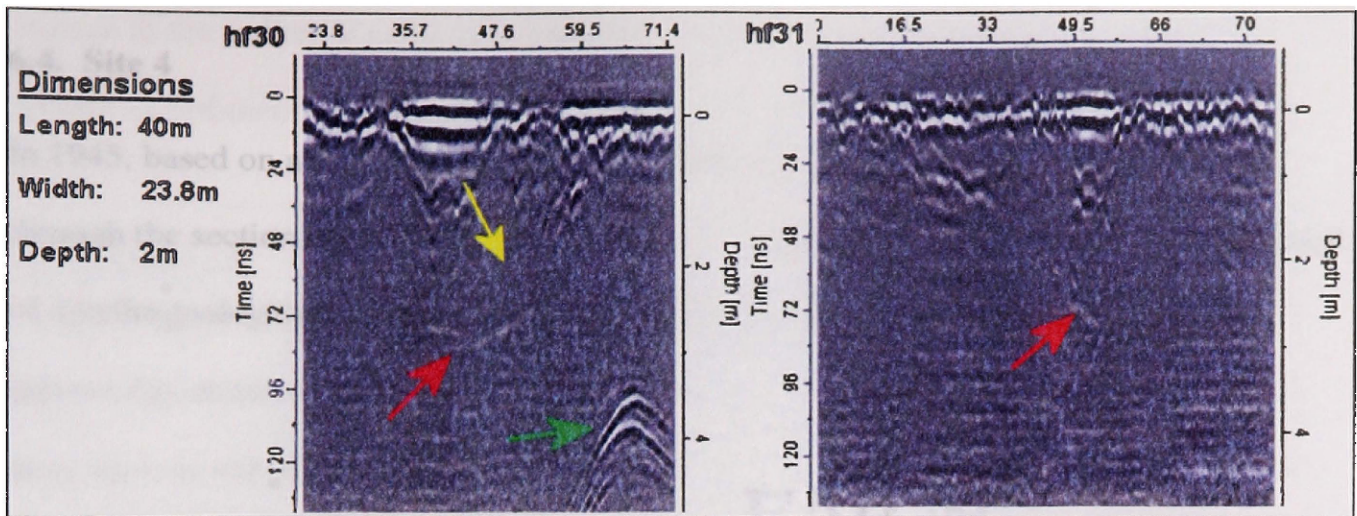


**Figure 22. Hayfield transects hf30 and hf31 (15x vertical exaggeration). Red arrow denotes trough-shaped reflector in transect hf30 and dipping reflector in transect hf31. The yellow arrow denotes a zone of absorption and the green arrow denotes diffraction hyperbolae. Length dimension is for both the trough-shaped reflector and dipping reflector. Width and depth dimensions are for the imaged paleochannel only.**



#### 6.4. Site 4

In 1945, based on aerial photography, the Middle Fork of the Flathead River flowed through the section of the floodplain known as Wally Creek. Wally Creek is the location of a hydrogeological study to determine if there is a preferential flowpath from the present day channel of the Middle Fork to Beaver Creek (Johnson, 2003). From this area, there is one transect of interest with respect to trough-shaped paleochannel reflectors (Figure 23).

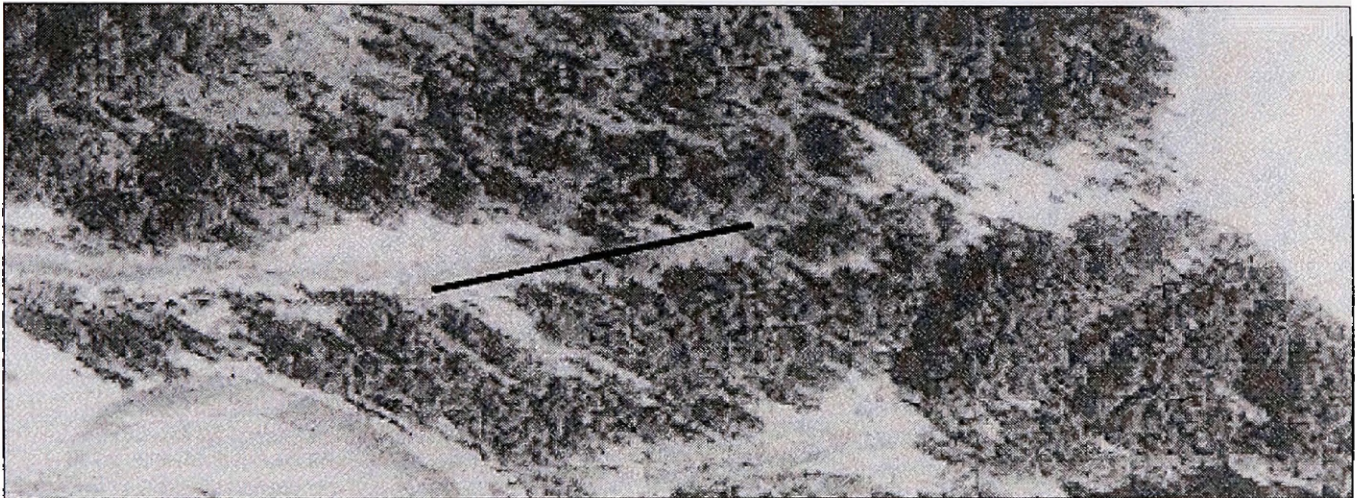


**Figure 23. Wally Creek transect wc05 (black line). Length of transect is approximately 162m**

In transect wc05 (Figure 24) a trough-shaped, undulating reflector, denoted by the red arrow, is present and indicative of a paleochannel. The interpreted paleochannel has a width of 39 meters and a depth of 1.5 meters. Other transects in the area do not show a similar reflector pattern. The other reflector of interest in this particular transect is located at a depth of approximately one-half meter and slightly undulates at a horizontal position between 70 meters and 127 meters. This reflector most likely represents a

change in the sediment package within the area of this particular transect. Such a change in sediment package could be a transition from sand to gravel, etc.

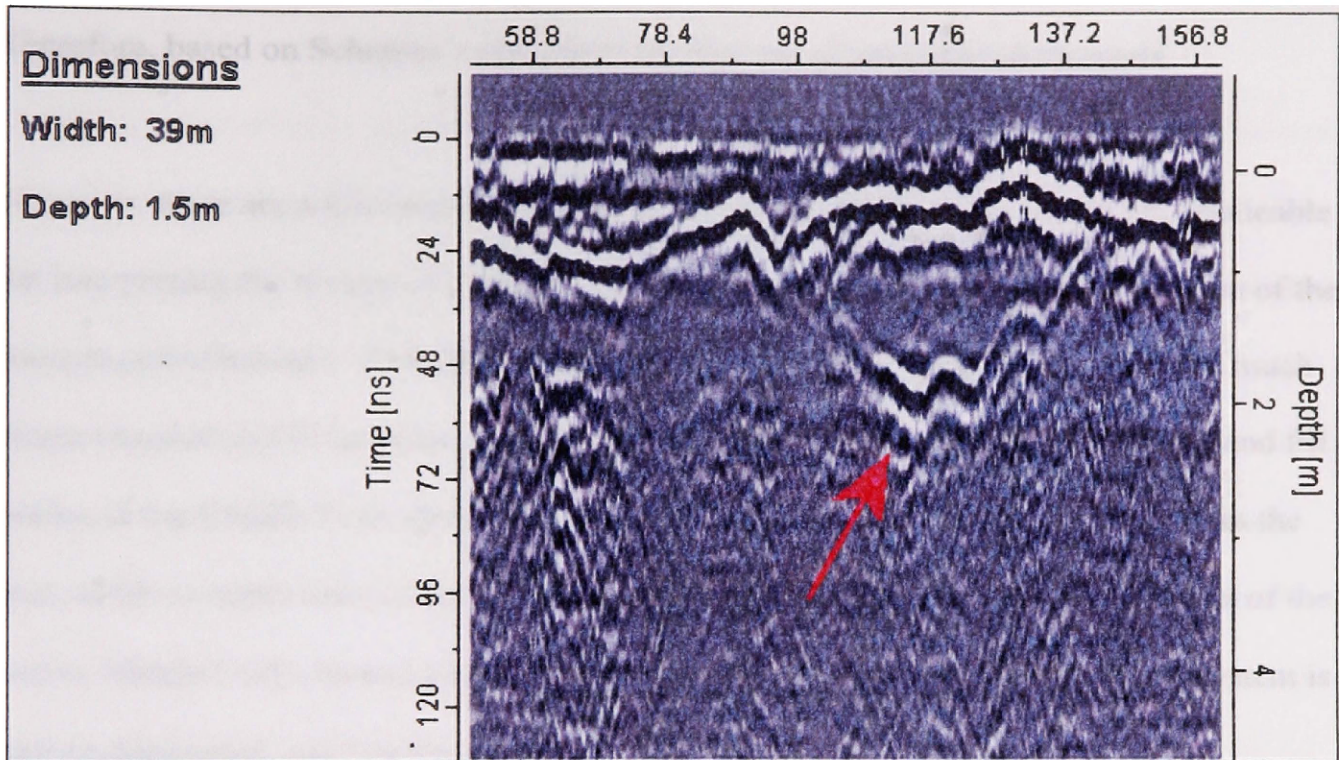


**Figure 24. Wally Creek transect wc05 (15x vertical exaggeration). Trough-shaped reflector denoted by red arrow. Length dimension absent due to trough-shaped reflector being present in only one transect from this locality.**

## 6.5. Channel Form

The width-to-depth ratio of a channel is related to the energy conditions of the fluvial system and therefore can provide insight into the transport processes that took place (Schumm, 1960). The value of the width-to-depth ratio places a channel into one of three categories: suspended load, mixed load, or bed load. Width-to-depth ratios that fall between 10 and 40 are indicative of mixed load channels (Galloway and Hobday, 1996). A mixed load channel transports a variety of sediment grain sizes in an environment with

a moderate gradient. In comparison, suspended load channels transport fine grains, such as silt and clay, and bed load channels transport coarse grains, such as gravel. The imaged paleochannels have width-to-depth ratios between the values of 12.5 and 26. Therefore, based on Schumm's classification they are all mixed load channels.

However, there are a few reasons that the Schumm classification system is not applicable for interpreting the energy conditions of the fluvial system at the time of deposition of the imaged paleochannels. First, the imaged paleochannels may only be one part of a much larger channel and if the other portions of that channel were eradicated by the cut and fill nature of the Middle Fork, then there is inadequate information to accurately obtain the true width-to-depth ratio of the former channel. Second, simple visual observation of the active Middle Fork channel bottoms and channel banks clearly indicate that the system is gravel-dominated, and has been for quite some time, indicating a bed load system. Third, width-to-depth ratios of the active channel range from 9 to 90 (Lorang, personal comm.) indicating that in a braided system the values are highly variable from one locality to another even though the entire system is a bed load system. Therefore, the width-to-depth ratio of an imaged paleochannel, in a fluvial environment such as that found at Nyack, is not an accurate method to classify the energy system of that environment preserved by the aforementioned paleochannel.

## **6.6. Diffraction Hyperbolae**

As previously mentioned, diffraction hyperbolae appear in transects throughout the study area (Figure 25) and are most likely the result of reflections off of large boulders.

Diffraction hyperbolae are predominantly located between depths of four to eight meters, with the minimum and maximum being approximately three meters and twelve meters, respectively (Figure 26). The majority of the diffraction hyperbolae depths are greater than the maximum depths of the imaged paleochannels. Therefore, based on the principle of superposition, the deposits represented by the diffraction hyperbolae are older than the deposits that produce the trough-shaped reflectors indicative of imaged paleochannels. The boulders represented by these diffraction hyperbolae are the result of 1) lag deposits and/or 2) glacial deposition. Lag deposits are very coarse materials that the fluvial system did not remove at a given time. Glacial deposition is the result of 1) large boulders plucked from one location and deposited down-glacier and/or 2) outwash from the mouth of a glacier.

Of note in Figure 25 is that 1) there is a linear trend from northeast to southwest with respect to the depth of the detected boulders and 2) there is a lack of detected boulders within most of the Hayfield section of the floodplain. The linear trend of increasing boulder depth indicates that the valley is deeper on the southwest side than to the northeast. This further implies that the southwest side of the valley, due to faulting, has down-dropped faster than the northeast side of the valley. Based on the depth trend of the boulders previously pointed out, the lack of boulders detected in the Hayfield section

implies that the boulders located there are too deep for detection with the antenna frequencies used for this survey.

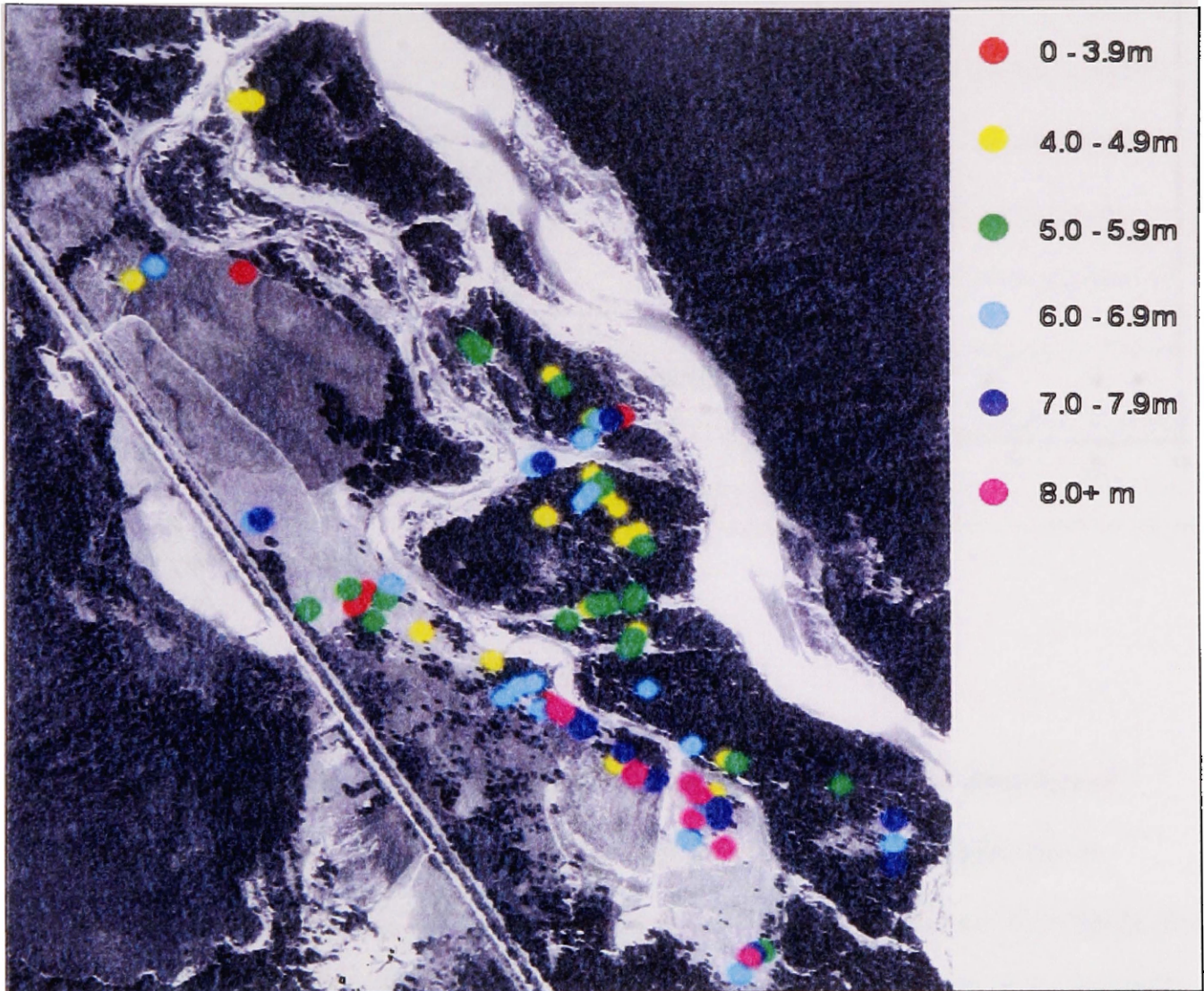


**Figure 25. Distribution of diffraction hyperbolae throughout the floodplain. Depths shown are calculated values.**

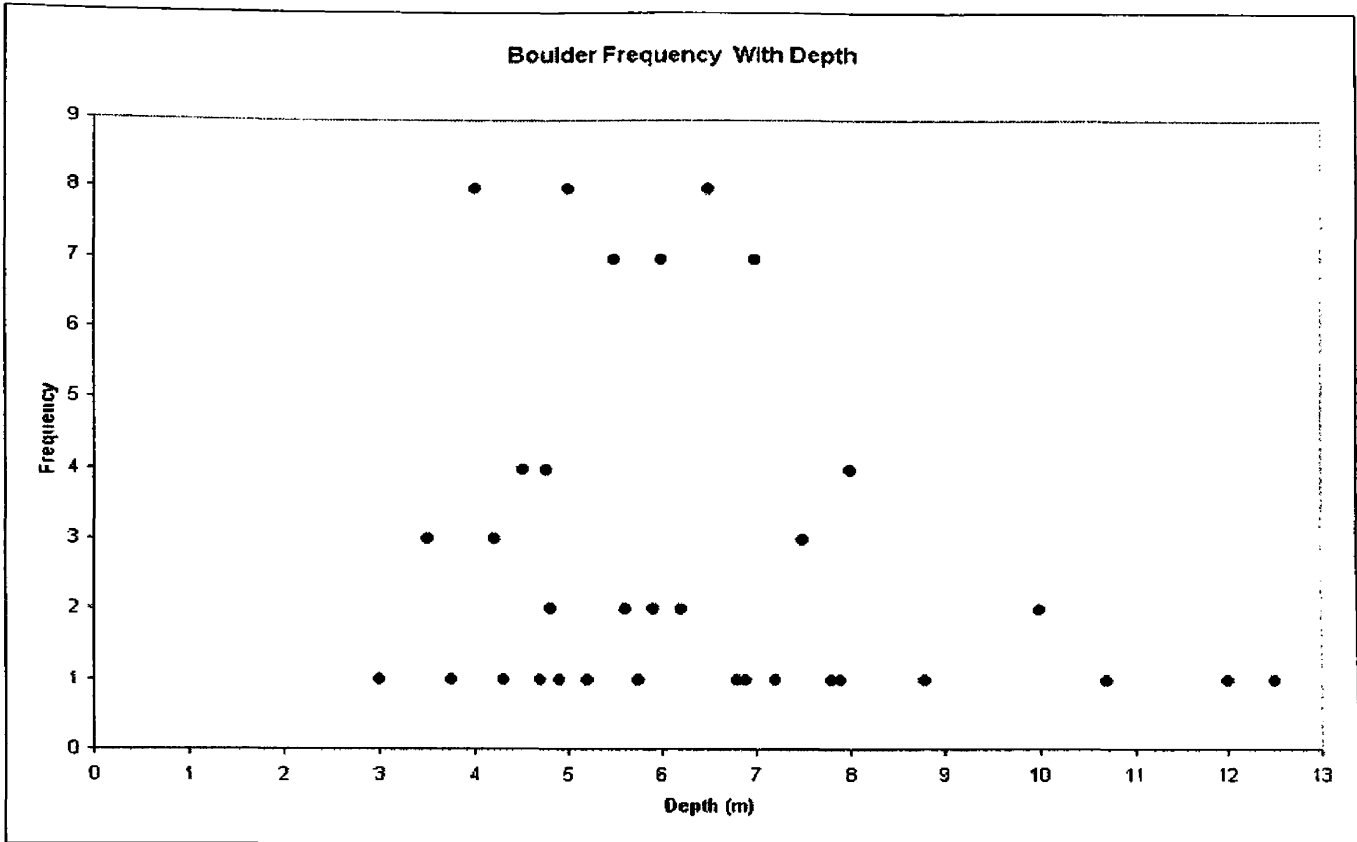


Figure 26. Boulder frequency with depth.

## 7. Conclusion

My survey of the Nyack floodplain provides imagery that indicates the presence of paleochannels within the floodplain. Morphologically, the paleochannels vary in average width from nineteen to thirty-nine meters, in average depth from nine-tenths of a meter to two meters, and in length from forty to one hundred meters. In three localities, paleochannels exist below surface swales. However, the longitudinal extents of the associated surface swales are on the order of two times or longer than the paleochannels that are beneath. This indicates that while swales are possible indicators of paleochannels, there is not a one-to-one relationship between them with respect to their width and length. Furthermore, the four paleochannels of the Nyack floodplain lack

connectivity between one another and only comprise, approximately, one percent of the total amount of transects acquired during this survey.

Diffraction hyperbolae reflectors are present throughout the floodplain. These reflectors are due to the presence of boulders because of 1) lack of anthropogenic artifacts and 2) there is no relationship between forest cover and diffraction hyperbolae at this locality. The diffraction hyperbolae occur at varying depths between three and twelve meters below the subsurface. The deepest boulders are located along the southwest portion of the floodplain suggesting that the valley fill here is deeper than to the northeast. Due to superposition, deposition of the boulders associated with the diffraction hyperbolae took place before deposition of the paleochannels. In general, boulder zones begin one to two meters before the paleochannels.

Reflectors in the Nyack floodplain are chaotic and discontinuous over the study area. The chaotic nature of these reflectors is due to the predominance of interbedded sands and gravels that comprise the floodplain. The discontinuous nature of the reflectors is due to the cut and fill nature of the Middle Fork of the Flathead River. Also evident in the data collected are zones of absorption. These zones are interspersed throughout the floodplain and are indicative of fine-grained sediments such as silts and clays.

This survey was unable to detect the water table with the exception of a few transects in the Beaver Creek area of the floodplain during the latter part of the field season. The lack of detection of the water table is due to the damped input pulse of the GPR, which

obscures the first one-half to one and one-half meters of the subsurface. With the water table being located within this obscured range for much of the field season, its detection was not possible.

The subsurface of the Nyack floodplain is comprised of interbedded sands and gravels interlaced with zones of silts and clays. Due to the cut and fill nature of the fluvial system, it is difficult to pinpoint specific packages as the sediment is continually reworked. At a few localities within the floodplain, paleochannels are partially preserved. Below these paleochannels, exist boulders dispersed throughout the floodplain and are found at increasing depth as one moves across the floodplain from the northeast to the southwest. Shallow subsurface stratigraphy of the Nyack floodplain is complex, due to reworking by the Middle Fork, and in most cases not readily definable using ground penetrating radar of 100 and 200 MHz.



## References

- Bano, Maksim, G. Marquis, B. Niviere, J.C. Maurin, and M. Cushing. 2000. Investigating alluvial and tectonic features with ground-penetrating radar and analyzing diffraction patterns. *Journal of Applied Geophysics*. 43. 33-41.
- Beres, Milan Jr. and Haeni, F.P. 1991. Application of Ground-Penetrating Radar Methods in Hydrogeologic Studies. *Ground Water*. 29. 375-386.
- Boggs, Sam Jr. 1995. *Principles of Sedimentology and Stratigraphy*. Upper Saddle River, New Jersey: Prentice-Hall.
- Bridge, John, R. Collier, and J. Alexander. 1998. Large-scale structure of Calamus River deposits (Nebraska, USA) revealed using ground-penetrating radar. 1998. *Sedimentology*. 45. 977-986.
- Davis, J.L. and Annan, A.P. 1989. Ground-penetrating radar for high-resolution mapping of soil and rock stratigraphy. *Geophysical Prospecting*. 37. 531-551.
- Dominic, David F., K. Egan, C. Carney, P.J. Wolfe, and M.R. Boardman. 1995. Delineation of shallow stratigraphy using ground penetrating radar. *Journal of Applied Geophysics*. 33. 167-175.
- Galloway, W.E. and D.K. Hobday. 1996. *Terrigenous Clastic Depositional Systems: Applications to Fossil Fuel and Groundwater Resources*. Berlin, Germany: Springer-Verlag.
- Gawthorpe, R.L., R.E. Li Collier, J. Alexander, J.S. Bridge, and M.R. Leeder. 1993. Ground penetrating radar: application to sandbody and heterogeneity studies. *Characterization of Fluvial and Aeolian Reservoirs*. Geological Society Special Publication 73. 421-432 Ed. North, C.P. and Prosser, D. J.
- Huggenberger, P., E. Hoehn, R. Beschta, and W. Woessner. 1998. Abiotic aspects of channels and floodplains in riparian ecology. *Freshwater Biology*. 40. 407-425.
- Huggenberger, Peter, E. Meier, and A. Pugin. 1994. Ground-probing radar as a tool for heterogeneity estimation in gravel deposits: advances in data-processing and facies analysis. *Journal of Applied Geophysics*. 31. 171-184.
- Isbell, Brad. 2002. Personal communication.
- Johnson, Adam. 2003. Preliminary Hydrogeological and Ground Penetrating Radar Investigation of Preferential Flow Zones in a Gravel-Dominated Floodplain, Northwestern Montana. University of Montana M.S. Thesis.

- Jol, Harry M., D.G. Smith, and R.A. Myers. 1996. Digital Ground Penetrating Radar (GPR): A New Geophysical Tool for Coastal Barrier Research (Examples from the Atlantic, Gulf, and Pacific Coasts, U.S.A.). *Journal of Coastal Research*. 12. 960-968.
- Leclerc, Rene F. and Edward J. Hickin. 1997. The internal structure of scrolled Floodplain deposits based on ground-penetrating radar, North Thompson River, British Columbia. *Sedimentology*. 21. 17-38.
- Lesmes, David P., Scott M. Decker, and David C. Roy. 2002. A multiscale radar-stratigraphic analysis of fluvial aquifer heterogeneity. *Geophysics* 67. 1452-1464.
- Miall, A.D. 1996. *The Geology of Fluvial Deposits: Sedimentary Facies, Basin Analysis, And Petroleum Geology*. Berlin, Germany: Springer-Verlag.
- Olhoeft, Gary R. 2000. Maximizing the information return from ground penetrating Radar. *Journal of Applied Geophysics* 43. 175-187.
- Poole, G.C., R.J. Naiman, J. Pastor, and J.A. Stanford. 1997. Uses and limitations of ground penetrating RADAR in two riparian systems. *Groundwater/Surface Water Ecotones: Biological and Hydrological Interactions and Management Options*. 140-148 Ed. Janine Gilbert, et al. United Kingdom: Cambridge University Press.
- Poole, Geoffrey C., J.A. Stanford, C.A. Frissell, and S.W. Running. 2002. Three-dimensional mapping of geomorphic controls on flood-plain hydrology and connectivity from aerial photos. *Geomorphology*. 48. 329-347.
- Reynolds, John M. 1997. *An Introduction to Applied and Environmental Geophysics*. Chichester, UK: John Wiley & Sons
- Schumm, Stanley A. 1960. The shape of alluvial channels in relation to sediment type. U.S. Geological Survey Professional Paper 352-B. 17-30
- Smith, D.G. and Harry M. Jol. 1995. Ground penetrating radar: antenna frequencies and maximum probable depths of penetration in Quaternary sediments. *Applied Geophysics*. 33. 93-100.
- Smith, D.G. and Harry M. Jol. 1997. Radar Structure of a Gilbert-type delta, Peyto Lake, Banff National Park, Canada. *Sedimentary Geology*. 113. 195-209.

- Stanford, Jack A. and J.V. Ward. 1988. The hyporheic habitat of river ecosystems. *Nature*. 335. 64-66.
- Stanford, Jack A. and J.V. Ward. 1993. An ecosystem perspective of alluvial rivers: connectivity and the hyporheic corridor. *Journal of the North American Benthological Society*. 12. 48-60.
- Stanford, J.A., J.V. Ward, and B.K. Ellis. 1994. Ecology of the Alluvial Aquifers of the Flathead River, Montana. *Groundwater Ecology*. 367-390. Ed. Janine Gilbert, Et al. San Diego, CA: Academic Press.
- van Overmeeren, R.A. 1998. Radar facies of unconsolidated sediments in The Netherlands: A radar stratigraphy interpretation method for hydrogeology. *Journal of Applied Geophysics*. 40. 1-18.
- Vandenbergh, J. and R.A. van Overmeeren. 1999. Ground penetrating radar images of Selected fluvial deposits in the Netherlands. *Sedimentary Geology*. 128. 245-270.
- Ward, J.V., J.A. Stanford and N.J. Voelz. 1994. Spatial distribution patterns of Crustacea in the floodplain aquifer of an alluvial river. *Hydrobiologia*. 287. 11-17.

**Appendix A**  
**Transect Start/End Points and Length**

Transect Name	Start Point (UTM)		End Point (UTM)		Length (m)
	Easting	Northing	Easting	Northing	
up01	0291992	5370582	0292066	5370600	50.5
up02	0291972	5370603	0292052	5370621	55.0
up03	0291962	5370615	0292044	5370634	53.5
up04	0291956	5370631	0292040	5370645	62.5
up05	0291928	5370660	0292009	5370697	61.5
up06	0291912	5370677	0291993	5370724	57.0
up07	0291910	5370687	0291984	5370733	74.0
up08	0291906	5370695	0291976	5370739	60.0
up09	0292039	5370533	0292107	5370610	100.0
up10	0292026	5370535	0292100	5370622	114.0
up11	0291795	5370823	0292071	5370916	283.5
up12	0291806	5370910	0292065	5370948	256.5
up13	0291812	5370979	0292058	5370978	244.5
up14	0291819	5371013	0292053	5371013	229.3
up15	0291822	5371047	0292035	5371036	212.0
up16	0291822	5371074	0291983	5371072	151.0
up17	0291822	5371074	0291867	5371132	60.5
up18	0291778	5371091	0291805	5371143	47.0
up19	0291748	5371104	0291779	5371153	41.5
up20	0291725	5371121	0291759	5371168	50.0
up21	0291700	5371139	0291748	5371183	58.0
up22	0291683	5371163	0291720	5371204	50.0
up23	0291652	5371180	0291708	5371242	80.6
up24	0291626	5371208	0291664	5371258	57.0
up25	0291604	5371225	0291633	5371271	50.0
up26	0291580	5371242	0291611	5371285	43.6
up27	0291555	5371269	0291586	5371302	41.6
up28	0291536	5371285	0291569	5371323	42.0
up29	0291481	5371269	0291547	5371334	92.0
up30	0291449	5371298	0291532	5371371	106.0
up31	0291435	5371312	0291529	5371392	122.1
up32	0291398	5371344	0291450	5371427	93.0
up33	0291378	5371368	0291426	5371450	94.5
up34	0291348	5371385	0291375	5371453	71.5
up35	0291263	5371430	0291272	5371495	57.0
up36	0291230	5371429	0291243	5371585	154.5
up37	0291199	5371434	0291218	5371626	192.0
up38	0291196	5371652	0291127	5371461	197.8
up39	0291100	5371506	0291173	5371674	185.5
up40	0291075	5371535	0291158	5371698	179.0

up41	0291047	5371568	0291139	5371671	140.0
------	---------	---------	---------	---------	-------

Transect Name	Start Point (UTM)		End Point (UTM)		Length (m)
	Easting	Northing	Easting	Northing	
hf01	0290375	5372414	0290626	5372590	296.6
hf02	0290644	5372582	0290395	5372386	283.9
hf03	0290413	5372358	0290743	5372582	378.4
hf04	0290770	5372565	0290448	5372307	411.2
hf05	0290460	5372279	0290875	5372491	468.5
hf06	0290903	5372473	0290610	5372044	511.1
hf07	0290631	5372015	0291110	5372312	543.2
hf08	0291125	5372279	0290994	5372207	143.3
hf09	0291018	5372179	0291149	5372192	114.0
hf10	0291133	5372126	0291036	5372130	104.4
hf11	0291040	5372121	0291140	5372121	90.2
hf12	0290968	5372201	0290646	5371983	356.3
hf13	0290658	5371960	0290954	5372149	338.8
hf14	0290971	5372119	0290691	5371931	330.7
hf15	0290686	5371901	0290997	5372099	349.1
hf16	0291016	5372065	0290728	5371848	335.3
hf17	0290745	5371832	0291090	5371998	380.6
hf18	0291036	5371932	0290766	5371804	303.1
hf19	0290704	5371775	0291043	5371897	282.2
hf20	0291056	5371867	0290853	5371772	222.7
hf21	0290853	5371742	0291060	5371813	218.5
hf22	0291061	5371775	0290861	5371713	206.3
hf23	0290870	5371683	0291067	5371760	212.4
hf24	0291088	5371722	0290867	5371644	228.0
hf25	0290877	5371618	0291097	5371701	228.8
hf26	0291114	5371675	0290899	5371589	226.8
hf27	0290917	5371560	0291115	5371663	217.3
hf28	0291107	5371645	0290963	5371520	189.3
hf29	0290935	5372284	0290802	5372524	341.4
hf30	0290769	5372532	0290835	5372508	72.8
hf31	0290820	5372488	0290733	5372480	89.0

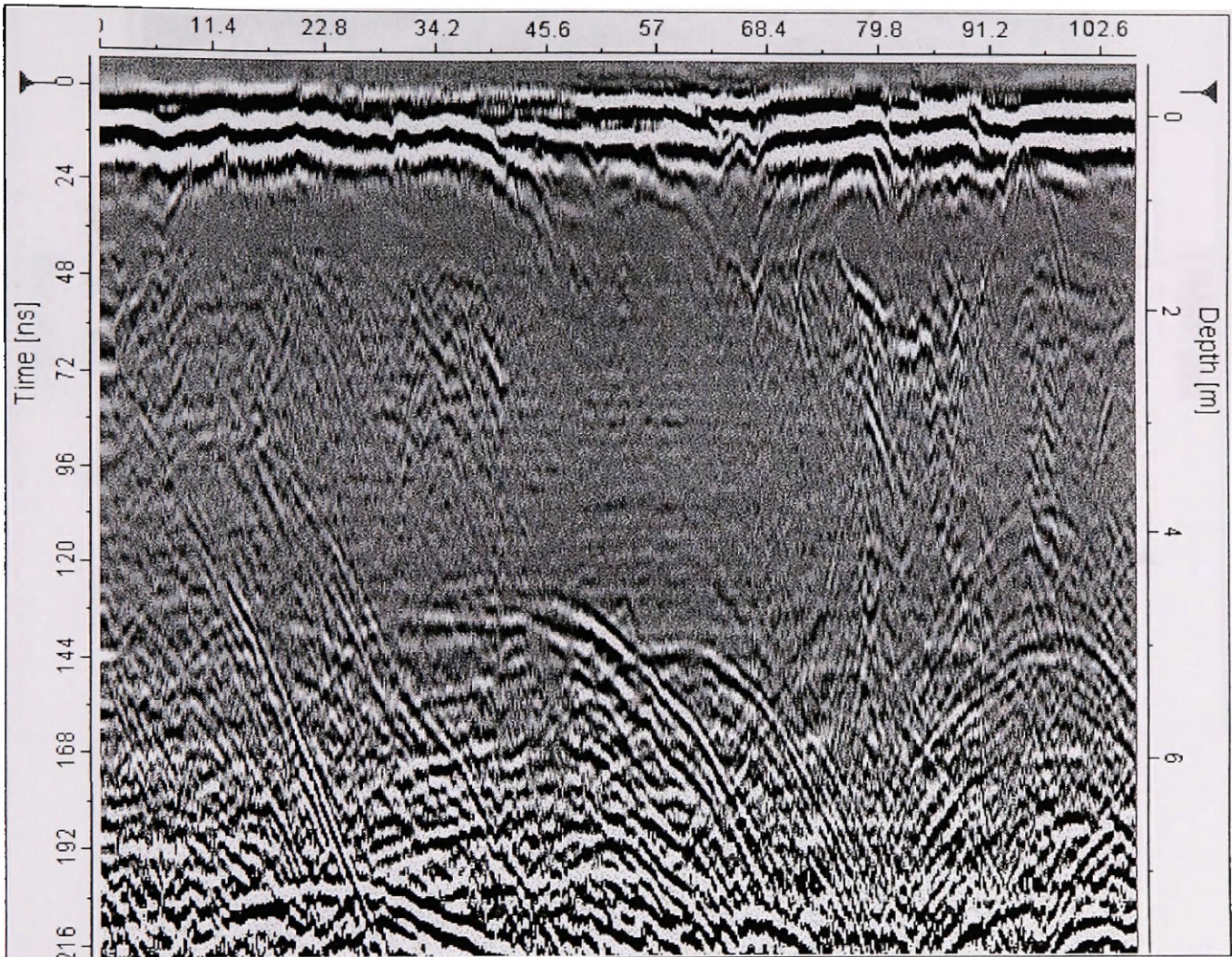
Transect Name	Start Point (UTM)		End Point (UTM)		Length (m)
	Easting	Northing	Easting	Northing	
bc01	0291791	5371541	0291761	5371440	107.9
bc02	0291478	5372039	0291491	5371961	83.7
bc03	0291515	5371972	0291510	5372058	90.2
bc04	0291590	5372052	0291591	5371998	59.0
bc05	0291911	5372007	0291850	5372119	126.8
bc06	0291850	5372119	0291809	5372131	45.1
bc07	0291809	5372131	0291713	5372114	98.1
bc08	0291713	5372114	0291570	5372000	187.0
bc09	0291570	5372000	0291465	5371962	112.5
bc10	0291713	5372114	0291658	5372109	68.1
bc11	0291658	5372109	0291615	5372141	54.2
bc12	0291615	5372141	0291579	5372222	75.4
bc13	0291579	5372222	0291535	5372252	62.4
bc14	0291535	5372252	0291496	5372311	58.7
bc15	0291496	5372311	0291448	5372325	54.9
bc16	0291448	5372325	0291352	5372303	98.8
bc17	0291352	5372303	0291356	5372367	61.3
bc18	0291356	5372367	0291321	5372388	36.9
bc19	0291321	5372388	0291349	5372506	110.5
bc20	0291349	5372506	0291302	5372555	72.8
bc21	0291302	5372555	0291268	5372618	77.6
bc22	0291268	5372618	0291293	5372655	40.8
bc23	0291052	5373085	0291162	5372805	333.1
bc24	0291162	5372805	0291293	5372655	240.5
bc25	0291162	5372805	0290855	5372945	367.0
bc26	0290855	5372945	0290745	5373030	169.9
bc27	0290745	5373030	0290911	5373240	284.7
bc28	0291060	5373062	0290991	5373096	80.3
bc29	0290970	5373092	0290776	5373001	208.7
bc30	0291527	5371916	0291445	5371762	199.3
bc31	0291445	5371762	0291189	5371716	263.1
bc32	0291519	5371852	0291700	5371754	210.0
bc33	0291700	5371754	0291791	5371541	254.2
bc34	0291761	5371440	0291868	5371208	296.3
bc35	0291868	5371208	0292136	5371086	319.4
bc36	0292136	5371086	0292444	5371048	306.8
bc37	0292444	5371048	0292433	5370773	282.9
bc38	0292433	5370773	0292416	5370677	103.0
bc39	0292444	5371048	0292513	5371089	88.1
bc40	0291700	5371754	0291818	5371803	141.7
bc41	0291771	5371799	0291810	5371736	61.9
bc42	0291771	5371799	0291621	5372017	243.5

bc43            0291716    5371956    0291598    5371825    231.6

<b>Transect Name</b>	<b>Start Point (UTM)</b>		<b>End Point (UTM)</b>		<b>Length (m)</b>
	<b>Easting</b>	<b>Northing</b>	<b>Easting</b>	<b>Northing</b>	
wc01	0291833	5371569	0291775	5371624	89.8
wc02	0291722	5371568	0291673	5371526	81.5
wc03	0291631	5371582	0291574	5371478	129.4
wc04	0291609	5371579	0291575	5371522	81.1
wc05	0291594	5371557	0291724	5371594	161.5

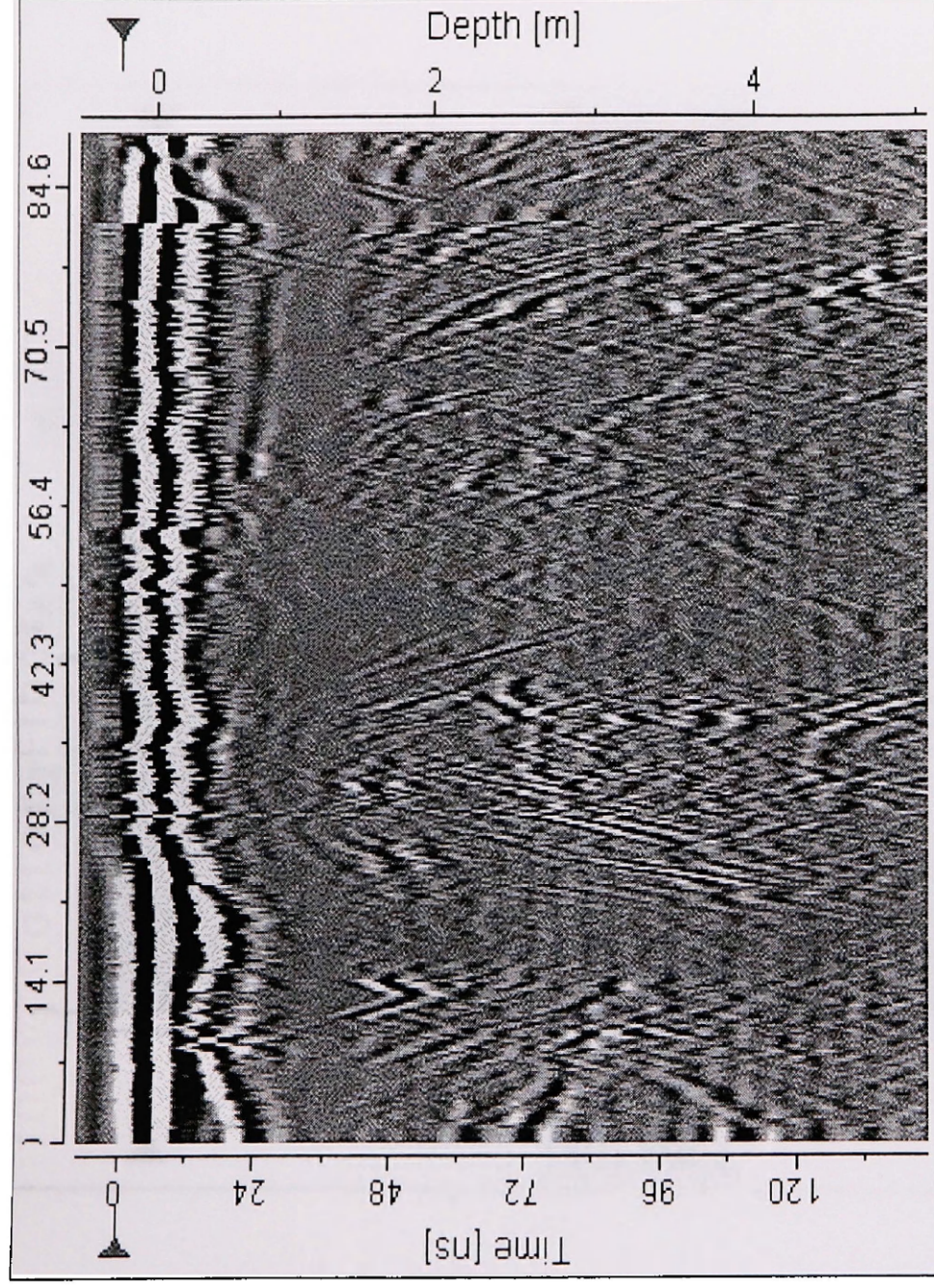
**Appendix B**  
**Representative Radargrams of the Nyack Floodplain**

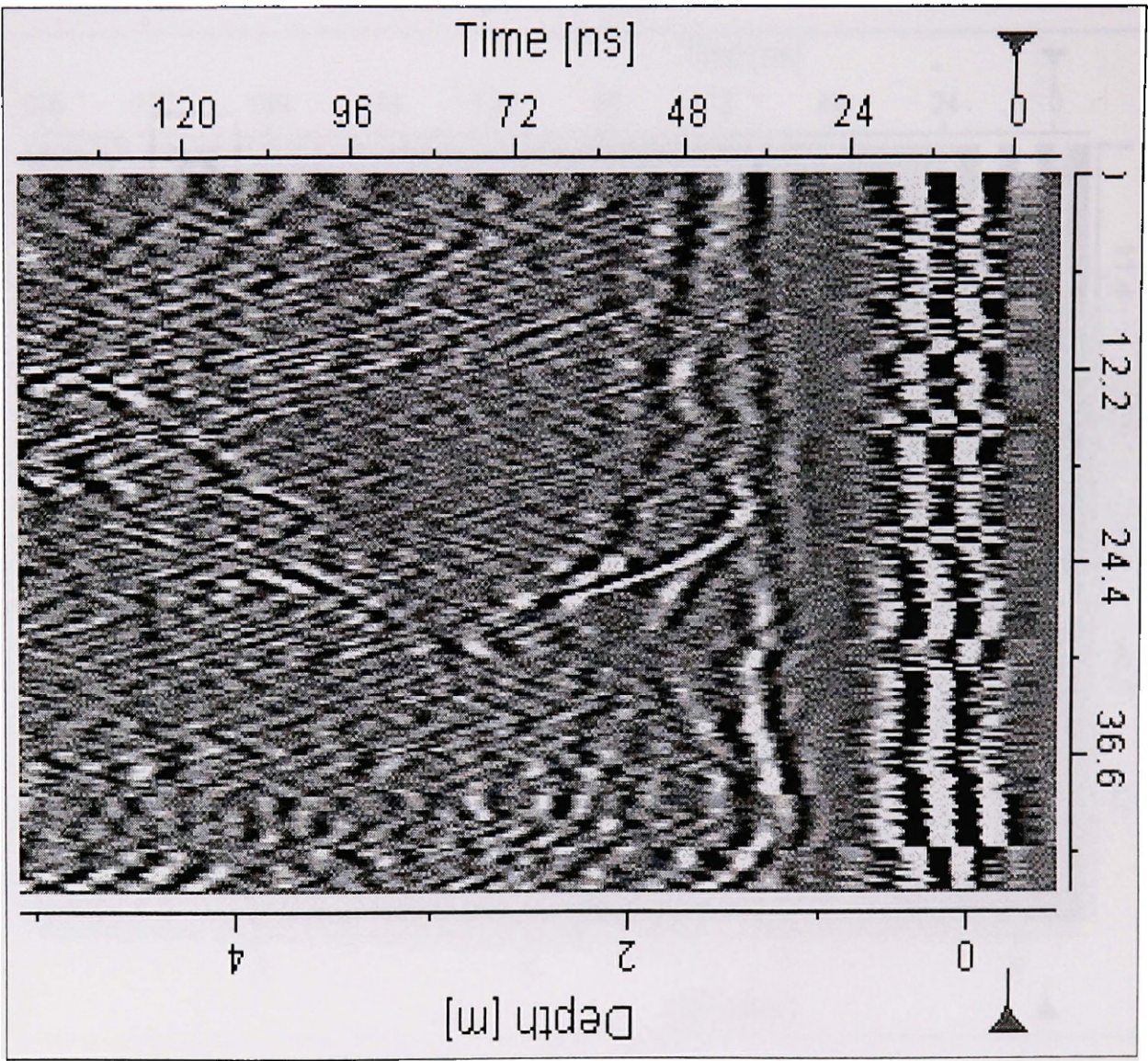
**bc01**





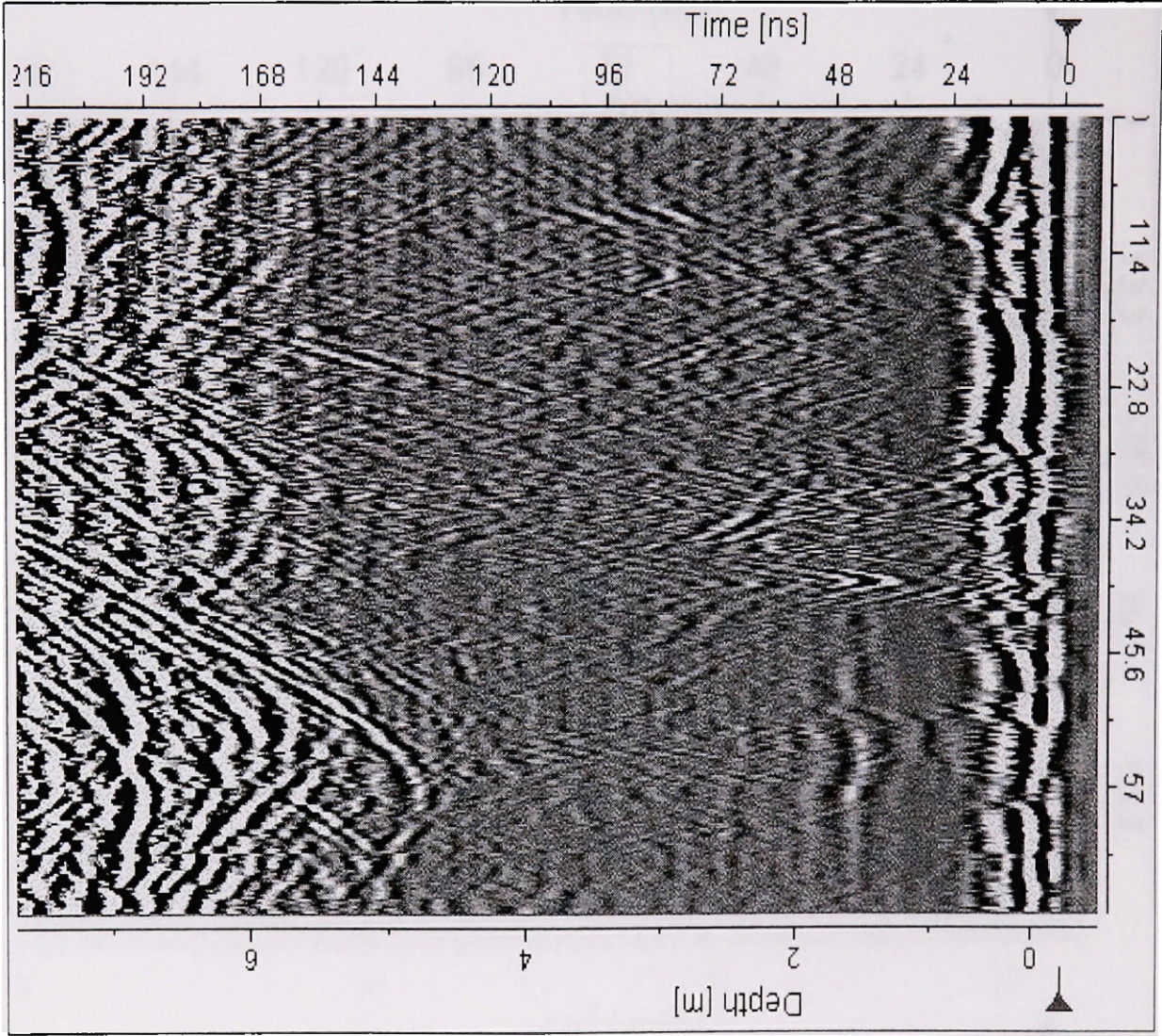
bc03

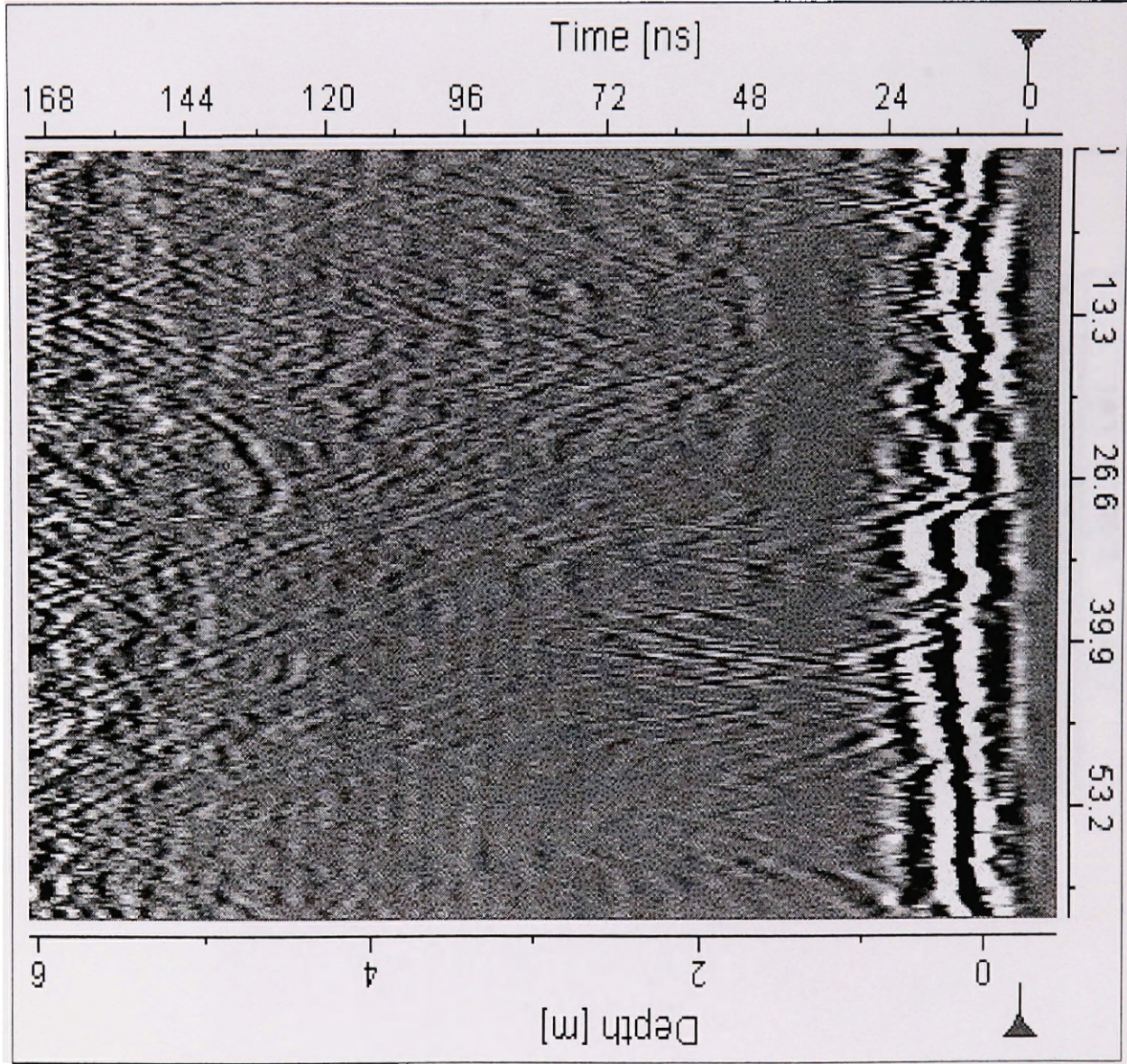




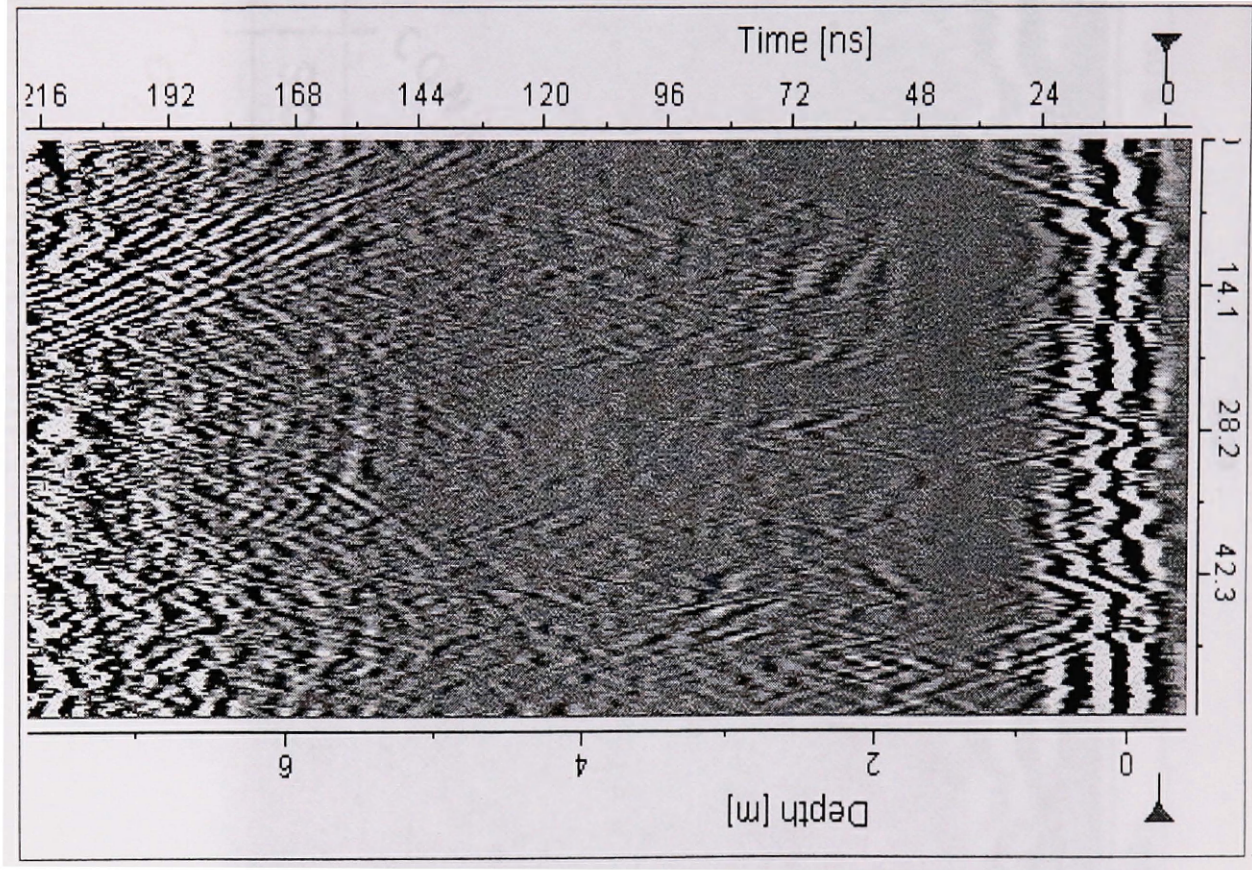
bc06

bc10

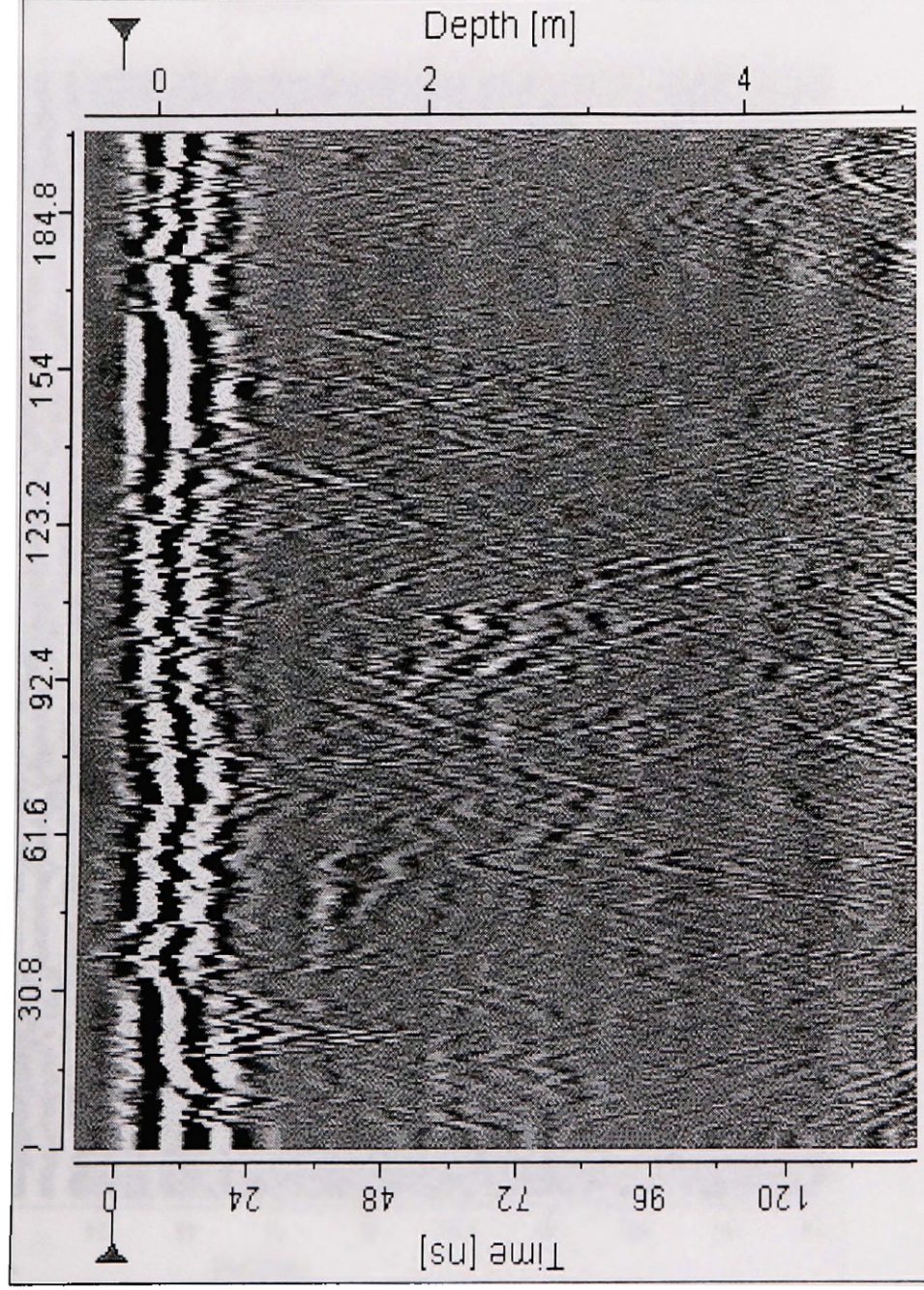




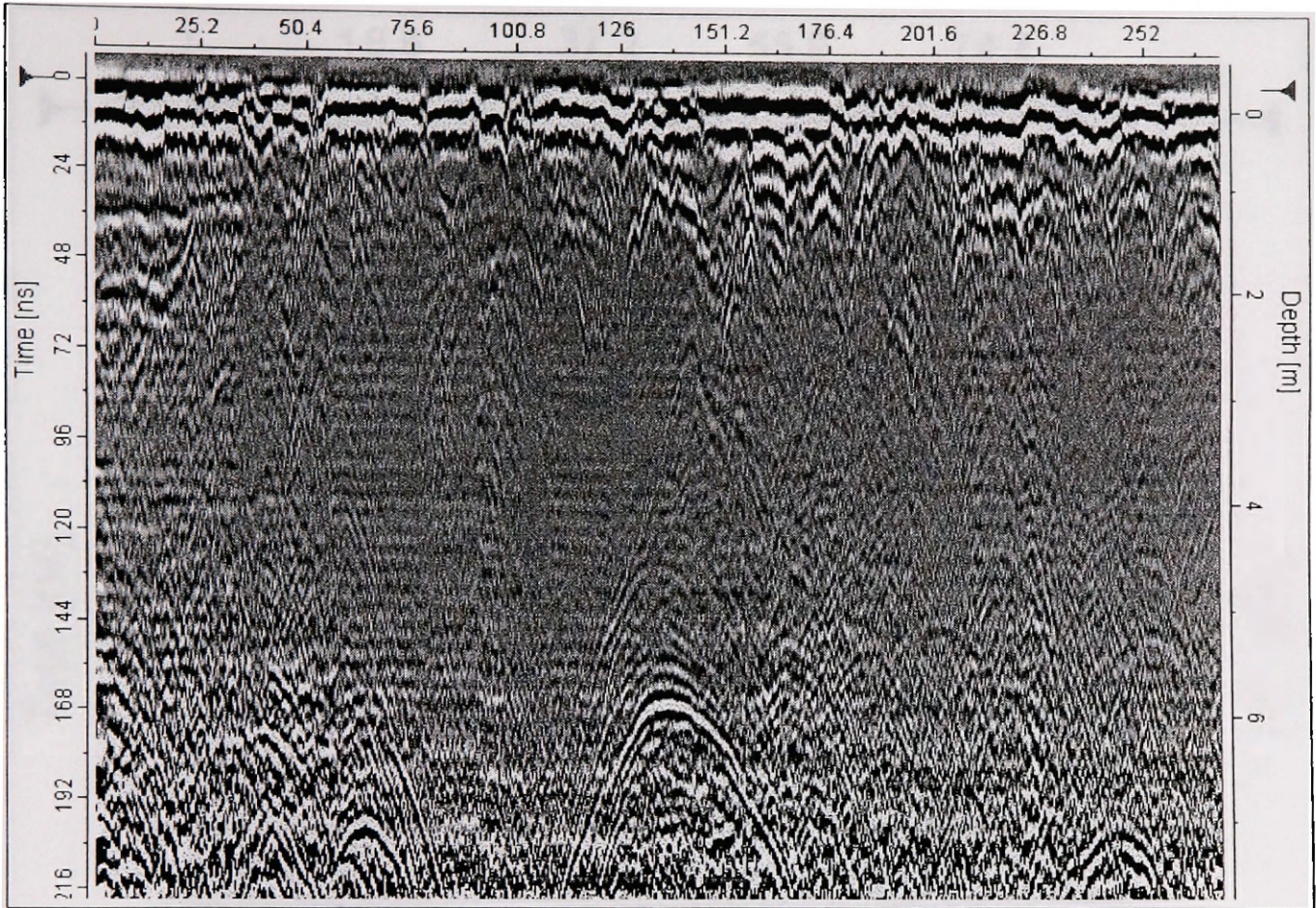
bc15



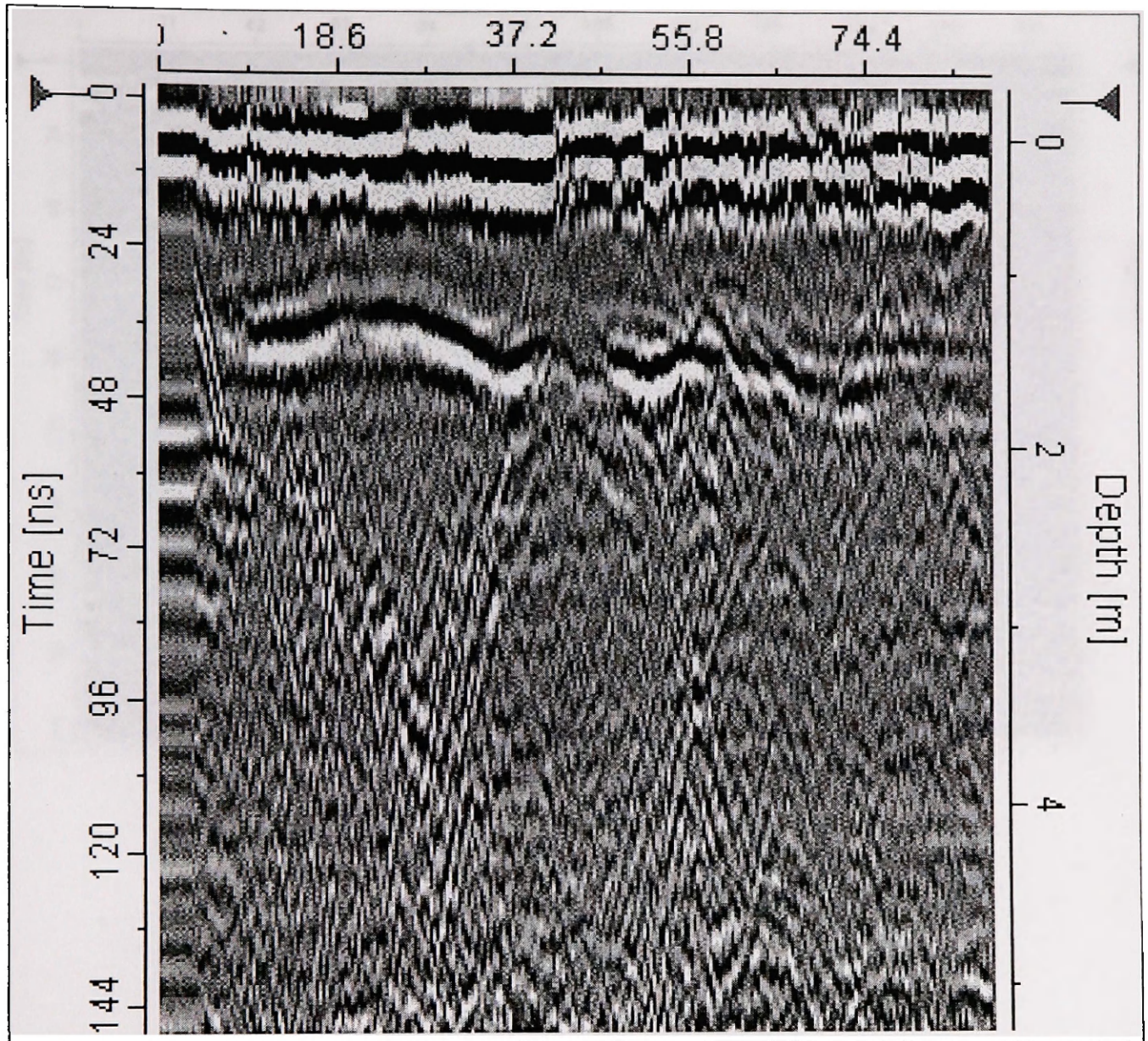
bc29



bc37

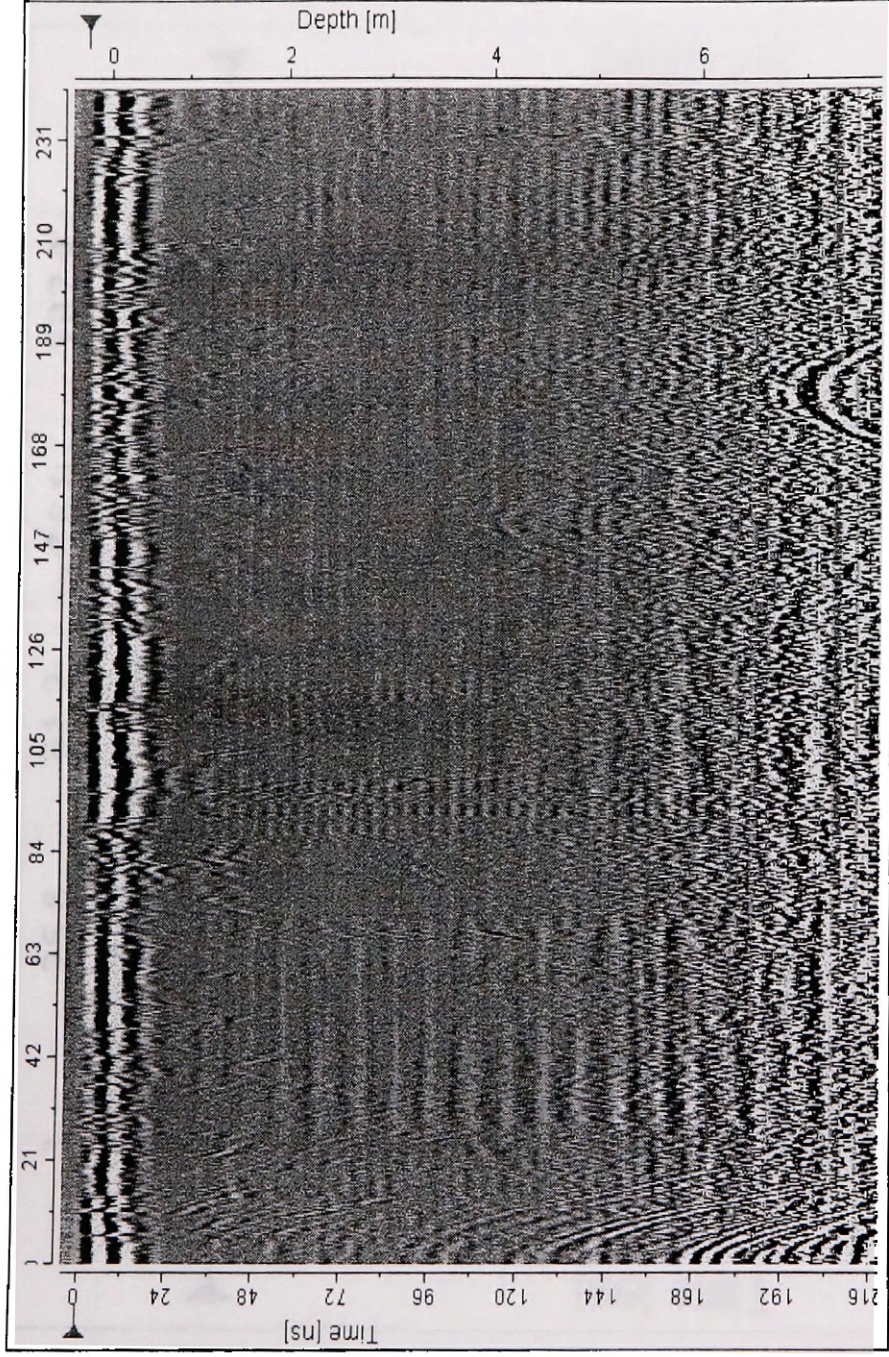


bc39

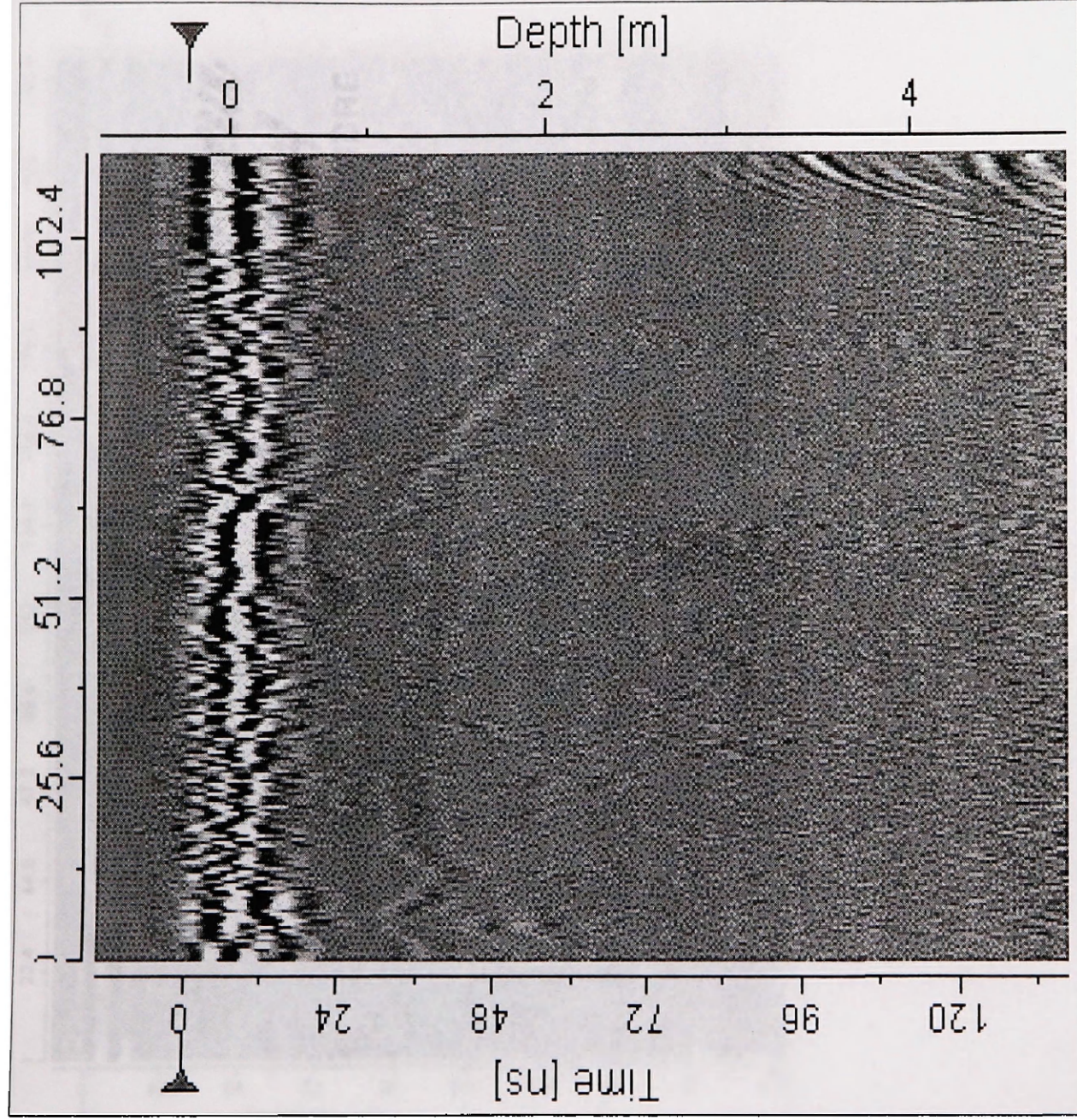




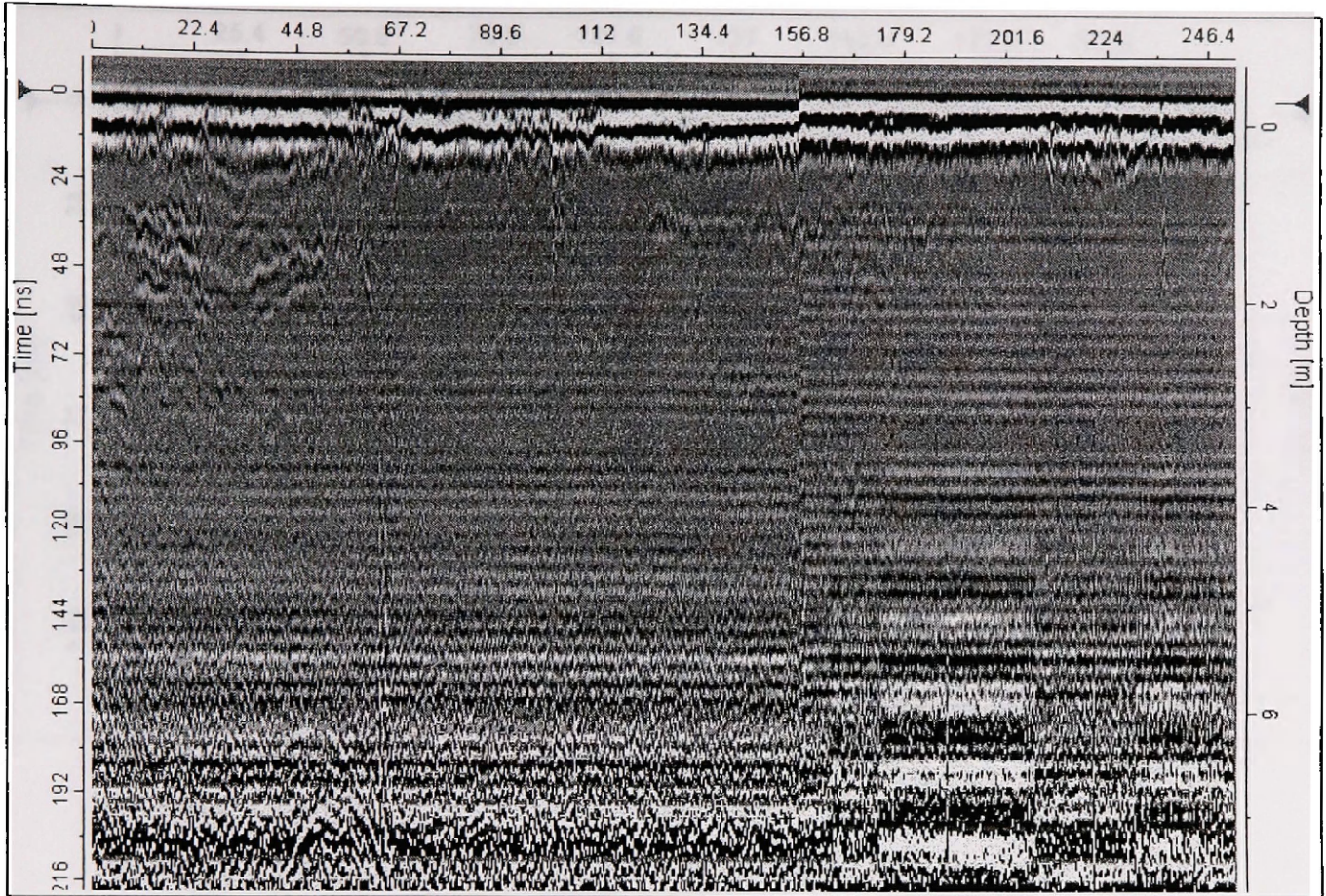
hf01



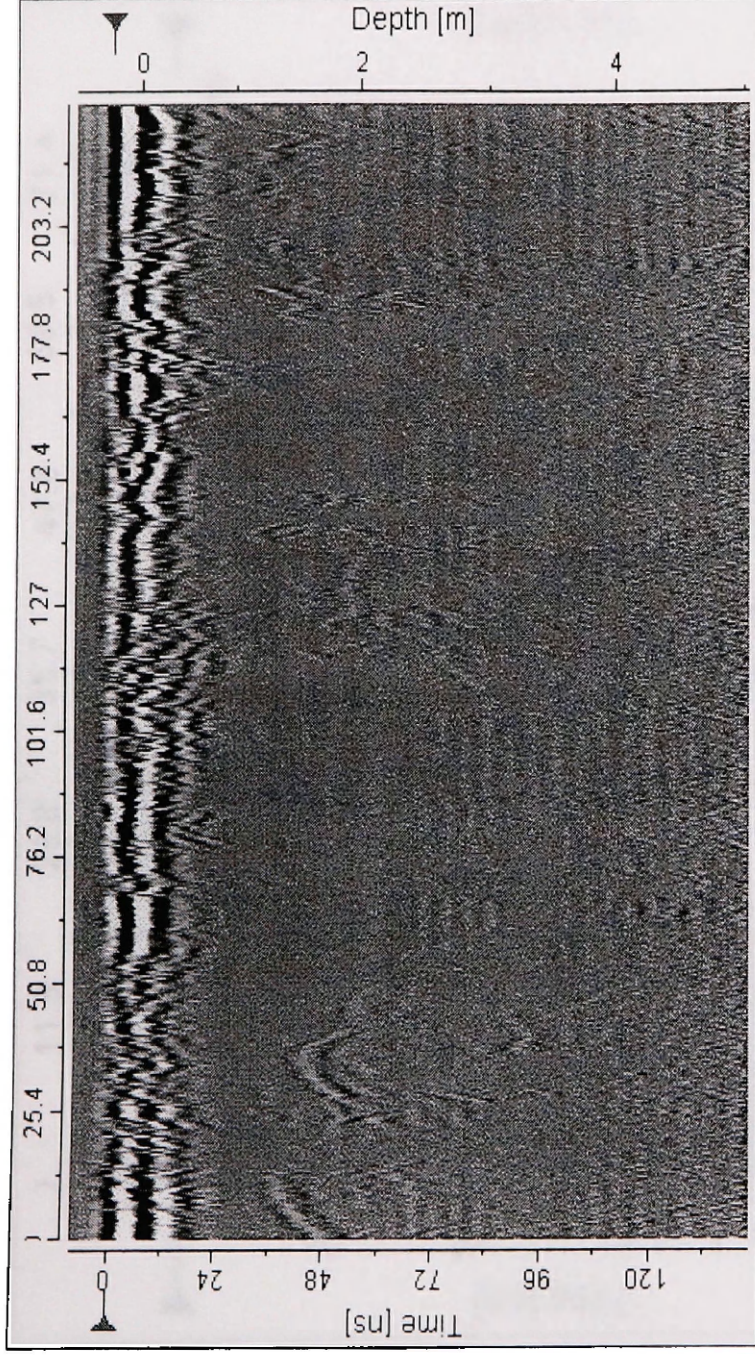
hf09



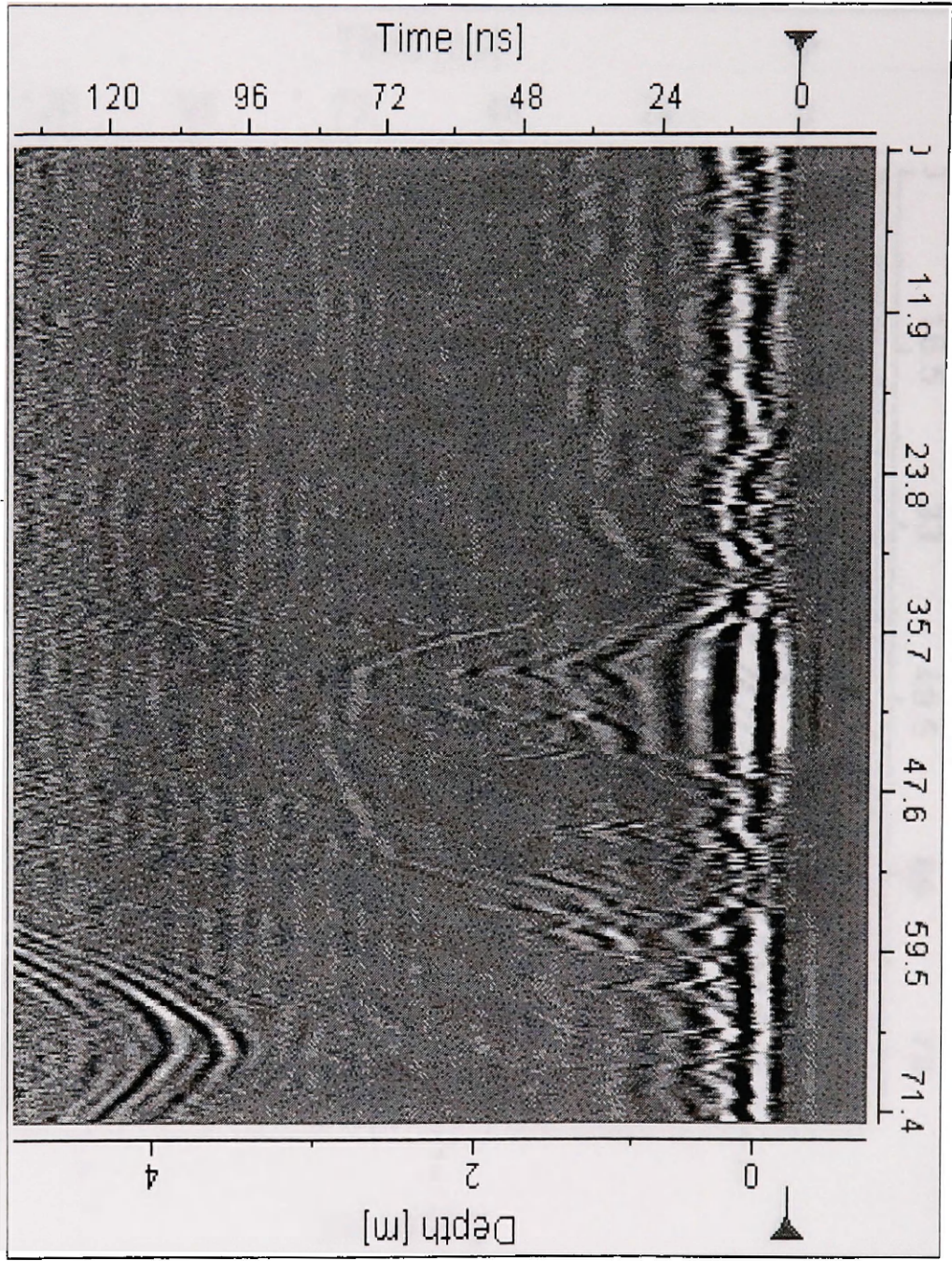
# hf19

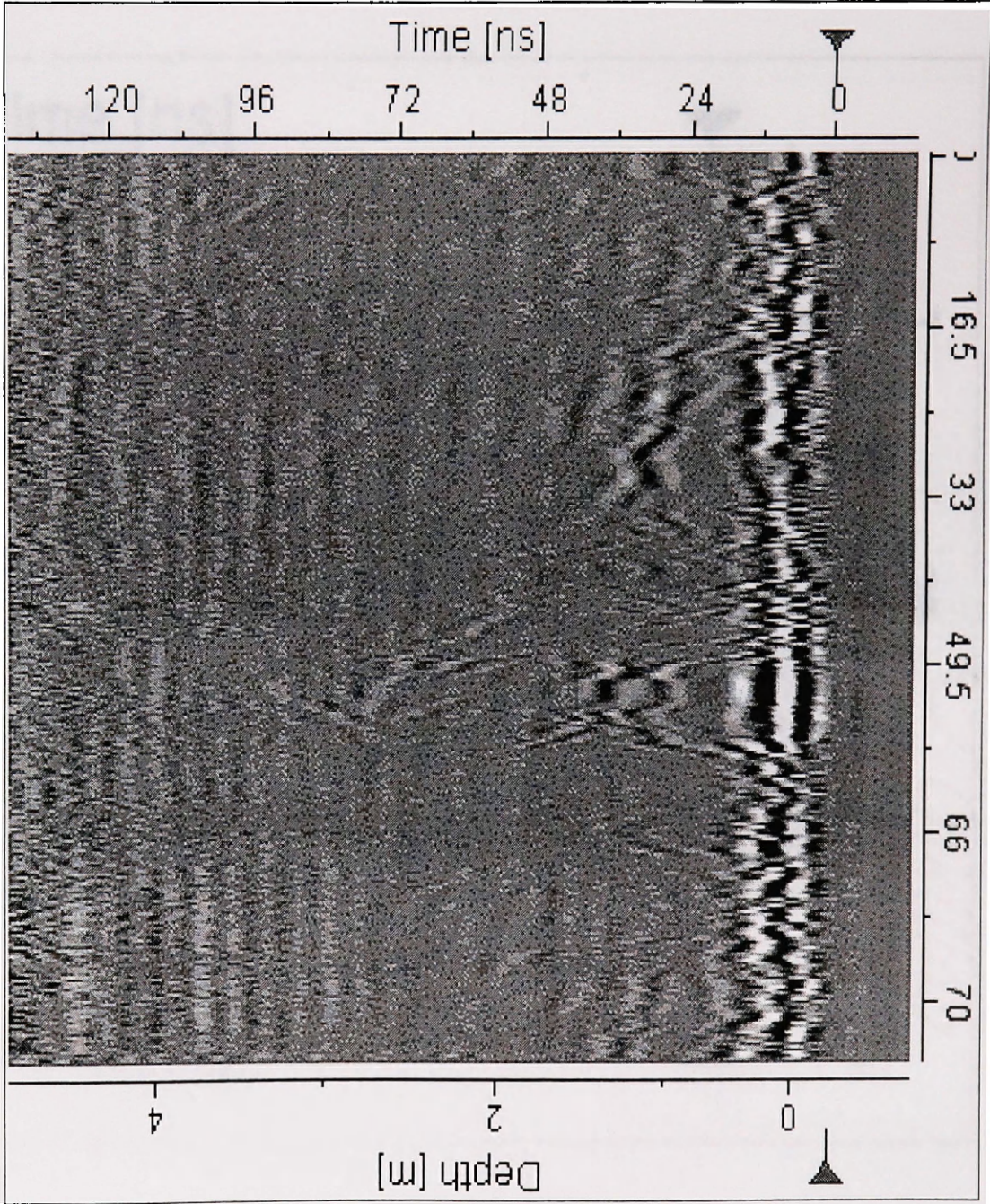


hf25



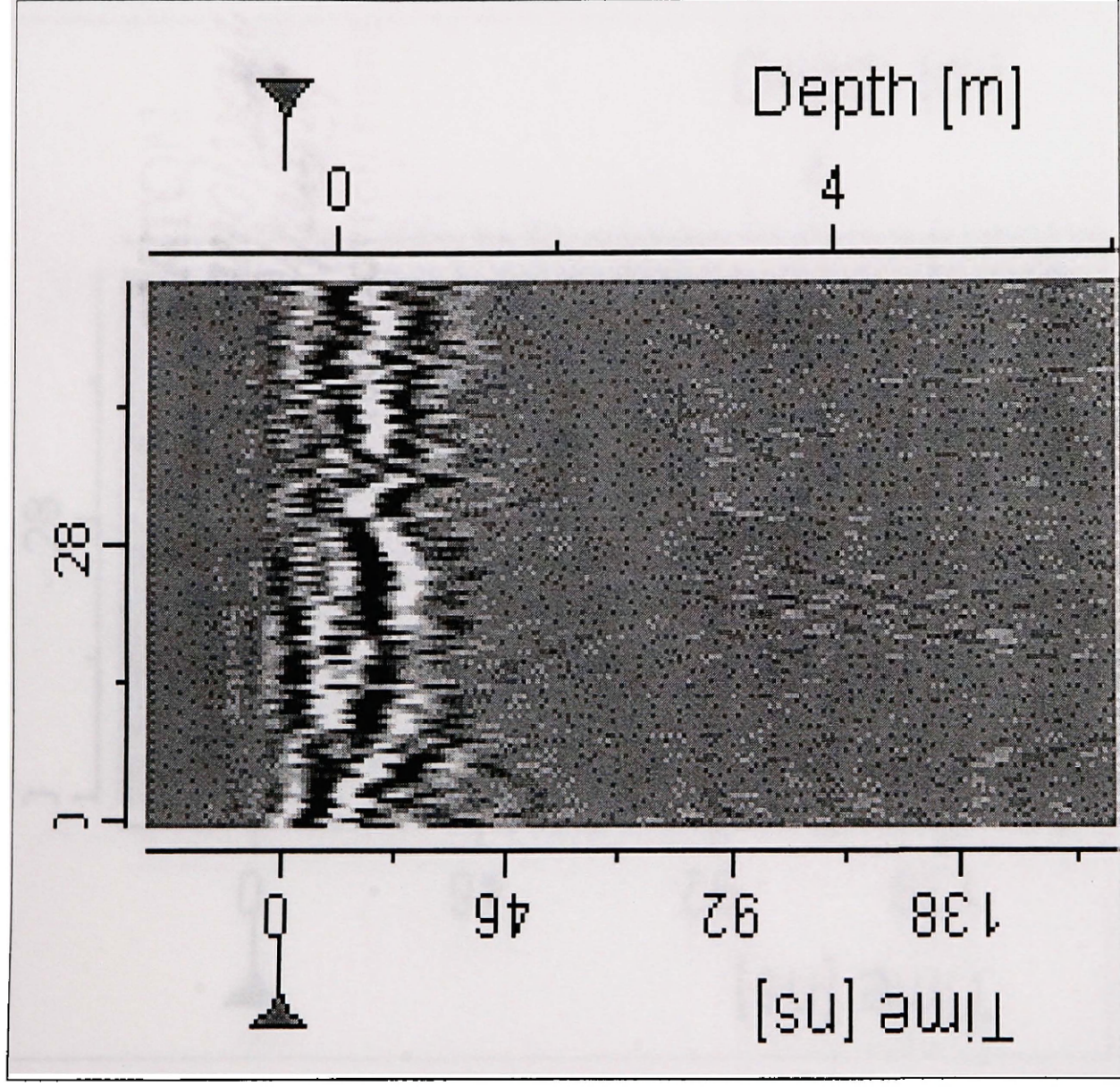
h30

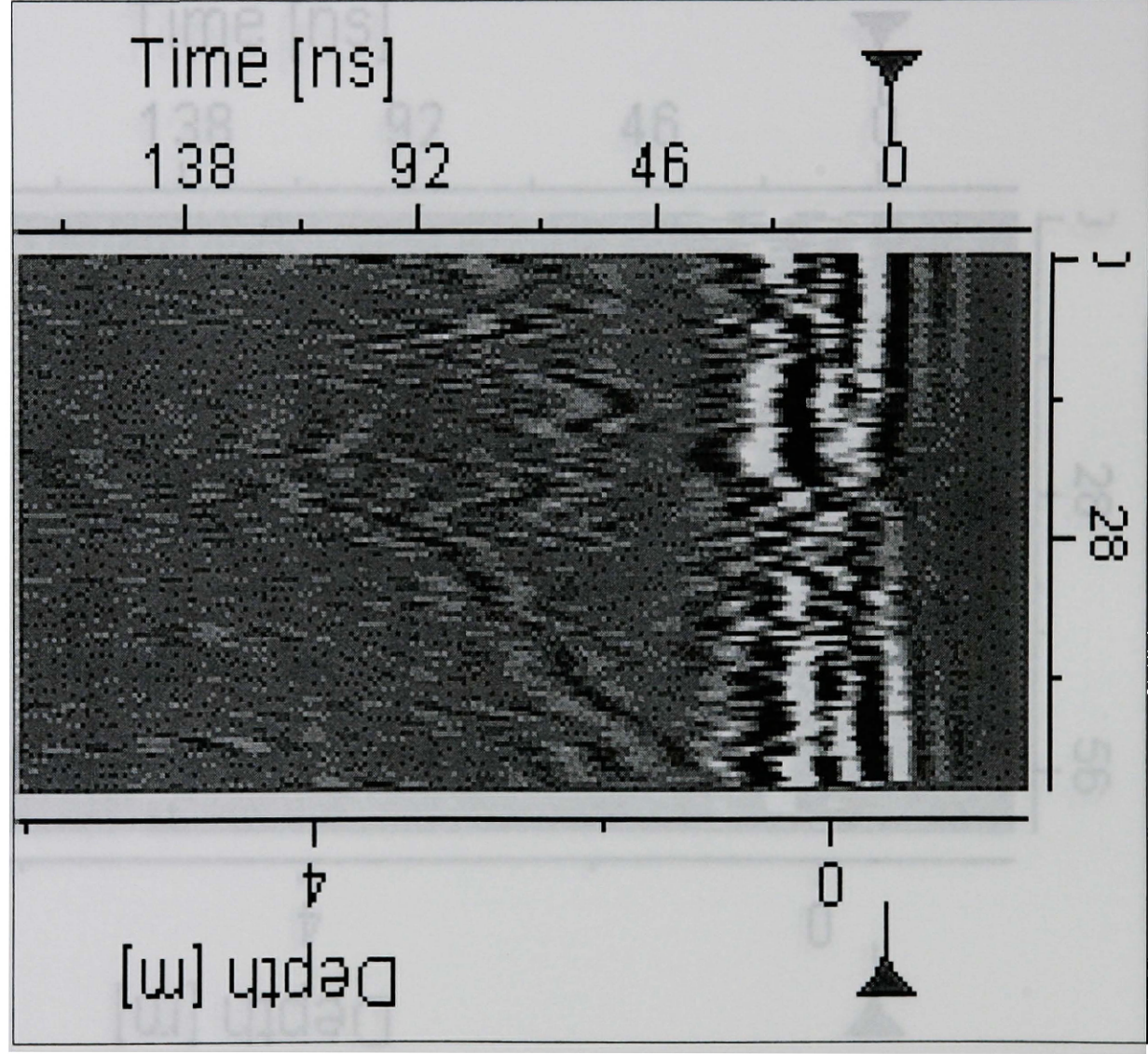




h31

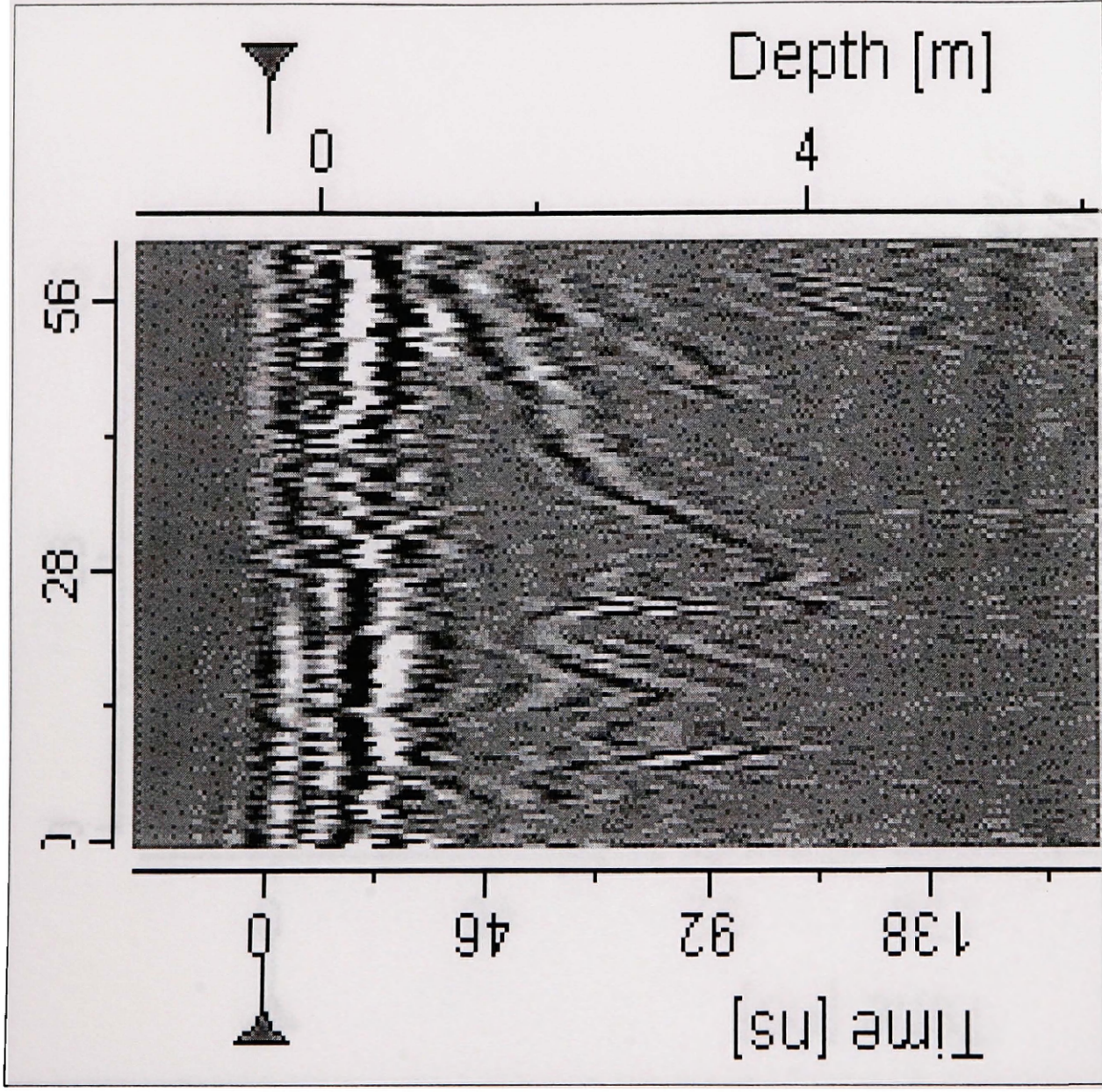
up02

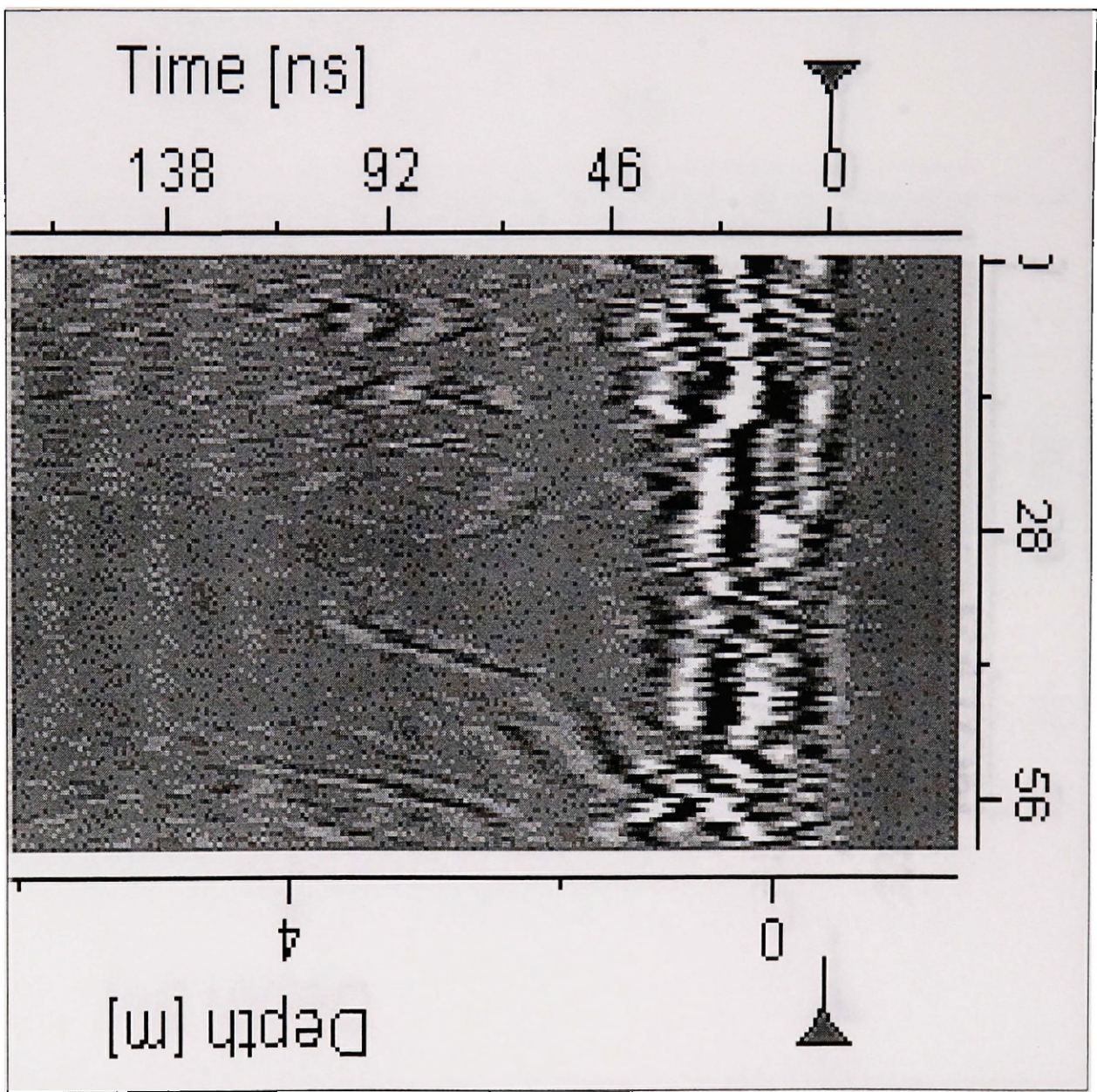


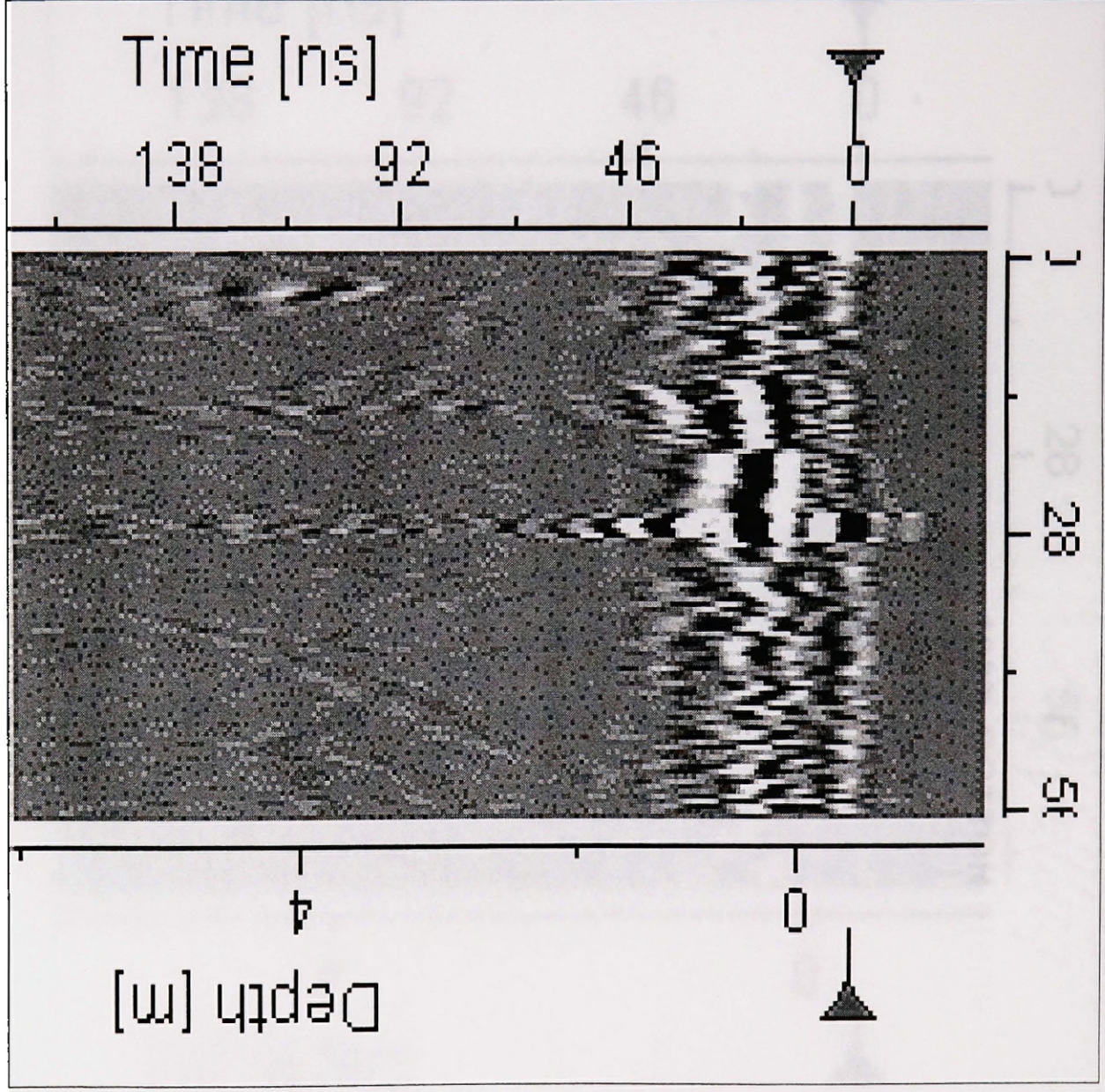




up04

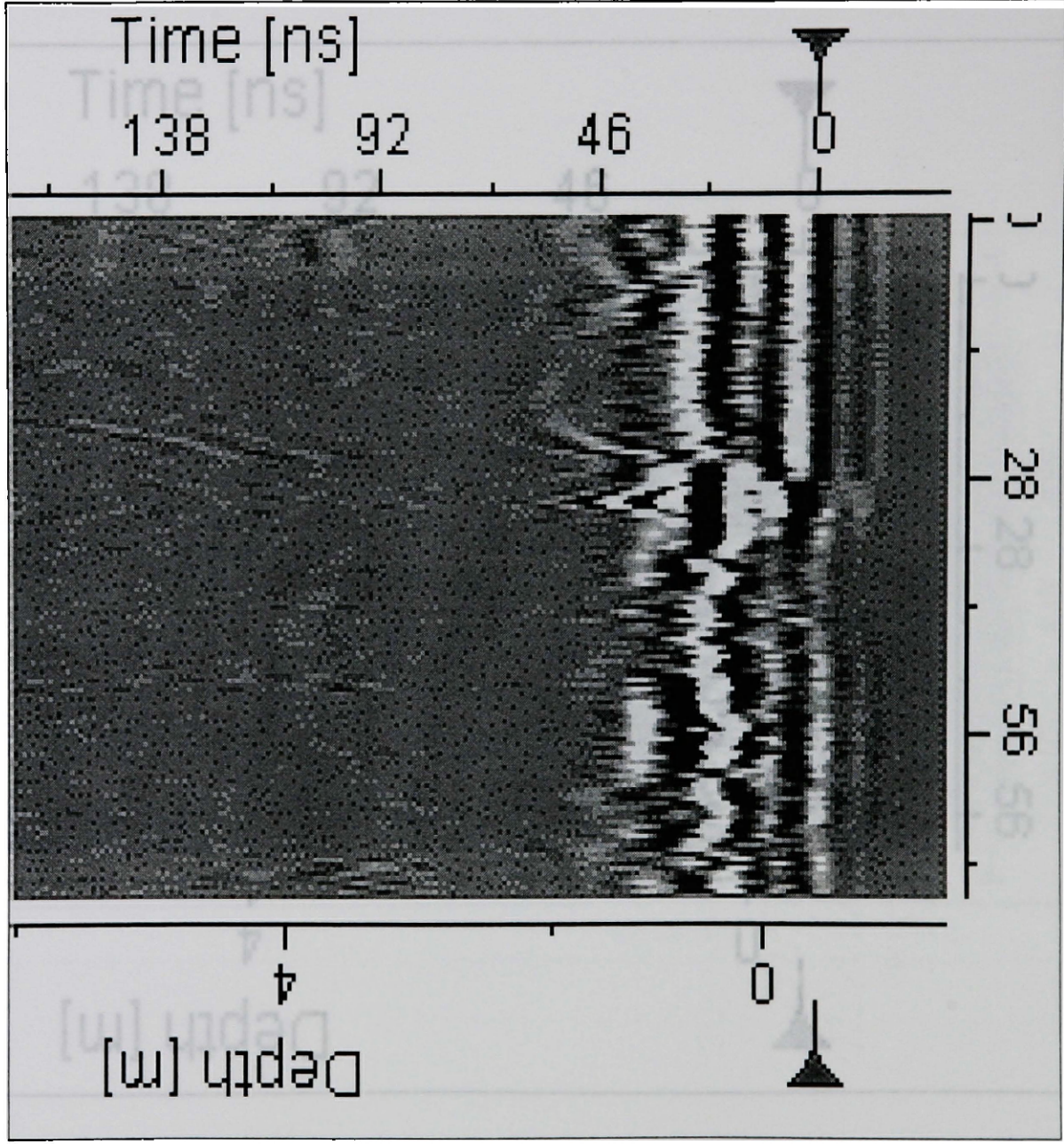


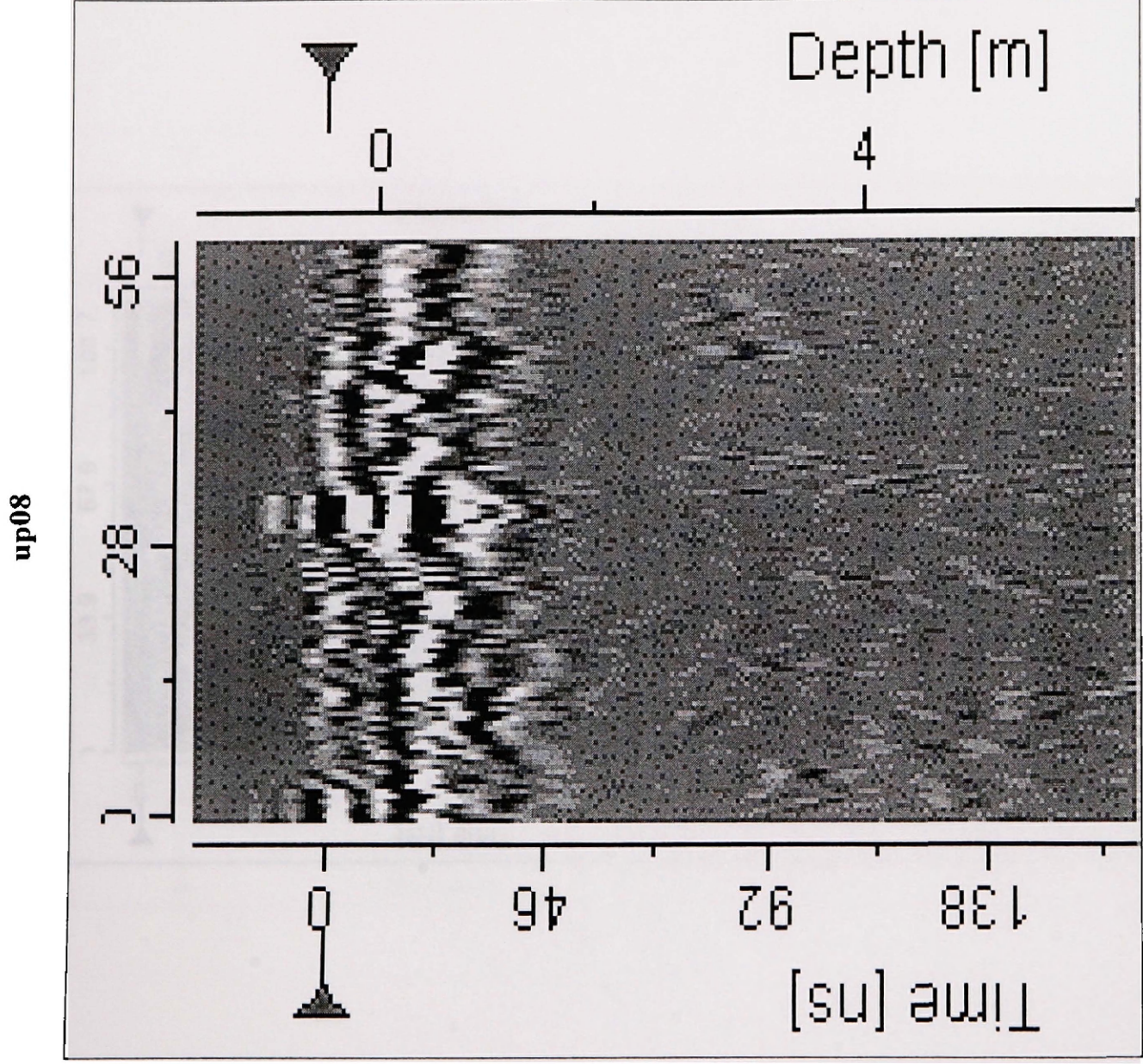




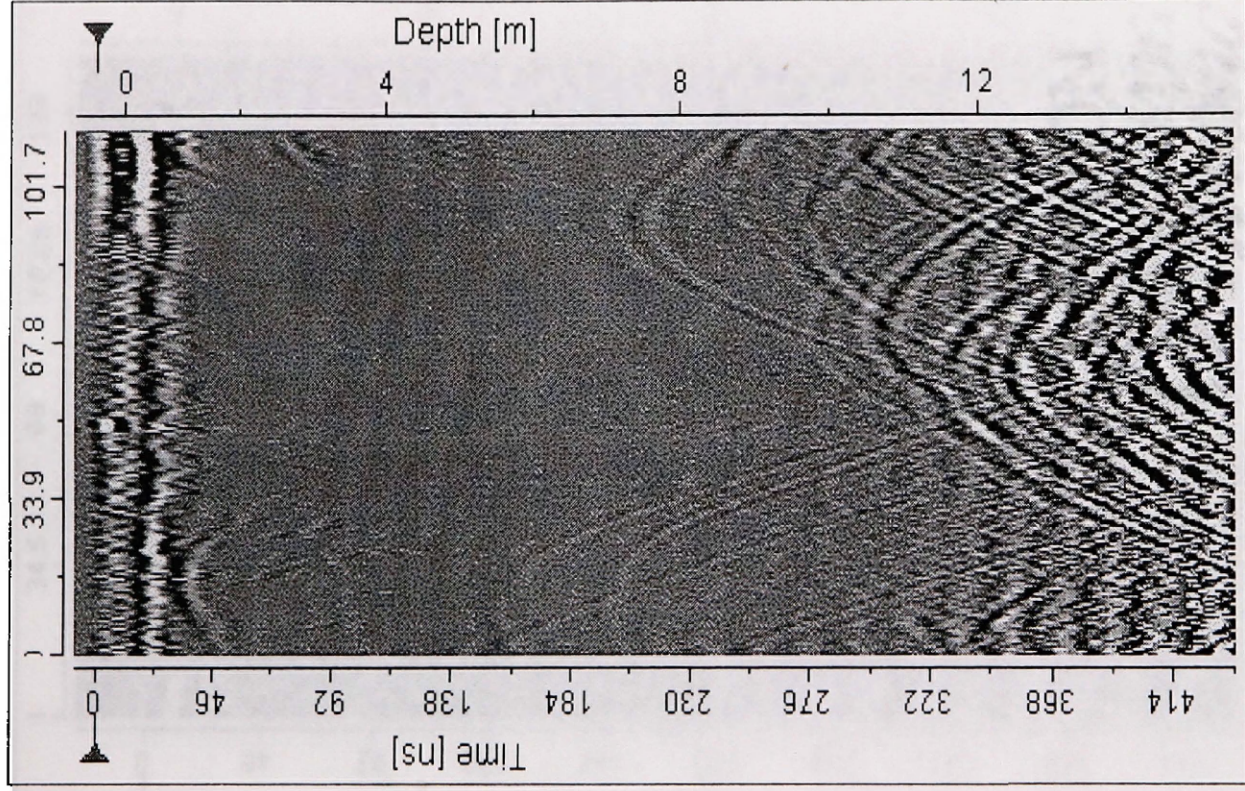
up06

up07

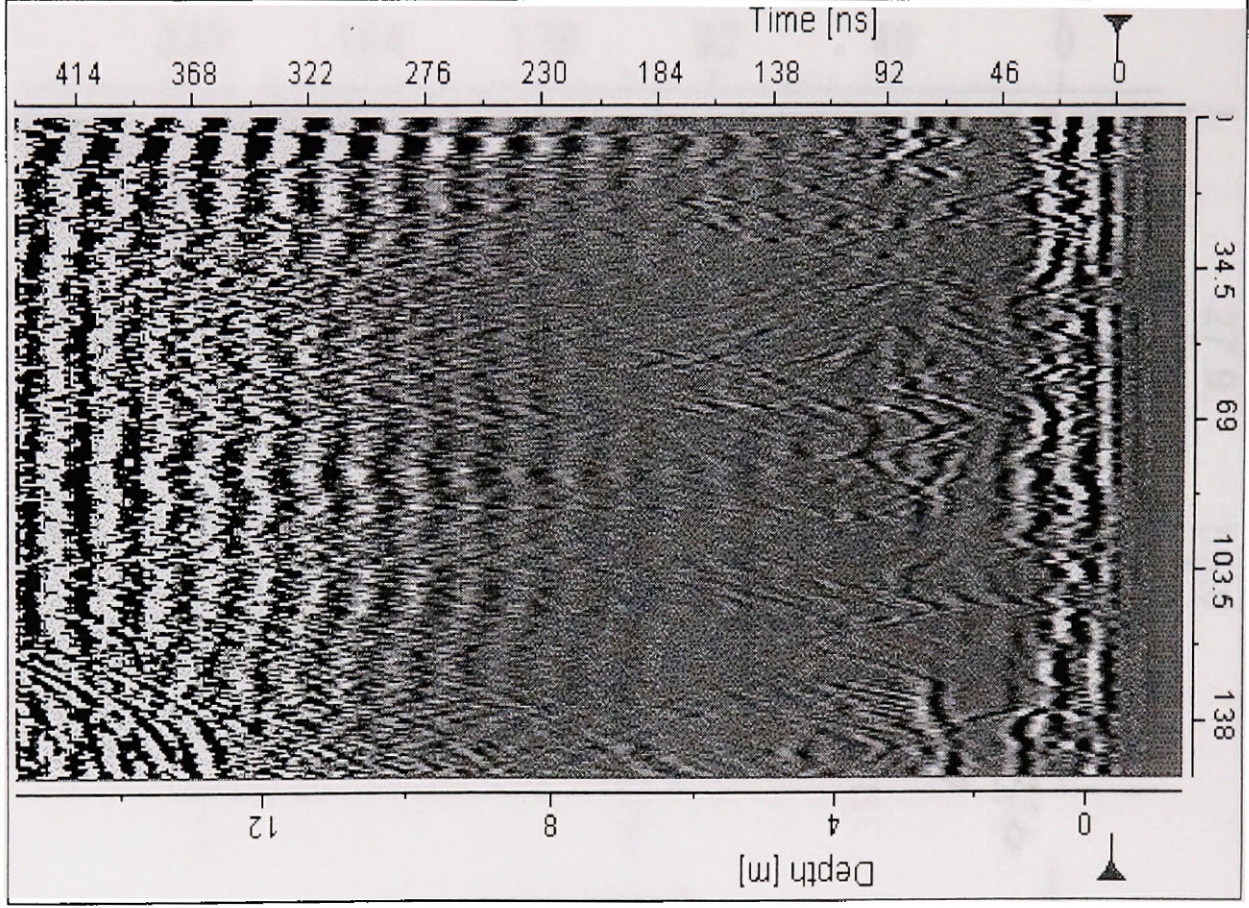




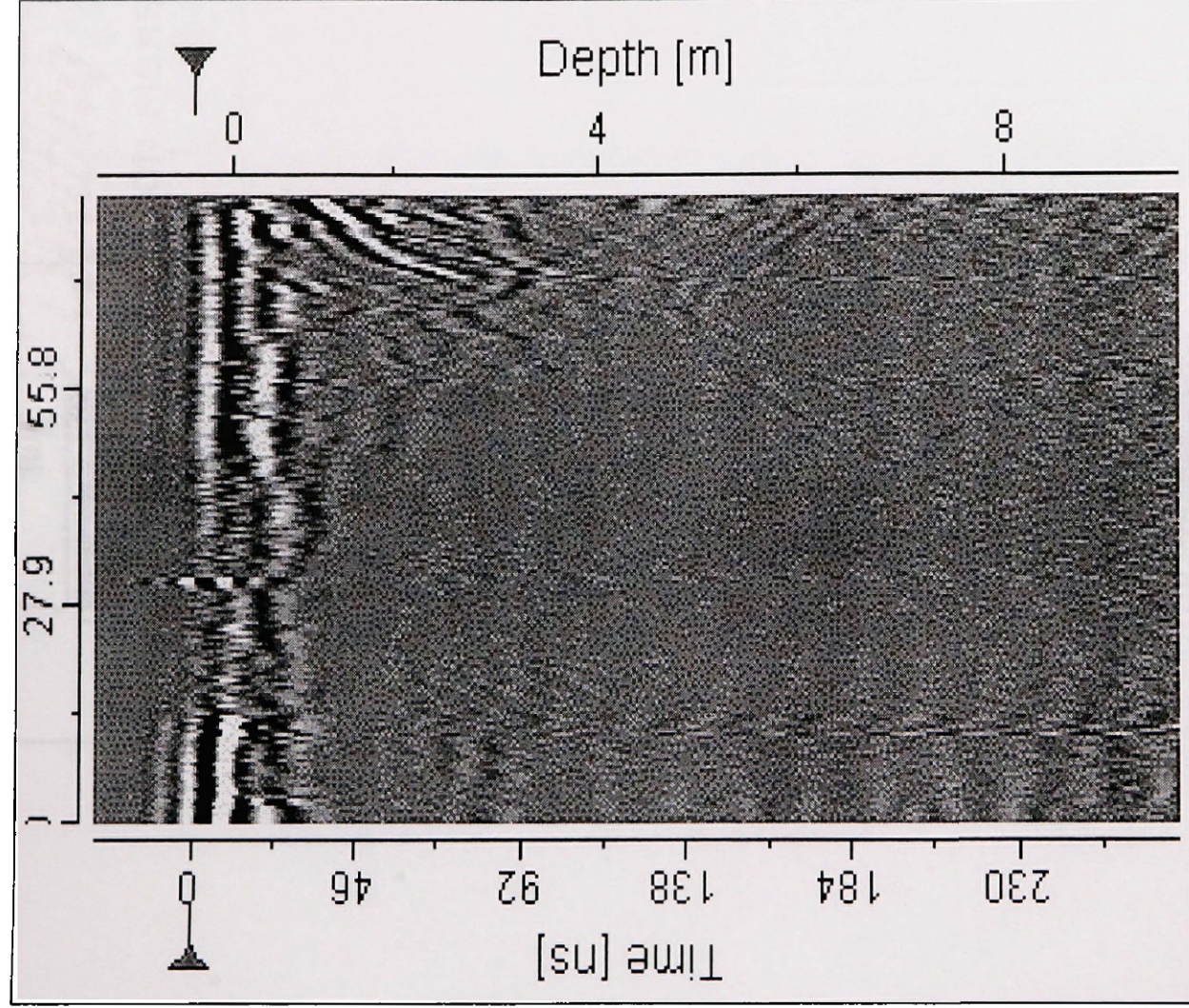
up10



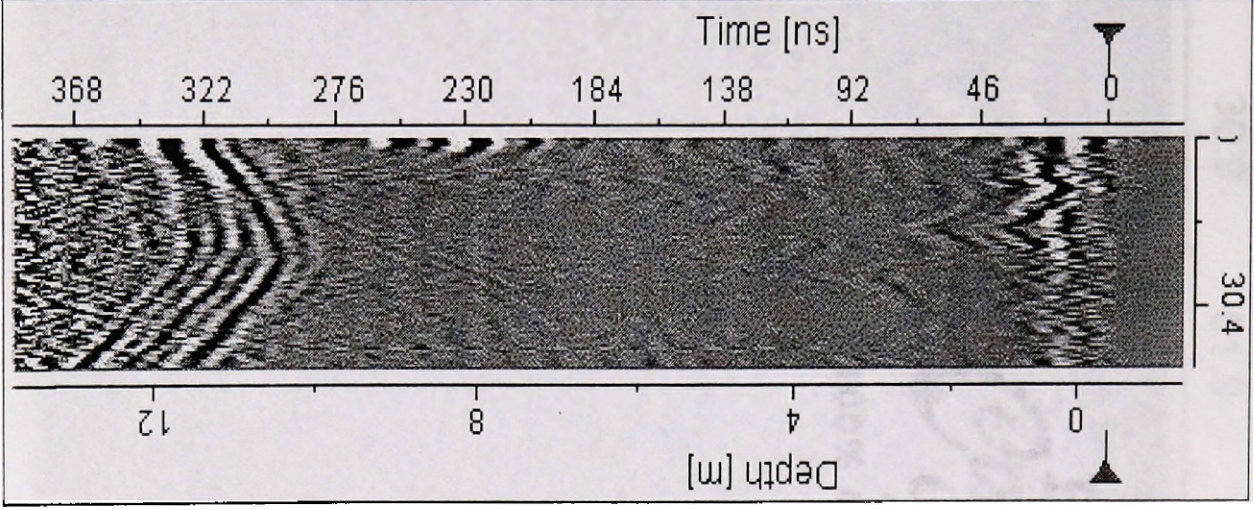
up16



up23

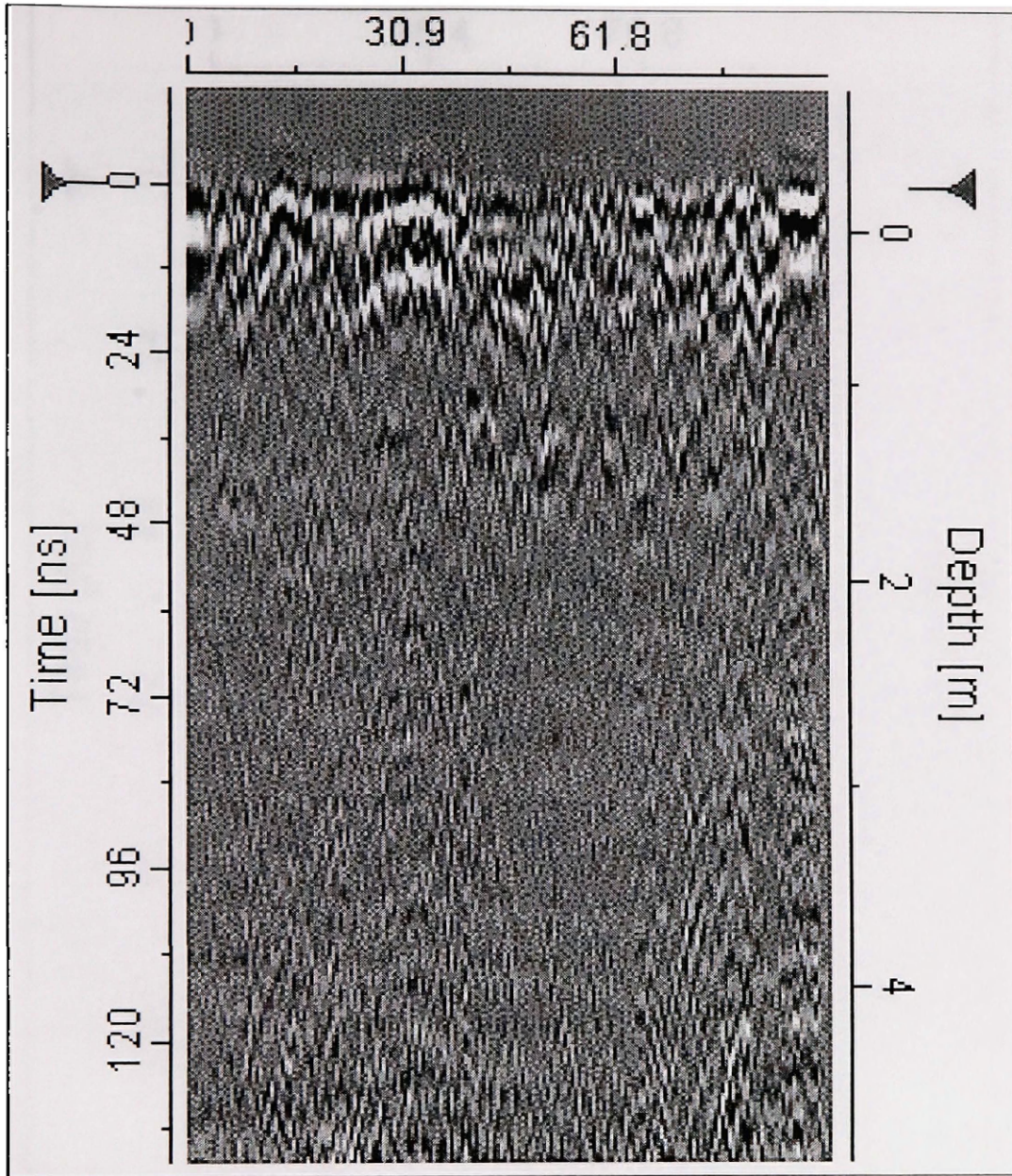




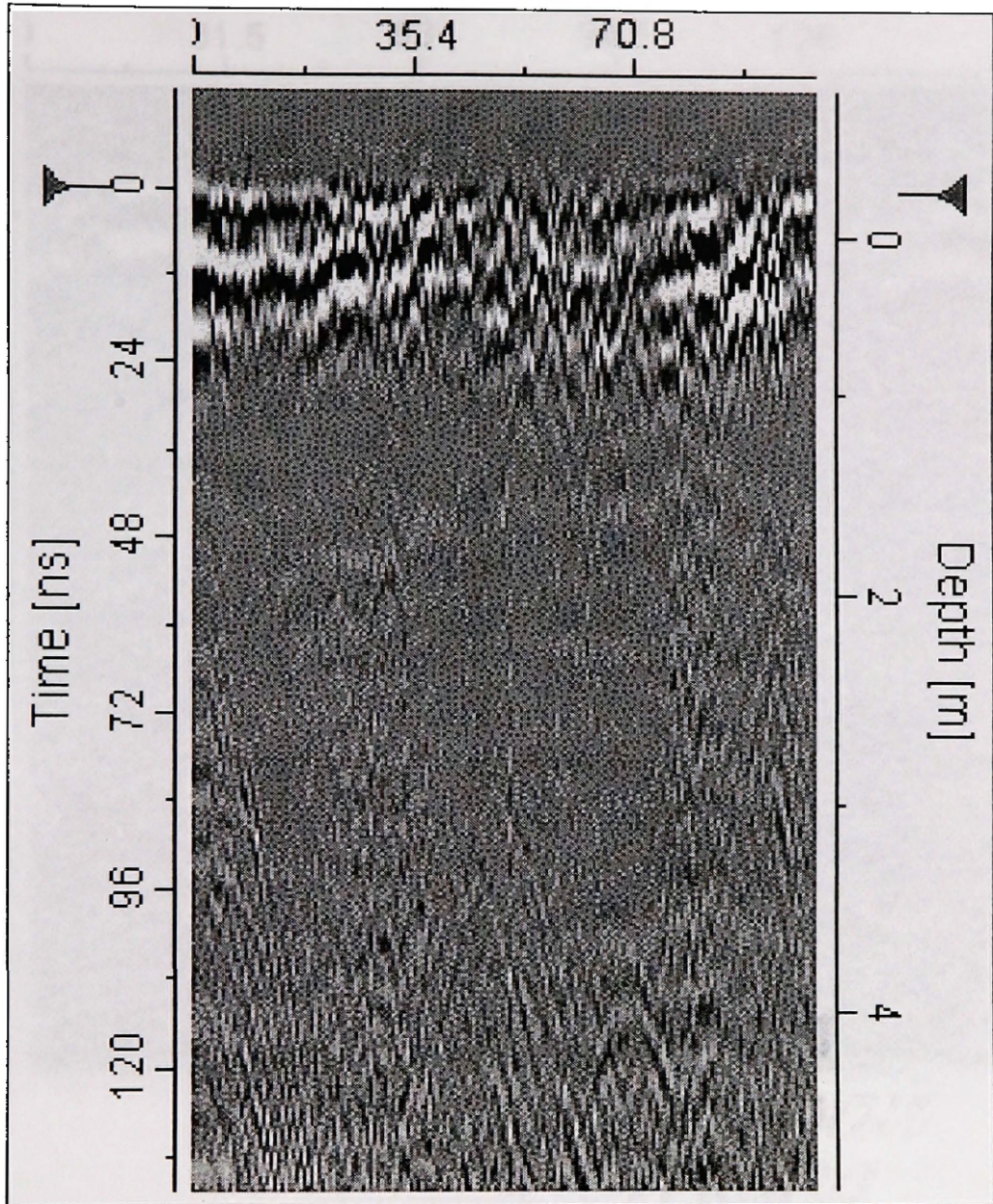


up27

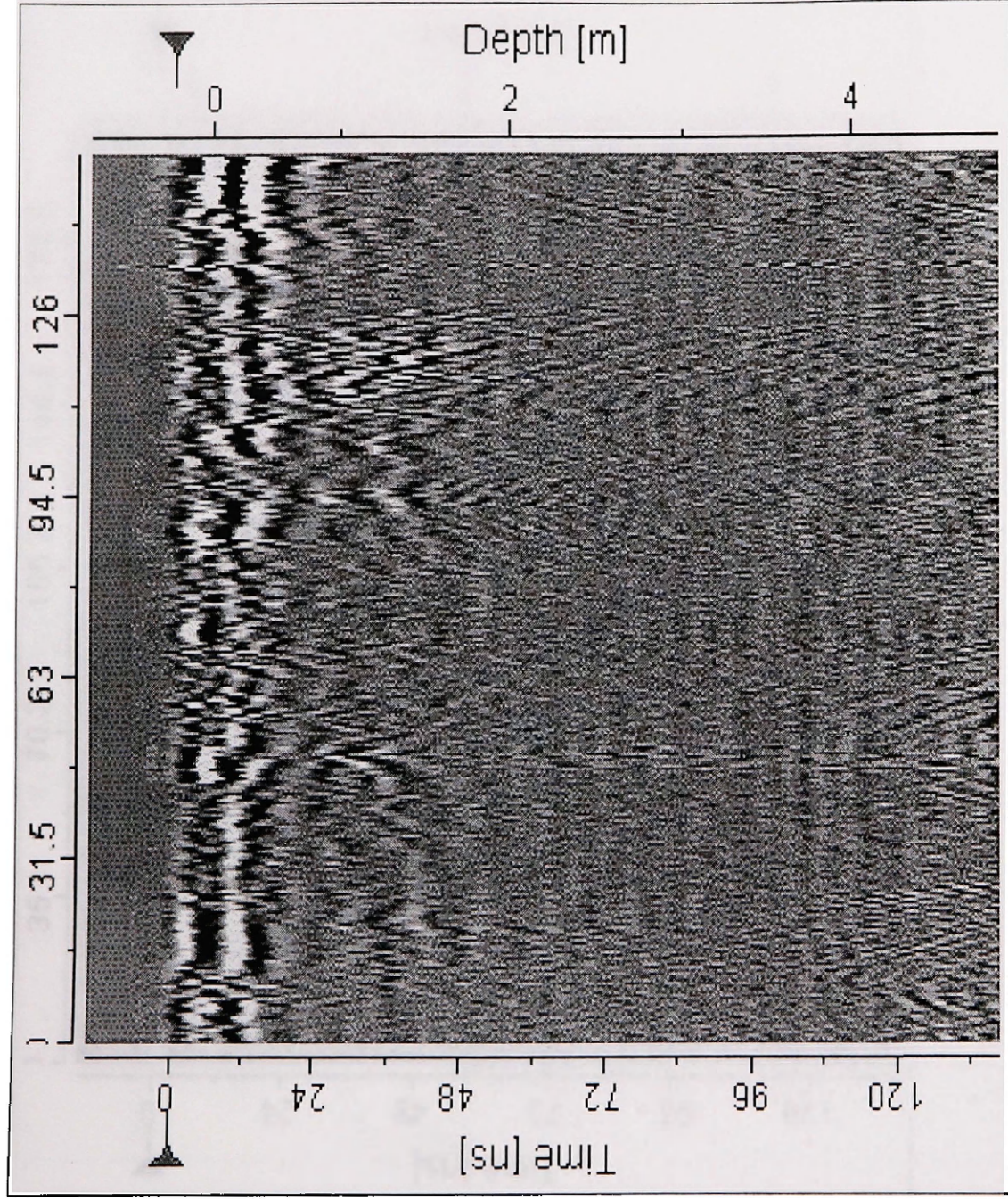
up33



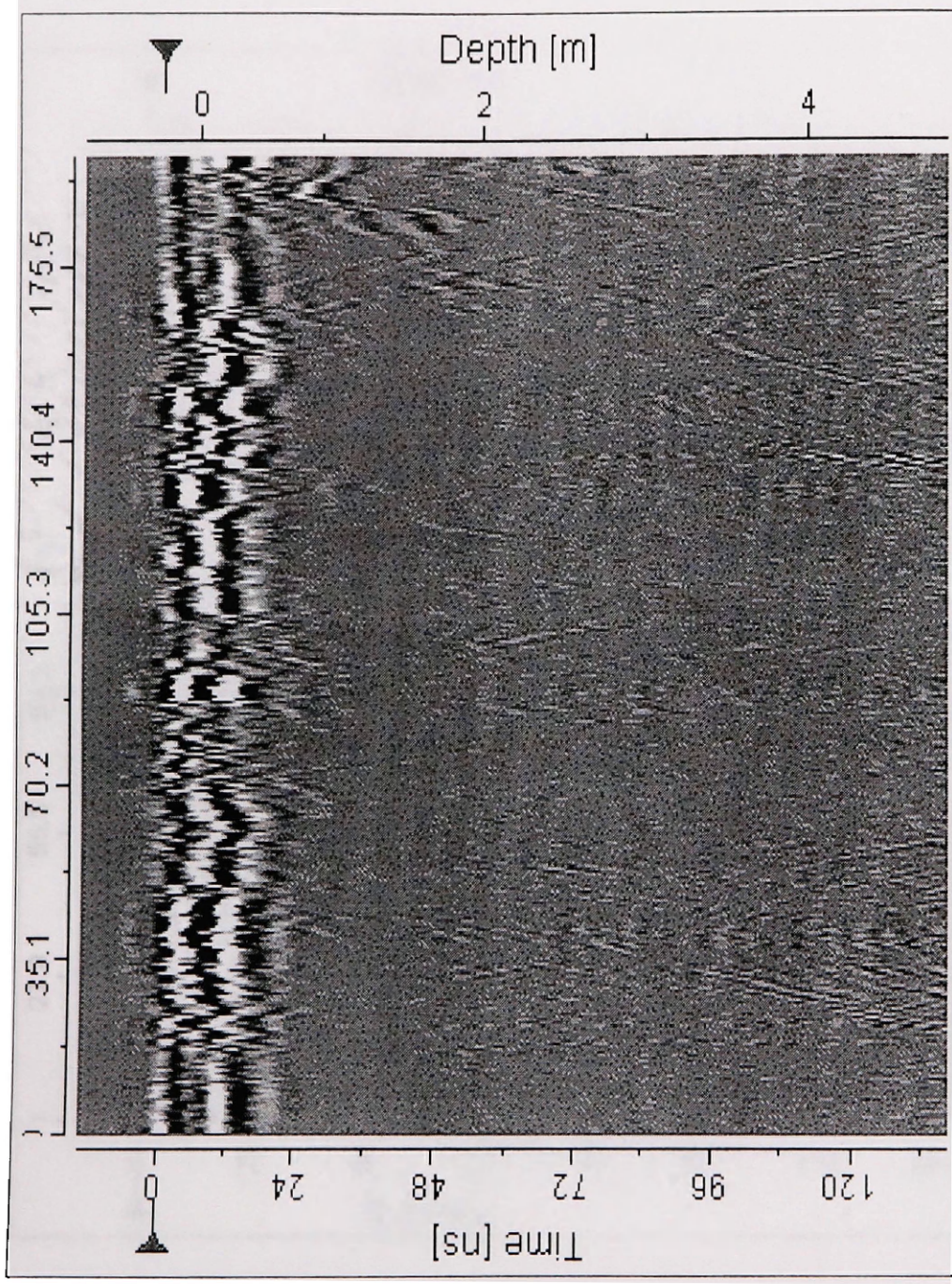
up33

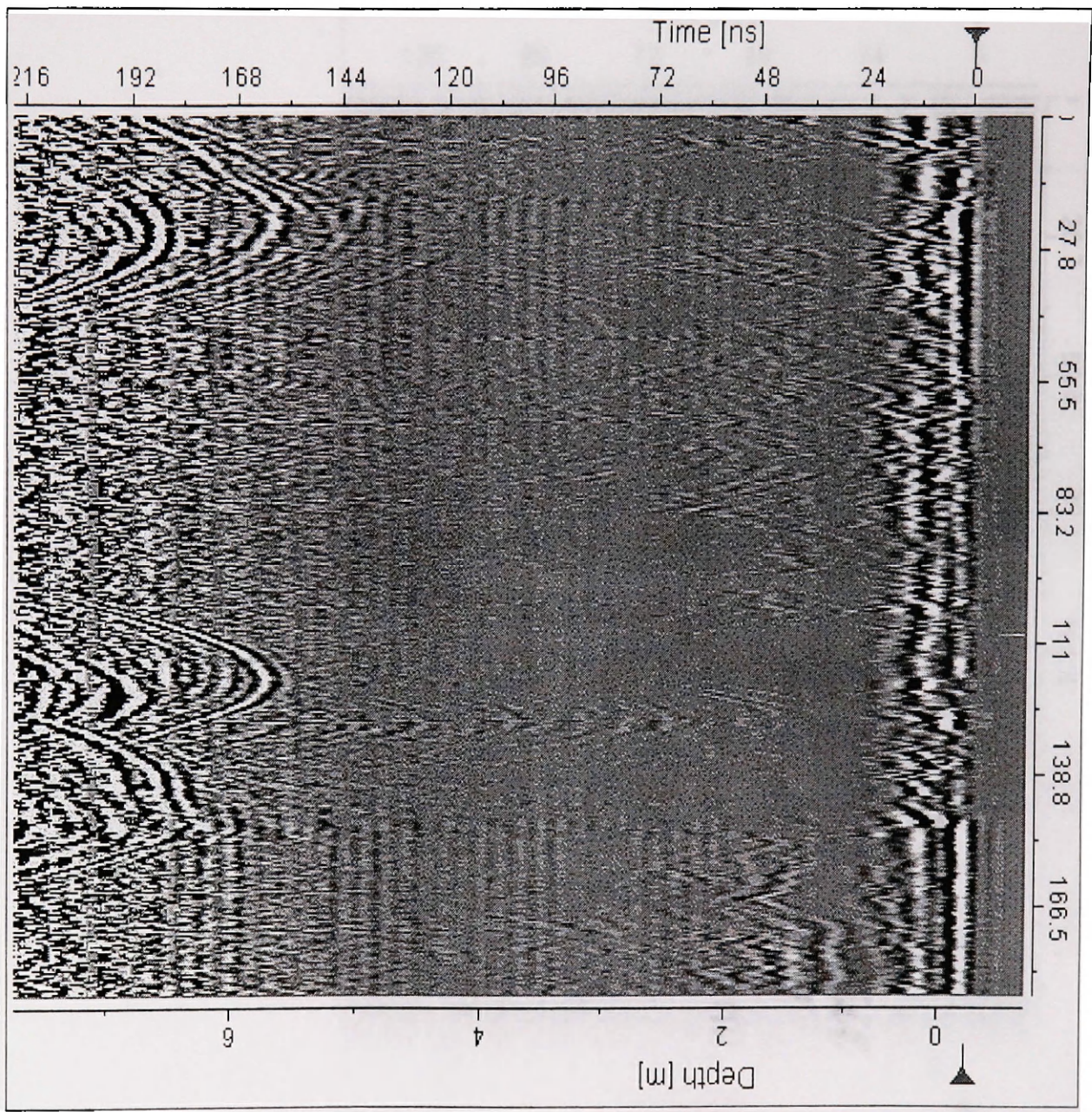


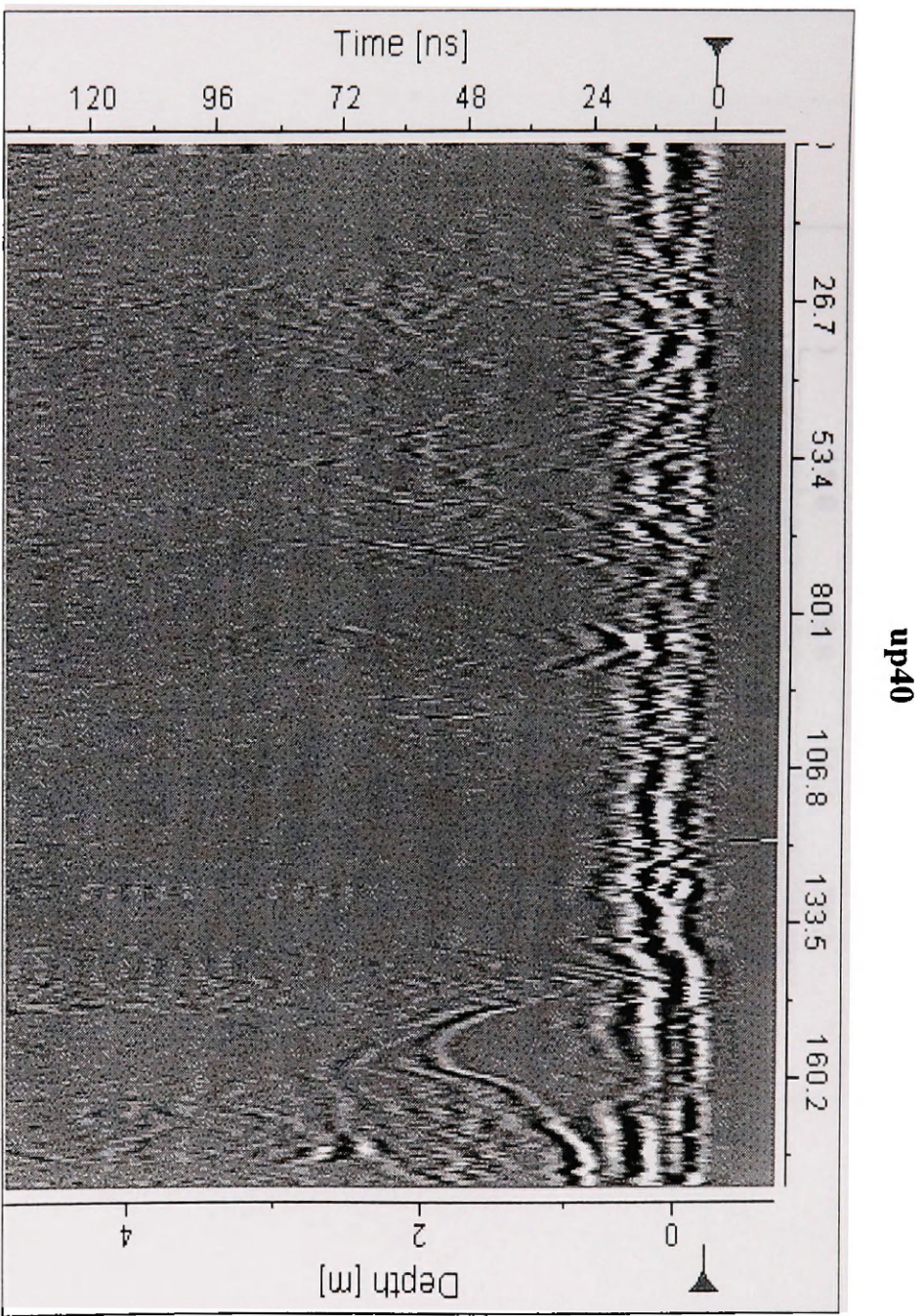
up36



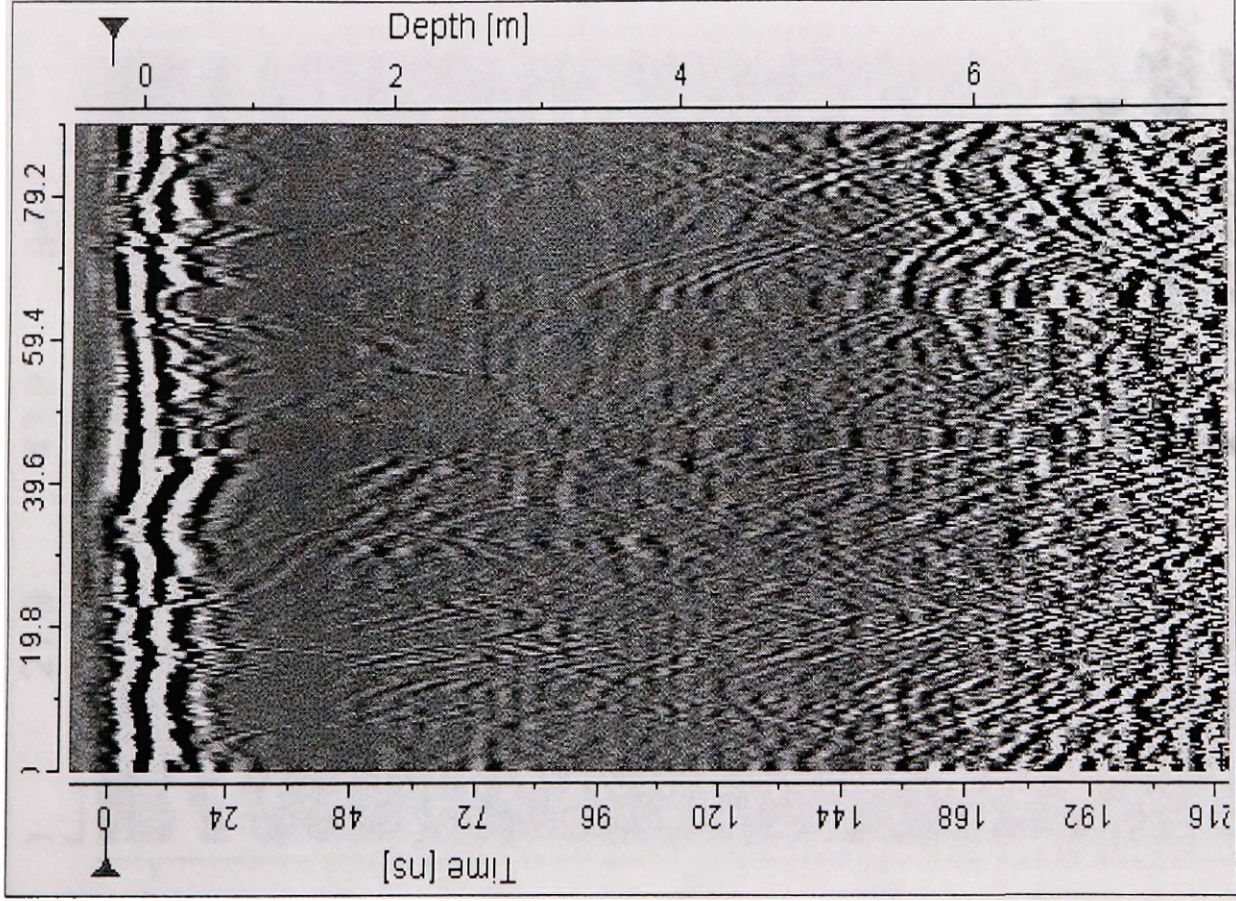
up38





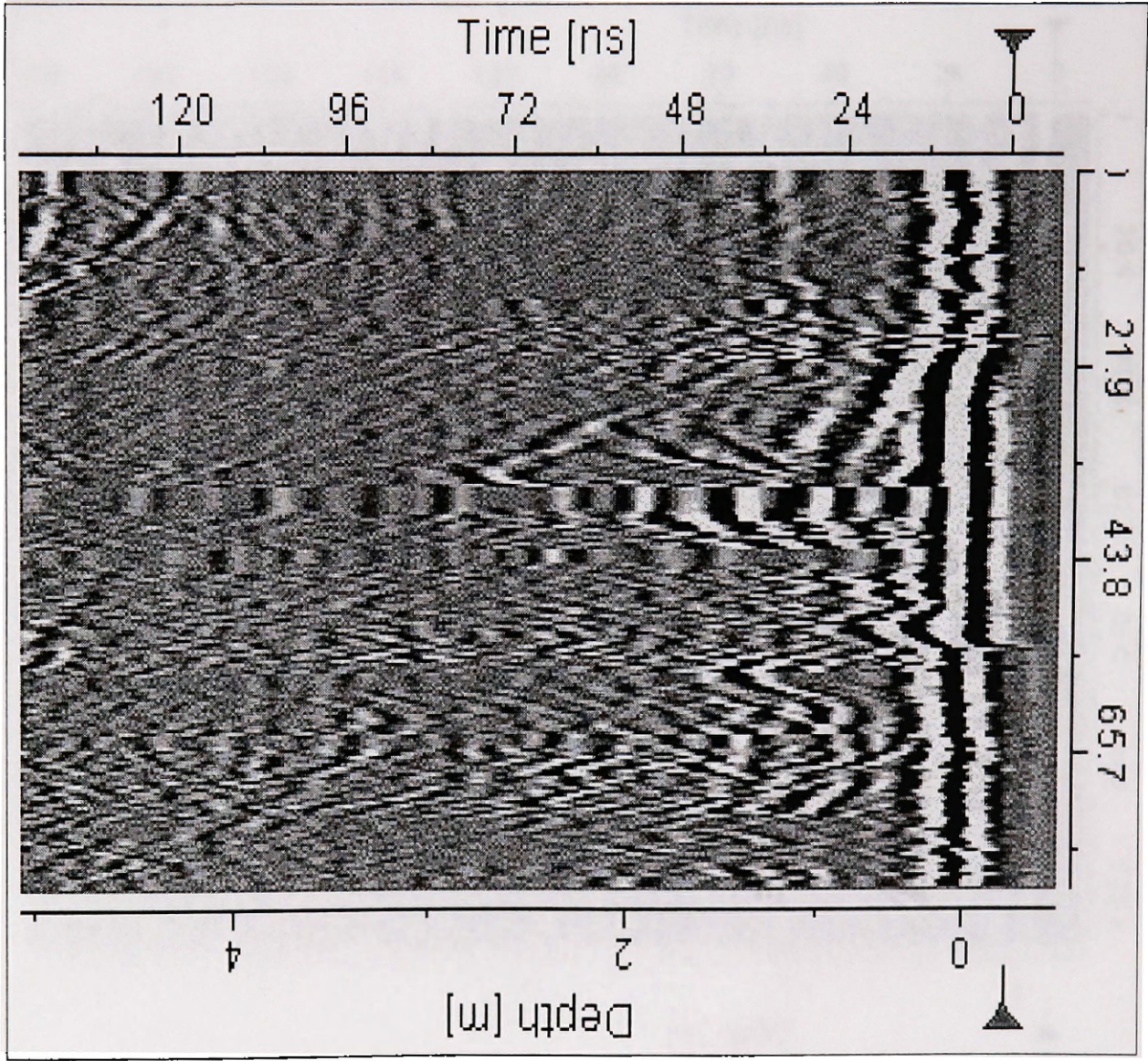


wc01

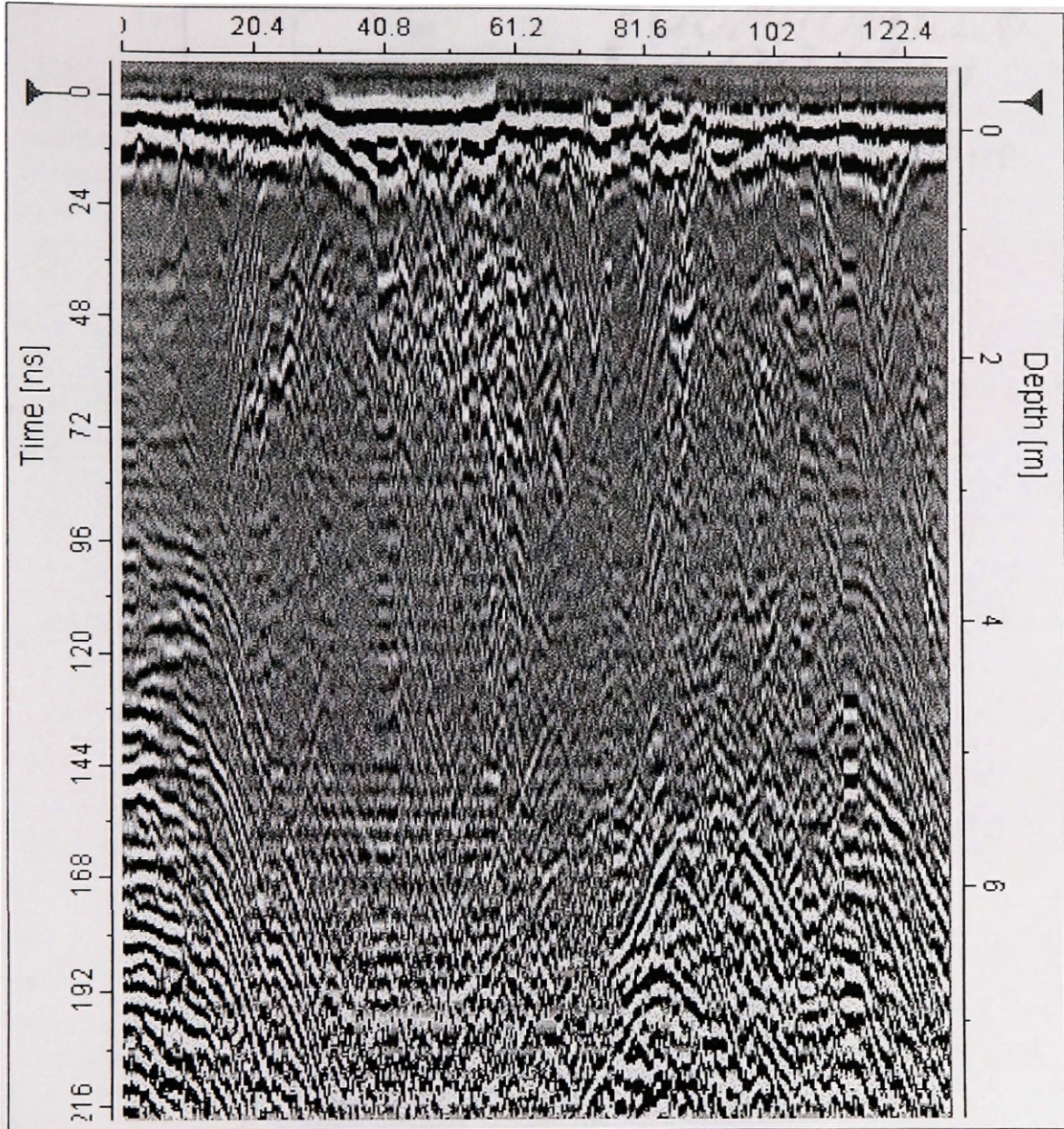




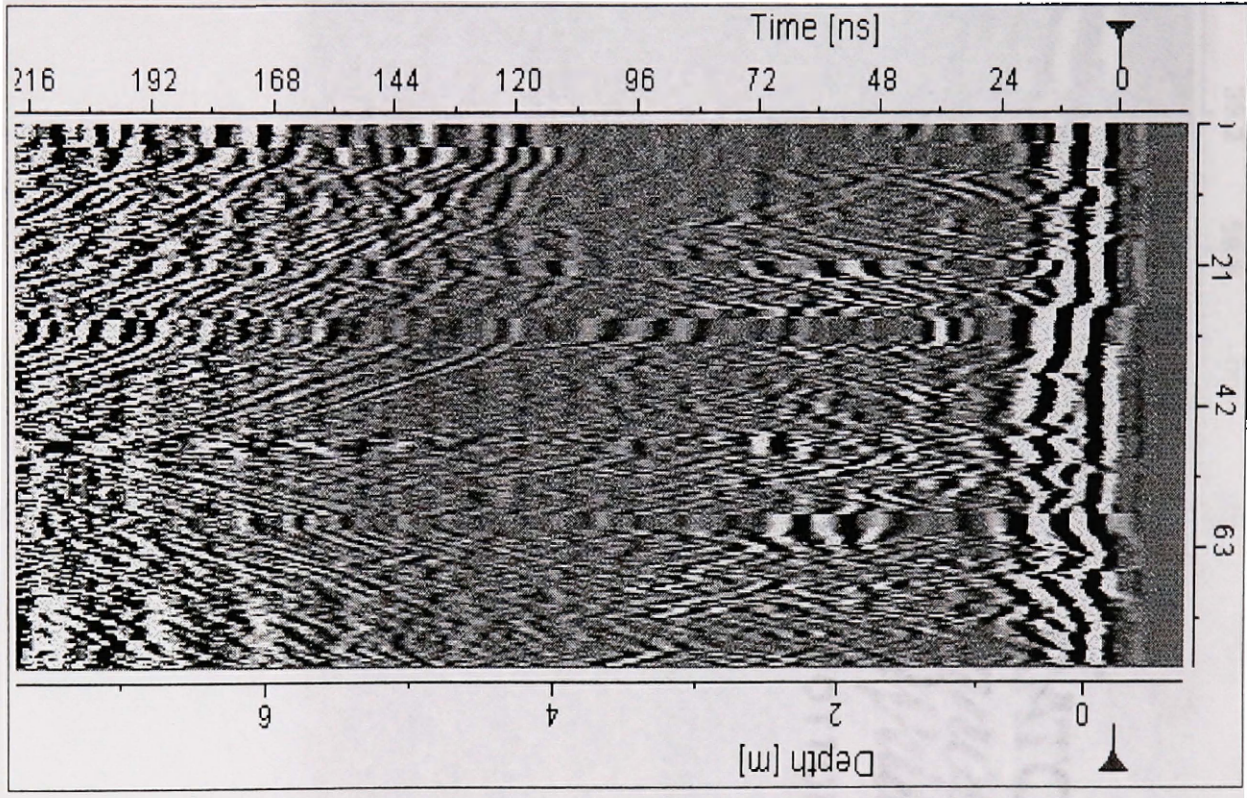
wc02



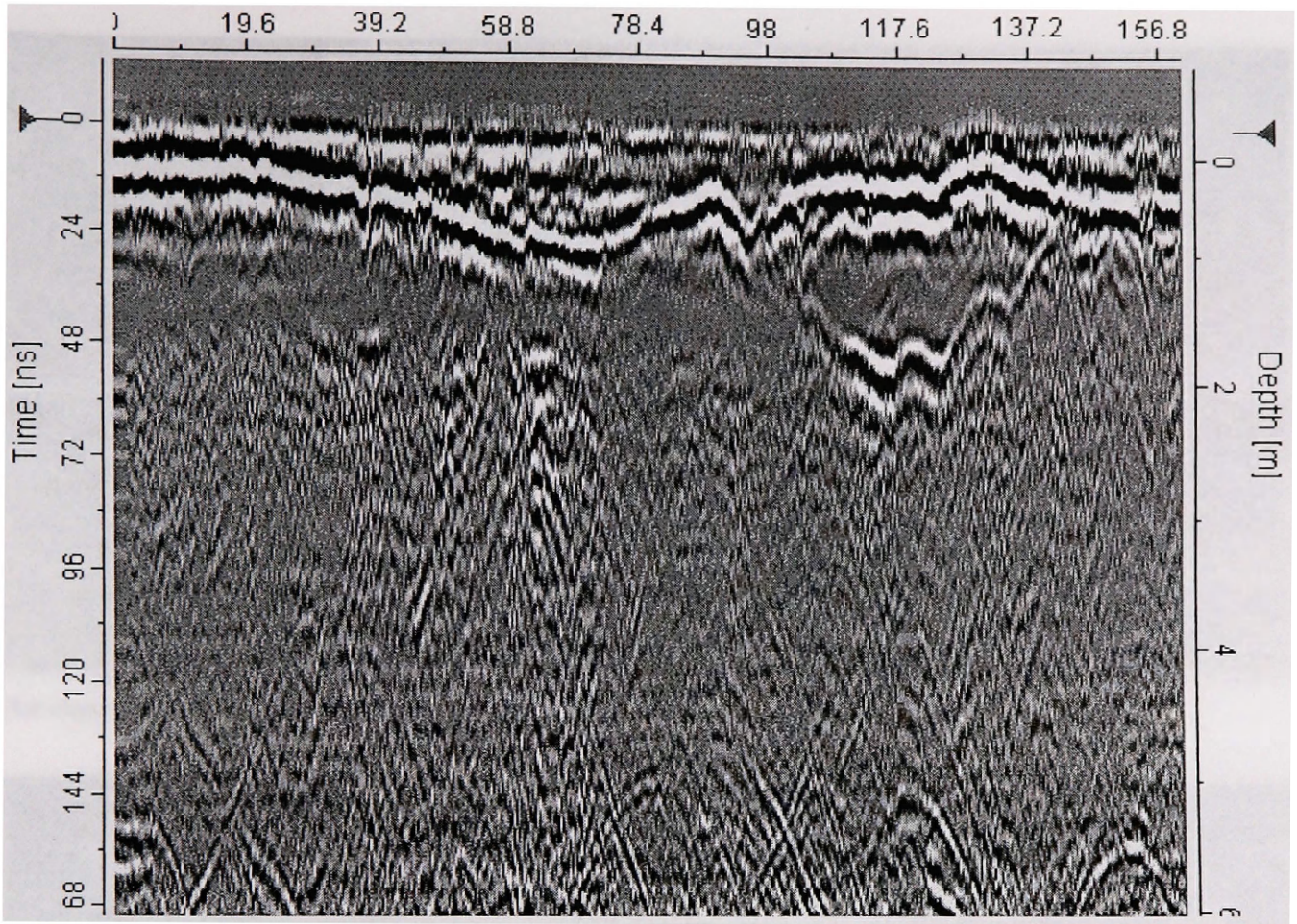
wc03



wc04



wc05



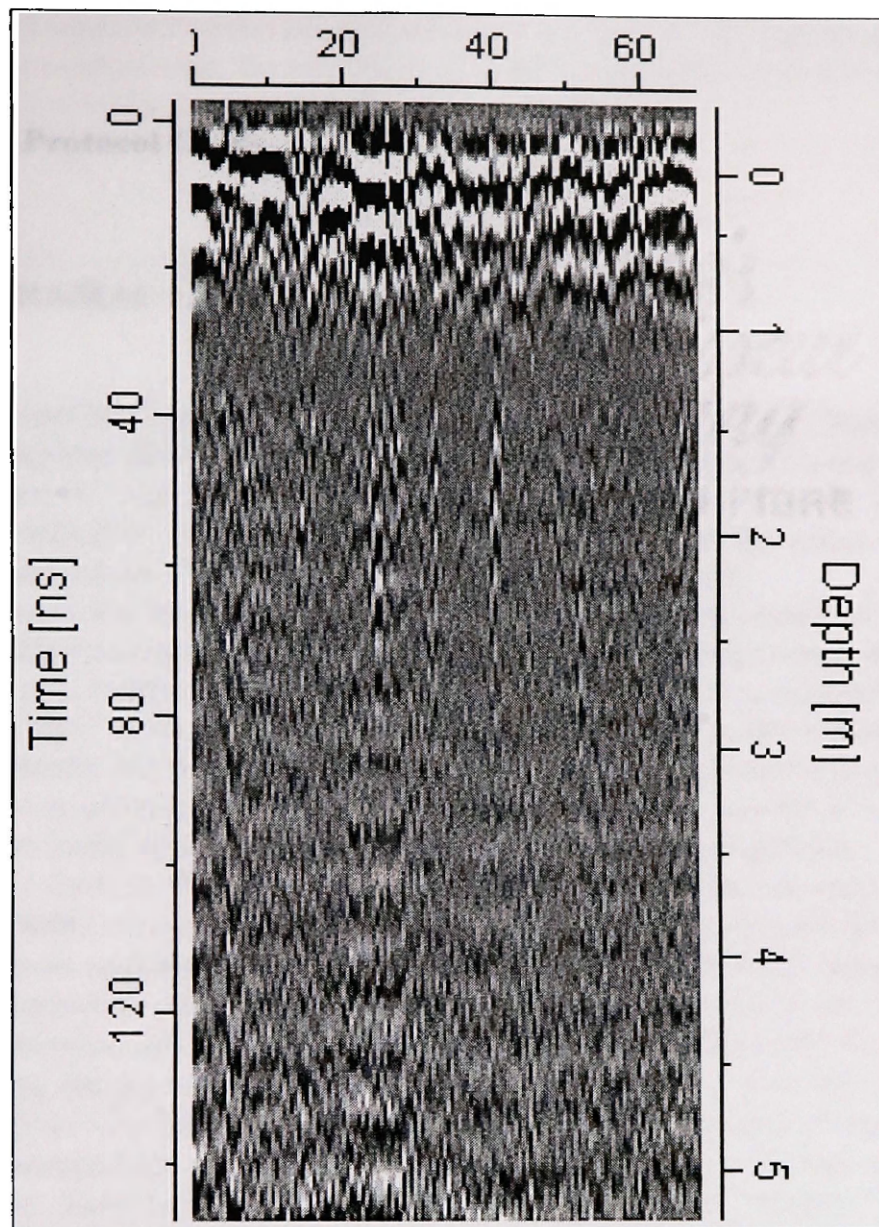
**Appendix C**  
**Polson, MT Gravel Pit**



**An exposure along eastern face of Polson gravel pit.**



**Another exposure along the eastern face of the Polson gravel pit.**



Radargram from the Polson gravel pit. Horizontal reflectors present are not due to layered stratigraphy, but ringing in the GPR system due to the electronic phenomena of wow.

## Appendix D RAMAC GPR Protocol Guide

Last Revised January 28, 2003

### Setting up the RAMAC GPR

1. Connect the battery packs to the transmitter and receiver electronics. The transmitter electronics has a single fiber optic cable connector on top with a *T* next to it. The receiver electronics has dual fiber optic cable connectors on top with an *R* next to one connector and a *D* next to the other. Be sure that battery packs are latched to each piece of electronics.
2. Connect the battery pack to the control unit (located inside of backpack).
3. Attach transmitter and receiver electronics to the transmitter and receiver antenna, respectively. Matching up the appropriate male/female serial pairs does this. Also, be certain to latch the electronics to the antennae.
4. Assemble the wooden antenna handles and attach them to the transmitter and receiver electronics. Do not pull hard on latch. If you have to pull hard, then rotate latch hooks counterclockwise to extend them upwards. This provides more slack to the latches. Use the 0.6 meter wooden separator bars for the 200 MHz antenna, the 1.0 meter wooden separator bars for the 100 MHz antenna, and the 2.0 meter separator bars for the 50 MHz antenna.
5. Connect one end of the single jumper fiber optic cable to the transmitter electronics and the other end to the control unit. The control unit has the letter *T* near the appropriate fiber optic cable connector. You must line up the notch on the fiber optic cable connector with the groove in the connector for the electronics. Once the notch is lined up, push down, and rotate to lock cable. Feed one end of the cable through the velcro window in the backpack so that the backpack may be zipped up with the cables connected to the control unit. NOTE: It is beneficial to have a small resealable plastic bag so that all the protective caps for the cables and cable connectors can be stored and not be lost.
6. Connect one end of the dual jumper fiber optic cable to the receiver electronics and the other end to the control unit. The control unit has the letters *R* and *D* next to the appropriate fiber optic cable connectors. NOTE: Make certain that if you have the black side of the fiber optic cable connected to *R* on the electronics that the black side is also connected to *R* on the control unit. Feed one end of the cable through the velcro window in the backpack so that the backpack may be zipped up with the cables connected to the control unit.

7. Attach one end of the parallel cable to the back of the laptop and the other end to the control unit. Be certain to feed one end of the cable through the velcro window in the backpack.

### **Performing a Measurement with the RAMAC GPR**

1. Record the start point of the desired line with a GPS unit.
2. Measure out the distance of the desired line.
3. Record the end point of the desired line with a GPS unit.
4. Turn on the power to the laptop
5. Turn on the power to the transmitter and receiver electronics (power switches located on side).
6. Turn on the power to the control unit (power switch is located on side of unit). At this time, the three lights on the control unit and the lights on the electronics should be flashing.
7. Double click on the icon for the Groundvision software to load the program.
8. Click the *Start* (F5) key in the menu to create a new measurement. In the dialog box specify the name of the file, the directory it is to be saved in, the trigger mechanism, the antenna type, and then click the *Settings* button on the dialog.
9. In the settings dialog box, make sure the antenna separation is correct for the antenna type being used, set the desired trig interval, set the number of stacks to 4. Then, click the *Search for Time Zero* button two to three times so that the first arrival will occur near the top of the trace window. Then click *OK*.
10. When ready to begin the measurement, click the *Start Measurement* button.
11. Collect data along the desired line.
12. When ready to quit the data collection, click the *Stop* (F6) button.
13. Close the window for the measurement data. This is to ensure that data collection does not resume with the current file if the *Start* (F5) is accidentally pressed.



## Filtering RAMAC GPR Data using RAMAC Groundvision

1. Access the Filter Manager Dialog Box. This is done by first going to the *Radargram* menu and selecting *Filter*.
2. Highlight the *DC Filter* option and click *Add>>*.
3. In the *DC Filter* dialog, maintain the default settings and click *OK*.
4. Highlight the *Band Pass Filter* option and click *Add>>*.
5. In the *Band Pass Filter* dialog, maintain the default settings and click *OK*.
6. Highlight the *Time Gain Filter* option and click *Add>>*.
7. In the *Time Gain Filter* dialog, in the left window, adjust the red highlighted area so that it is just below the input wave pulse. Then, alter the linear gain and exponential gain to satisfy that the exponential gain is a value approximately ten percent less than the linear gain and also to satisfy that the newly gained signal in the left window does not have its extremes outside of the window. Once you are satisfied with the gained signal, click *OK*.
8. Highlight the *Subtract Mean Trace* option and click *Add>>*.
9. In the *Subtract Mean Trace* dialog, click *Total Average* as the subtraction method and click *OK*.
10. In the Filter Manager Dialog Box, click *OK* to see the newly filtered data.
11. If the data needs to be filtered again for better results, remove all the filters and start over.

## **Problems Encountered with the RAMAC GPR**

1. The laptop brace will come loose unexpectedly and start to drop the laptop.
2. The fiber optic cables become easily hung-up on brush or start to get pulled under the antennae if they are too low to the ground.
3. Data collection will suddenly cease with the error “Communication Interruption” if the unit undergoes too much vibration. This problem was encountered when walking with the unit and also when attempting to use the unit with a four-wheeler.

## **Pitfalls/Limitations of the RAMAC GPR**

1. Effective depth of penetration is approximately six to ten meters. Unable to get an image of the subsurface below those depths.
2. Unable to operate unit in areas of heavy brush due to the lack of maneuverability of the unit and also the increased risk of snagging the fiber optic cables.
3. Laptop battery life is approximately 2.5 – 3 hours.
4. GPR battery life is approximately 6 – 8 hours. NOTE: The battery life range is an estimate.

Recharge time for one set of GPR batteries is approximately 8 hours.